

**MONOTONIC AND CYCLIC FRACTURE BEHAVIOUR OF
AISI 304LN STAINLESS STEEL**

Himadri Roy

MONOTONIC AND CYCLIC FRACTURE BEHAVIOUR OF AISI 304LN STAINLESS STEEL

*Thesis submitted to the
Indian Institute of Technology, Kharagpur
For award of the degree*

of

Doctor of Philosophy

by

Himadri Roy

Under the guidance of

Prof. K. K. Ray

and

Dr. S. Sivaprasad, NML, Jamshedpur



DEPARTMENT OF METALLURGICAL AND MATERIALS ENGINEERING

INDIAN INSTITUTE OF TECHNOLOGY KHARAGPUR

JULY 2011

© 2011 Himadri Roy. All rights reserved.

Dedicated to

My Beloved Wife
(Dolan Roy)

My Son
(Hriddesh Roy)

&

My Parents
(Mr. Tapan kumar Roy & Mrs. Rita Roy)

APPROVAL OF THE VIVA-VOCE BOARD

/ /2011

Certified that the thesis entitled **MONOTONIC AND CYCLIC FRACTURE BEHAVIOUR OF AISI 304LN STAINLESS STEEL** submitted by **HIMADRI ROY** to the Indian Institute of Technology, Kharagpur, for the award of the degree of Doctor of Philosophy has been accepted by the external examiners and that the student has successfully defended the thesis in the viva-voce examination held today.

(Member of the DSC)

(Member of the DSC)

(Member of the DSC)

(Supervisor)

(Supervisor)

(External Examiner)

(Chairman)

CERTIFICATE

This is to certify that the thesis entitled **Monotonic and Cyclic Fracture Behaviour of AISI 304LN Stainless Steel**, submitted by **Himadri Roy** to Indian Institute of Technology, Kharagpur, is a record of bona fide research work under our supervision and we consider it worthy of consideration for the award of the degree of Doctor of Philosophy of the Institute.

(Dr. S. Sivaprasad)

Scientist 'E-II'

Material Science and Technology Division
National Metallurgical Laboratory, Council
of Scientific and Industrial Research,
Jamshedpur-831 007, INDIA.

(Prof. K. K. Ray)

Professor

Department of Metallurgical and Materials
Engineering and Steel Technology Centre
Indian Institute of Technology,
Kharagpur-721 302, INDIA

Date:

DECLARATION

I certify that

- a. The work contained in the thesis is original and has been done by myself under the general supervision of my supervisors.
- b. The work has not been submitted to any other Institute for any degree or diploma.
- c. I have followed the guidelines provided by the Institute in writing the thesis.
- d. I have conformed to the norms and guidelines given in the Ethical Code of Conduct of the Institute.
- e. Whenever I have used materials (data, theoretical analysis, and text) from other sources, I have given due credit to them by citing them in the text of the thesis and giving their details in the references.
- f. Whenever I have quoted written materials from other sources, I have put them under quotation marks and given due credit to the sources by citing them and giving required details in the references.

(Himadri Roy)

ACKNOWLEDGEMENTS

I would like to express my great gratitude to my thesis advisor, **Professor Kalyan Kumar Ray**, for his guidance and encouragement during my PhD study. His instruction and support have always been a tremendous help during the preparation of this thesis. His broad and profound knowledge, his integral view on research, and his warm and encouraging smile have made a deep impression on me. It is a great pleasure and a great experience to conduct this thesis under his supervision, and I look forward to collaborate with him and expect more support in future research work. I would like to thank my advisor **Dr. S.Sivaprasad**, Scientist, CSIR-NML, Jamshedpur for encouraging me to investigate the topic of this work which I found very interesting and being a friend the most, philosopher and guide in giving me the complete working freedom. I will remain forever indebted to him for making my dream successful.

I would like to thank my DSC members **Prof. S.Ghosh**, **Prof. R.Mitra** and **Prof. B. Maity** (Mech. Engg. Deptt.), who have provided continued encouragement with critical discussions whenever required. I would also like to thank all the faculty members of Department of Metallurgical and Materials Engineering, IIT Kharagpur for their moral support. I extend my gratitude and thanks to **Dr. S. Tarafder** and **Dr. N. Parida**, both Deputy Director, CSIR-NML, Jamshedpur, for their invaluable suggestions during technical discussions, sustained interest, moral support and encouragement to carry out this investigation. My heartfelt thanks to **Prof. G. Biswas**, Director, CSIR-CMERI who continuously assessed the research work carried out by me for this thesis work. My special thanks to **Mr. A. K. Shukla**, Head, NDT & Metallurgy Group, CSIR-CMERI who helped me in every possible manner to complete my research work being in CSIR-CMERI. I would also like to express my deepest gratitude to **Dr. H.N.Bar**, **Dr. N.Narasaiah** and **Dr. J.K.Sahu**, all Scientist in CSIR-NML, Jamshedpur, for their kindness, help and support in various stages of my research work. The help rendered by **Dr. Swapan Das**, **Mr. A.Das**, **Mr. A.Metia**, **Mr. T.Chowdhury**, **Mr. S.Paul** of Material Science and Technology Division, NML is highly acknowledged.

It is my pleasure to thank all my colleagues in CSIR-CMERI, who always encouraged me pursuing research work and cheered me up at all my depressing moments. Lots of appreciations are reserved for my friends **Sharmillee**, **Subir da**, **Ayan**, **Rajdeep**, **A.Kumar**, **R.N.Jha**, **V.Toppo**, **Krishna**, **Manab**, **Anindya**, **Ashish**, **Poulami**, **Arya**, **Srijan**, **Siddhartha** and **Kaustav** for making my stay in Kharagpur, pleasant and memorable. My sincere thanks to all those who helped me directly and indirectly during my stay at Kharagpur and made it a memorable one.

Last but definitely not the least; my family has always been behind me and always been a source of support in my life. I dedicate this thesis to my son **Hrididesh (Googlu)** and wife **Dolan**. I am thankful for their patience for all these years and giving me the time and space to work on. I am indebted to my parents **Mr. T.K.Roy** and **Mrs. Rita Roy** in making me whatever I am today. I am also grateful to my in-laws **Mr. Samir Chatterjee** and **Late Mrs. Ira Chatterjee** for their moral support.

Himadri Roy

List of Symbols

Symbol	Description
a_N	Crack length up to machine notch
a	Crack length
a_o	Crack length after pre-cracking
Δa	Crack extension
b	Remaining ligament after cracking
B_{eff}	Effective specimen thickness
B_{net}	Net Specimen thickness
C	Paris Constant
C_p	Heat Capacity
C_1, C_2	Constant in J -crack extension relation
da/dN	Fatigue crack growth rate per cycle
e_t	Percentage total elongation
e_u	Percentage uniform elongation
E	Young's modulus
J_i	Fracture initiation toughness
J_{QC}	Cyclic J -integral
J_{QAE}	Conditional fracture toughness estimated using AE parameters for monotonic loading condition
J_{CAE}	Conditional fracture toughness estimated using AE parameters for cyclic loading condition
ΔJ_D	Dowling's operational J
ΔJ	Effective values of stress intensity factor ranges in terms of J
K	Stress intensity factor
K_{Ic}	Plane strain fracture toughness
K_{max}	Maximum value of stress intensity factor
ΔK	Stress intensity factor range
ΔK_o	Initial stress intensity factor range
ΔK_{eff}	Effective stress intensity factor
m	Exponent of the Paris equation
n	Strain hardening exponent
N	Number of cycles in fatigue test
N_f	Number of load cycles to failure under load controlled test

P	Load
P_{AE}	Critical load obtained during AE test for fracture toughness estimation
P_{max}	Maximum load
P_Q	Critical load for fracture toughness estimation
r_p	Plastic zone size
R	Stress ratio
T_J	Tearing modulus
V	Load line displacement
ΔV	Incremental plastic displacement
V_p	Plastic component of clip gauge displacement
W	Specimen width
W	Strain energy
γ_s	Surface energy
γ	Strain rate sensitivity
γ_{eff}	Effective surface energy for cleavage crack propagation
δ	Crack opening displacement
ρ	Density
$\partial G/\partial a$	Rate of change of elastic energy release rate
ν	Poisson's ratio
σ_0	Flow stress
σ_{ys}	Yield strength
σ_{UTS}	Ultimate tensile strength

List of Abbreviations

Abbreviation	Description
AE	Acoustic emission
AECE	Acoustic emission cumulative counts
AHWR	Advanced heavy water reactors
AISI	American iron and steel institute
ASM	American society of metals
ASME	American society for mechanical engineers
ASTM	American society for testing materials
CCL	Compliance crack length
CL	Transverse - longitudinal direction
CMOD	Crack mouth opening displacement
COD	Crack opening displacement
CT	Compact tension specimen
CTOD	Crack tip opening displacement
DIM	Deformation induced martensite
EPFM	Elastic plastic fracture mechanics
FCGR	Fatigue crack growth rate
GTAW	Gas tungsten arc welding
IPIRG	International piping integrity research group
LBB	Leak before break
LC	Longitudinal-transverse direction
LCF	Low cycle fatigue
LEFM	Linear elastic fracture mechanics
LLD	Load line displacement
LSC	Leakage size crack
NDE	Non-destructive examination
NOC	Normal operating condition
NSC	Net section collapse
PHT	Primary heat transport pipings
RA	Percentage reduction in area
SAE	Society of automotive engineers
SEM	Scanning electron microscope
SMAW	Submerged metal arc welding
SSE	Safe shutdown earthquake
SZW	Stretch zone width
UTS	Ultimate tensile strength

ABSTRACT

Fracture behaviour of AISI 304LN stainless steel and its weldment has been studied employing J -integral approach with and without superimposed cyclic load reversals in order to assess their structural integrity under simulated seismic loading condition and to compare their fracture behaviour in cyclic vis-à-vis monotonic loading. Conventional J -integral tests were carried out on specimens having notch in LC and CL configurations. Cyclic J - R experiments have been conducted (i) under displacement control with various combinations of R-ratio and incremental plastic displacement, and (ii) under load control (henceforth called *cyclic fracture tests*) for various magnitudes of monotonic peak loads. All cyclic J - R and cyclic fracture tests were carried out using specimens with LC orientation. Examinations of fracture surface and crack tip profiles have been made to understand the micro-mechanisms of fracture. In addition, acoustic emission (AE) methods were used synergistically with fracture toughness tests to detect the onset of crack initiation. Characterization of microstructures and mechanical properties like, tensile and hardness values are necessary supplements in this study.

The obtained results and their analyses lead to the following inferences: (a) microstructure of the selected steel reveals predominantly austenite whereas its weldment exhibits austenitic matrix with 12-15% δ -ferrite (b) the strength and hardness of the selected weldment are higher than that of the base metal. The results of fracture studies under monotonic loading conditions showed that (a) average fracture toughness values for LC and CL orientations are similar with J_Q values of 1107 and 1062 kJ/m² respectively and (b) fracture toughness values of weldment are almost 50% lower than that of the base metal. The cyclic fracture behaviour of the selected steels leads to the following conclusions: (a) under displacement controlled cyclic J - R tests, fracture toughness is found to degrade with (i) decrease in stress ratio from -0.5 to -1.0 and (ii) decrease in plastic displacement from 0.5 mm to 0.1 mm and (b) under load controlled cyclic fracture tests the steels are found to fail in a limited number of load cycles even when the load amplitude is sufficiently below the collapse load estimated from monotonic tests. Examination of the fracture surfaces and crack tip profiles revealed that degradation in initiation fracture toughness and their resistance to crack propagation at $R < 0$ is due to re-sharpening of the crack tip during compressive loading. Synergistic analyses of fracture test and AE results assist to demarcate the region of blunting, crack initiation and crack propagation under both monotonic and cyclic J - R tests. In generalization, it can be said that fracture resistance of the selected steels under cyclic loading is considerably lower than that obtained from monotonic J -integral experiments and the initiation fracture toughness value obtained from AE parameters provide a conservative estimate.

Keywords: AISI 304LN stainless steel; Weldment; Monotonic J - R ; Cyclic J - R ; Displacement control; Load control; Acoustic emission

CONTENTS

Subject	Page No.
Title Page	i
Certificate of Approval	iii
Certificate	iv
Declaration	v
Acknowledgements	vi
List of Symbols	vii
List of Abbreviations	ix
Abstract	x
Contents	xi
Chapter 1 Introduction	1
1.1 Objectives	3
Chapter 2 Literature review	5
2.1 Introduction	5
2.2 Fracture mechanics- an outline	5
2.2.1 LEFM vis-à-vis EPFM	5
2.2.2 CTOD parameter	6
2.2.3 <i>J</i> -integral parameter	7
2.2.4 Tearing modulus	9
2.3 Cyclic <i>J-R</i> curve	10
2.3.1 Dowling's low cycle fatigue analysis	11
2.3.2 Cyclic <i>J-R</i> curve for $R > 0$ and $R < 0$	14
2.4 Load-controlled cyclic fracture tests	19
2.5 Acoustic emission signal characterization	22
2.5.1 Principles and sources of acoustic emission	22
2.5.2 Types of acoustic emission signals	23
2.5.3 Acoustic emission during ductile fracture	23
2.6 AISI 304LN stainless steel used in nuclear power plant	26
2.7 Appraisal of the problem	29

Chapter 3	The selected steel and its characteristics	31
3.1	Introduction	31
3.2	Experimental procedure	31
3.2.1	Chemical analysis	32
3.2.2	Metallographic specimen preparation	32
3.2.3	Metallographic examination	32
3.2.4	Hardness evaluation	34
3.2.5	Tensile testing	34
3.2.6	Fractographic examination	36
3.3	Results and discussion	36
3.3.1	Chemistry, microstructure and hardness	36
3.3.2	Tensile deformation behaviour	38
3.4	Summary	56
Chapter 4	Displacement controlled fracture behavior of AISI 304LN stainless steel and its weldment	59
4.1	Introduction	59
4.2	Experimental procedure	61
4.2.1	Specimen preparation and fatigue pre-cracking	61
4.2.2	Monotonic J -integral test	63
4.2.3	Cyclic J -integral test	65
4.2.4	Generation of J - R curve under monotonic and cyclic J -integral test	69
4.2.5	Fractography	72
4.3	Results and discussion	72
4.3.1	Determination of the monotonic J -integral fracture toughness	72
4.3.2	Determination of the cyclic J -integral fracture toughness	76
4.3.2.1	Effect of stress ratio on cyclic fracture toughness	77
4.3.2.2	Effect of plastic displacement on cyclic fracture toughness	80
4.3.2.3	Determination of critical J and dJ/da under cyclic J -integral tests	82
4.3.3	Micro mechanisms of fracture in the investigated steel	85
4.4	Conclusions	90
Chapter 5	Load controlled fracture behaviour of AISI 304LN stainless steel and its weldment	91
5.1	Introduction	91

5.2	Experimental procedure	93
5.2.1	Specimen preparation and fatigue pre-cracking	93
5.2.2	Load controlled cyclic fracture tests	93
5.3	Results and discussion	94
5.3.1	Load controlled cyclic fracture behaviour of AISI 304LN SS and its weldments	95
5.3.2	Load controlled vis-à-vis displacement controlled cyclic fracture tests of AISI 304LN SS and its weldments	96
5.3.3	Master curve to account for cyclic tearing in components and in specimens	99
5.4	Conclusions	103
Chapter 6	A comparative assessment of acoustic emission and conventional load-displacement analysis for detection of crack initiation	105
6.1	Introduction	105
6.2	Experimental procedure	106
6.2.1	Acoustic emission during fracture toughness test	106
6.3	Results and discussion	108
6.3.1	Detection of the point of crack initiation by AE characteristics	108
6.3.2	Determination of fracture toughness by AE technique	113
6.4	Conclusions	120
Chapter 7	General conclusions and suggestions for future work	121
	References	125
	Curriculum Vitae	

Introduction

Stainless steel of AISI 304LN grade (hence forth referred as AISI 304LN SS) and its weldments are extensively used in primary heat transport (PHT) piping systems of advanced heavy water reactors (AHWR) of nuclear power plants. The PHT piping and pressure vessels are currently designed and operated on the basis of leak before break (LBB) concept. The LBB analysis involves careful application of fracture mechanics principles in order to ensure that stable extension of postulated cracks or flaws in piping components which usually lead to benign leakage occurs prior to the onset of unstable fracture. For implementation of LBB in structural integrity analysis of piping components, it is therefore imperative that ductile fracture characteristics of the material used for fabricating PHT piping be fully understood.

The integrity of all types of structural components specifically with the possibility of being subjected to seismic events is currently being considered as one of the critical issues in the design of nuclear power plants. The load fluctuations during seismic activity are usually random in nature. As a consequence existing cracks in an engineering component experience either tensile or compressive load amplitudes of considerable magnitudes during seismic activity and this leads to their extension or growth. In order to incorporate seismic factors in design, knowledge related to the resistance to fracture under cyclic loading conditions must be gathered for LBB analysis of piping components.

The operating temperature range of this structural component is usually 301-573 K. The pipes used in PHT system possess typically outer diameter of the order of 320 mm with wall thickness of 25 mm. So any attempt to determine plane strain fracture toughness of the material from specimens cut from this component gets limited by curved sections having maximum thickness of 25 mm. This limitation related to specimen thickness allows one to carry out only assessment of elastic-plastic fracture toughness of the steel. The J -integral fracture toughness values of a few steels having similar compositions are reported in the literature (Wilkowski *et al.*, 1990; Olson *et al.*, 1994; Rudland *et al.*, 1996), but similar toughness indices of AISI 304LN SS and its weldment at ambient temperature are not available. Hence an investigation on the J -integral fracture behaviour

of AISI 304LN SS and its weldment was a-priori directed to understand their crack growth resistance behaviour. But the existing procedures for estimating fracture resistance of materials are considered inadequate to provide reliable information related to the fracture characteristics of component-materials subjected to seismic events because of the imposed uncertain nature of cyclic deformation. A component with an allowable defect size may be safe under conventional monotonic loading but may fail in a limited number of reversible load cycles as the latter may degrade the fracture resistance of the material in a significant manner. The effect of cyclic loading on fracture resistance of materials is currently not included in the design codes to assess the integrity of the PHT piping system. This problem has been recently realized by the engineering community, and thus attempts are being directed to assess the significance of superimposed cyclic loads for safe control of structural materials.

In order to incorporate seismic factors in design, the present design codes and practices (Scott, 2003) demand understanding of the deleterious effects of load reversals during conventional J -integral tests, often referred to as cyclic J - R test. However, the concept of cyclic J - R behaviour is of recent origin. Only a few laboratories over the world have directed efforts to understand this problem till now and the available literature on cyclic J - R behaviour of structural materials is scanty. There exists controversy over the applicability of J -integral test with compressive crack tip load-excursions that necessarily take place in cyclic J - R tests. The definition of J through crack extension is theoretically considered violated by unloading even in the standard J -integral tests (ASTM E 1820, 2009); but periodic partial unloading has been accepted in favour of an engineering solution by consensus (Landes *et al.*, 1979). So cyclic J -integral tests which incorporate higher unloading to different extents would cause severe violation of the theoretical definition of J , but at the present moment an understanding related to fracture resistance with superimposed load cycles possibly would emerge through this approach only for achieving engineering solutions (Tarafder *et al.*, 2003).

The extent of deleterious effect due to superimposed cyclic load seems to depend up on the magnitude of the compressive load and the frequency of load cycle. Thus, to understand the nature of seismic effect on structural components, one must examine fracture behaviour of materials under both load and displacement controlled modes, a

discipline of current interest with extremely limited available information. The primary objective of this study is to bring forward understanding related to fracture behaviour of AISI 304LN SS under cyclic loads involving both displacement and load control modes.

In addition, determination of initiation fracture toughness of ductile materials has always been a challenging task due to the ambiguity associated with the identification of the point of departure of the initial linear region of the fracture resistance curve which is considered to correspond to the initiation of cracking in a material. Acoustic emission (AE) is a technique that is capable of directly indicating this crack initiation point during fracture toughness tests using single specimen. A corollary objective of this investigation is also to illustrate some results related to monotonic and cyclic fracture resistance of the base metal and weldment of AISI 304LN SS estimated by ‘combined acquisition of load-crack length data for J -integral analysis coupled with synergistic generation of acoustic emission data to assess the point of crack initiation’.

In summary, the objectives of this investigation encompass studies on monotonic and cyclic fracture behaviour and acoustic emission signal characteristics during the fracture tests supplemented by suitable characterizations of the microstructural aspects and determination of conventional mechanical properties.

1.1 Objectives

The major objectives and the pertinent work-plan to fulfill the objectives of this investigation can be categorized into four broad modules. These are:

Module (I) To characterize the microstructure and to determine the related mechanical properties of the selected steel.

This module consists of (a) microstructural characterization of AISI 304LN SS base metal and its weldment, (b) measurement of austenite grain size in base metal and determination of volume fraction of δ -ferrite in the weldment and (c) determination of hardness and tensile properties of the steel and its weldment at ambient temperature.

Module (II) To study the displacement controlled fracture behaviour of the steel at ambient temperature.

This module comprises of (a) generation of monotonic J - R curves of the base metal and weldment at ambient temperature, (b) examining the effect of specimen configuration

(CL and LC orientations) on the monotonic J - R curves of the base metal, (c) generation of a series of cyclic J - R curves of the steels at different test conditions, (d) investigation of the effect of stress ratio and plastic displacement on the J - R curve, and (e) examination of the micro mechanisms of crack propagation in the steels during various types of loading conditions.

Module (III) To study the load controlled fracture behaviour of the steel at ambient temperature.

This module consists of (a) examination of the number of cycles to failure of the investigated steels, and (b) comparison of the obtained results on laboratory samples with corresponding available component data.

Module (IV) Comparative assessment of acoustic emission and conventional load-displacement analysis for detection of crack initiation

This module consists of (a) examination of AE signals during monotonic J -integral test and (b) examination of AE behaviour during cyclic J -integral tests of both base metal and weldment.

All the cyclic fracture tests have been designed and performed following a few earlier investigations. Attempts have been made to assign reasons and explanations for the observed results and to illustrate the practical utility of the generated data. The thesis has been structured into seven chapters. The significance of the research and the motivation behind this investigation are briefed in Chapter-1. Some pertinent literature background related to the current investigation has been presented in Chapter-2 prior to the obtained results and their discussion. Chapter-3 to Chapter-6 includes the results and discussion corresponding to the above-mentioned four modules. An overview of the conclusions derived from this work has been summarized briefly in Chapter-7 together with some proposed future work related to this area. All references quoted throughout the dissertation have been compiled at the end of Chapter-7.

Literature review

2.1 Introduction

This chapter deals with the terminologies of linear elastic and elastic-plastic fracture mechanics in section 2.2. Various fracture mechanics parameters such as stress intensity factor (K), crack tip opening displacement (CTOD), J -integral and tearing modulus, T_J have been defined and explained in brief. The engineering need and the concepts behind development of cyclic J - R curves are discussed in section 2.3. This section incorporates an overview of available reports on cyclic J - R curves under various types of loading. The significance of acoustic emission signal analysis during fracture toughness estimation is discussed in section 2.4. Finally a basis for the motivation for the present investigation is provided in section 2.5.

2.2 Fracture mechanics- an outline

Fracture mechanics encompasses stress analysis ahead of cracks, experiments and observations to suggest useful representation of forces that cause the development and extension of cracks. The crack extension behaviour is governed by the stress field distribution ahead of a crack tip as suggested by Irwin (1957). The material, in which crack propagation is accompanied by very small or insignificant deformation, predominantly behaves in linear elastic manner. Such materials come under the purview of Linear Elastic Fracture Mechanics (LEFM). On the other hand, if the crack propagation is accompanied by large plastic deformation, Elastic Plastic Fracture Mechanics (EPFM) approach is adopted to describe the crack driving forces ahead of a crack tip in the material.

2.2.1 LEFM vis-à-vis EPFM

The principle of linear elastic fracture mechanics (LEFM) is based on the unique distribution of stress ahead of a crack in a body under load. The amplitude of such a distribution is characterized by the stress intensity factor K , a critical value of which provides the driving force for existing cracks to propagate. The solution of the stress field ahead of a crack using linear elasticity can be given as:

$$\sigma_{ij} = \frac{K}{\sqrt{2\pi r}} f_{ij}(\theta) \quad \dots (2.1)$$

where, (r, θ) represent polar co-ordinates around the crack tip and $f_{ij}(\theta)$ are characteristic functions. The elastic stress field solution indicates the presence of a stress singularity at the tip of a crack. However in practice, most materials exhibit a yield stress above which these deform plastically. As a result there exists a region around the crack tip, which is plastically yielded. This region is called the plastic zone (PZ). The plastic zone size for a material with yield strength σ_{ys} is given as:

$$r_p = \frac{1}{n\pi} \left(\frac{K}{\sigma_{ys}} \right)^2 \quad \dots (2.2)$$

where the magnitude of n depends on the state of stress.

The employment of LEFM remains valid as long as the size of plastic zone is significantly small in comparison to the dimensions of the cracked geometry. In materials where the size of the plastic zone is large, fracture conditions are controlled by elastic-plastic fracture mechanics (EPFM). EPFM often uses the concept of non-linear elasticity to obtain solutions for equivalent plastic problems. Unlike LEFM, EPFM demands a careful understanding of the crack tip plasticity and currently this discipline provides a few established procedures for obtaining fracture criteria. These are: (i) Crack tip opening displacement (CTOD), (ii) J -integral and (iii) Tearing Modulus T_J .

2.2.2 CTOD parameter

Wells (1961) proposed that the failure of a cracked component can be characterized by the opening of the crack faces in the vicinity of a sharp crack tip known as crack tip opening displacement (CTOD). He showed that the concept of crack opening displacement was analogous to concept of critical crack extension force and thus the CTOD values could be related to the plane-strain fracture toughness, K_{IC} . Because CTOD measurements can be made even when there is considerable plastic flow ahead of a crack, such as would be expected for elastic-plastic or fully plastic behaviour, the technique may be used to establish critical design stresses or crack sizes in a quantitative manner similar to that of linear-elastic fracture mechanics.

Dugdale's strip yield model analysis (Dugdale, 1960) relates CTOD to the applied stress and the crack length as given below:

$$\delta = \frac{8\sigma_{ys} a}{\pi E} \left[\ln \left(\sec \frac{\pi a}{2\sigma_{ys}} \right) \right] \quad \dots (2.3)$$

where,

δ = crack tip opening displacement

σ_{ys} = yield stress, a = crack length,

σ = the applied stress and E = the elastic modulus

At $\sigma / \sigma_{ys} \ll 1$, at the crack instability the above expression can reduce to

$$\delta_{IC} = \frac{K_{IC}^2 (1 - \nu^2)}{\lambda E \sigma_{ys}} \quad \dots (2.4)$$

2.2.3 *J*-integral parameter

The path independent *J*-integral proposed by Rice (1968) can be used to characterize the stress-strain fields at the tip of a crack and to analyze the fracture process in elastic-plastic materials. *J* can be computed by an integration path taken sufficiently far from the crack tip to be substituted for a path close to the crack tip region. Thus, even though considerable yielding occurs in the vicinity of a crack tip, the behaviour of the crack can be inferred by considering a region away from the crack tip for the analysis. This technique can be used to estimate the fracture characteristics of materials exhibiting elastic-plastic behaviour. For linear elastic behaviour, the *J* integral is identical to *G*, the energy release rate per unit crack extension. Therefore *J* failure criterion for the linear-elastic case is identical to the K_{IC} failure criterion. For linear elastic plain-strain conditions,

$$J_{IC} = G_{IC} = \frac{1 - \nu^2}{E} K_{IC}^2 \quad \dots (2.5)$$

The energy line integral, *J* is defined for either elastic or elastic-plastic behaviour as follows

$$J = \int_{\tau} \left(W dy - T_i \frac{\partial u_i}{\partial x} ds \right) \quad \dots (2.6)$$

where, $W = \int_0^{\epsilon} \sigma_{ij} d\epsilon_{ij} = \text{Strain energy density} \quad \dots (2.7)$

$T_{ij} = \sigma_{ij} n_j = \text{Vector of surface tractions,}$

$u_i = \text{Displacement vector,}$

$s = \text{Element of arc length along contour } \Gamma .$

For any linear elastic or elastic plastic material treated by deformation theory of plasticity, Rice (1968) had shown path independence of the J integral parameter. The J integral can be interpreted as the potential energy difference between two identically loaded specimens having slightly different crack lengths i.e., a and $a+da$. The energy parameter J is given as,

$$J = -\frac{1}{B} \frac{\partial u}{\partial a} \quad \dots (2.8)$$

The definition is shown schematically in Fig. 2.1 where the shaded area is $\partial u = JB\partial a$. Begley and Landes (1972) developed compliance technique for evaluating J -integral, which made the fracture mechanics parameter more popular in comparison to other fracture mechanics parameters. Standard test procedure for determining the fracture toughness of the ductile materials in terms of J -integral has been developed and incorporated in ASTM standard E 1820-09 (2009). Generally compact tension, C(T) and single edge notch bend, SEN(B) specimens are used for J -integral testing of materials.

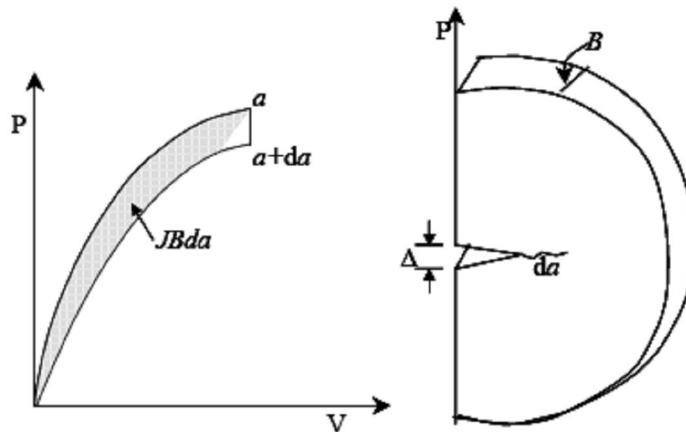


Fig. 2.1 Interpretation of J -integral

2.2.4 Tearing modulus

Materials having good ductility show appreciable plasticity at fracture and usually undergo slow and stable crack growth before fracturing. Thus, the crack will start growing at a critical value, J_{IC}/J_C , and hence it is useful to quantify the onset of fracture. But further increase of stress is required to sustain the crack growth. Apparently the crack resistance increases with crack growth, which is reflected in a higher value of J -integral. The crack resistance curve is called as R curve, J_R curve or J - R curve. Thus the criteria for stable crack growth can be written as

$$J = J_R \quad \dots (2.9)$$

fracture instability will occur when

$$J \geq J_R \quad \dots (2.10)$$

on differentiation

$$\frac{dJ}{da} \geq \frac{dJ_R}{da} \quad \dots (2.11)$$

In high toughness materials crack initiation is not the only relevance but propagation stage is also important, and it will have considerable lifetime left after the crack initiation. Therefore greater attention is now being focused on the investigation of both crack initiation and propagation behaviour of the materials. This has prompted several investigators to study the stability of crack growth based on the concept of J integral resistance curves.

Paris *et al.*, (1970) have proposed a dimensionless form for the crack growth resistance parameter. It has been denoted by T_J and is called as tearing modulus.

$$T_J = \frac{E}{\sigma_0^2} \frac{dJ}{da} \quad \dots (2.12)$$

where,

E = Elastic modulus of the material,

σ_0 = Flow stress of the material.

This parameter offers a convenient definition for crack growth toughness based on the J integral approach. Here dJ/da is the slope of J - Δa resistance curve in the stable crack growth region.

Thus the applied instability criterion is:

$$T_{\text{applied}} > T_{J \text{ material}}$$

Hutchinson and Paris (1979) have suggested that the assumption of J controlled crack growth is valid when the following conditions are fulfilled

$$\omega = \frac{b}{J} \frac{dJ_R}{da} \gg 1 \quad \dots (2.13)$$

$$\text{and} \quad a < 0.06b$$

for C(T) specimens, the value of ω may not be less than 10.

2.3 Cyclic J - R curve

The integrity of components during seismic events is one of the critical issues in the design of nuclear power plants. The load fluctuation during seismic activity may be random, with postulated cracks and flaws experiencing tensile as well as compressive loads of high magnitudes leading to their extension or growth far from the conventional fracture resistance (J_{IC}) determined under monotonic loading conditions. In order to incorporate seismic factors in design, the present design codes and practices (Scott, 2003) demand understanding the deleterious effects of load reversals during monotonic tensile loading. However, the concept of cyclic J - R behaviour is of recent origin. Only a few international laboratories have worked on this problem and the available literature on cyclic J - R behaviour of materials is scanty. Mogami *et al.* (1990) have first proposed cyclic J -integral tests to simulate the deleterious effects of periodic load reversals. But there exists controversy over the applicability of the J -integral to compressive crack tip load-excursions that take place in such tests. The definition of J through crack extension is theoretically considered violated in the standard J -integral tests (ASTM E 1820-09, 2009); but periodic partial unloading has been accepted in favour of an engineering solution by consensus (Landes *et al.*, 1979). Thus an understanding can be considered likely to emerge with respect to cyclic J -integral (Tarafder *et al.*, 2003).

Engineering components can be subjected to a wide variety of service loads and should be designed to operate safely under all such variations. The safety assessment for monotonic loading can be achieved using the concepts of K_{IC} , J_{IC} , or δ_c ; under fatigue loading it can be achieved using Paris law (Paris and Erdogan, 1963). This law is expressed as:

$$da/dN = C(\Delta K)^m \quad \dots (2.14)$$

where,

da/dN = crack growth rate of the material per cycle,

ΔK = applied elastic stress range

C and m are material constants.

When an engineering component is subjected to monotonic loading with intermittent cycling, neither the conventional monotonic fracture toughness values nor the Paris law constants are sufficient to predict its safe operating margins with reliability. This situation is not a mere hypothesis, but is documented by a Japanese group who recorded severe extent of load reversals on engineering components during a seismic event (Miura *et al.*, 1994). This aspect has been of serious concern for several critical engineering components like that in nuclear power plants. As a consequence attempts are being made over the last two decades to understand cyclic J - R curves.

2.3.1 Dowling's low cycle fatigue analysis

Dowling and Begley (1976) were the first to employ the J integral parameter in place of linear-elastic stress intensity factor, ΔK for cyclic crack growth. The cyclic J is evaluated by integrating the load-displacement data for each individual cycle. However, the integration is applied to the area DBCD as in Fig. 2.2, against the conventional understanding of J (area EBF E). The point 'D' in the schematic diagram is derived from the analysis of crack closure. Owing to the reversed plasticity during the part of a cycle having compressive load, the crack tip does neither experience any tensile load, nor opens fully, till a significant magnitude of the load is acquired during reload part of the cycle. The Dowling's ΔJ is referred to as an operational J value and it is a modification of the

classical J integral parameter. The Dowling's ΔJ methodology enables one to handle reverse loading, but the data analysis is complicated. This method needs the complete load-displacement data and information about crack closure during each cycle.

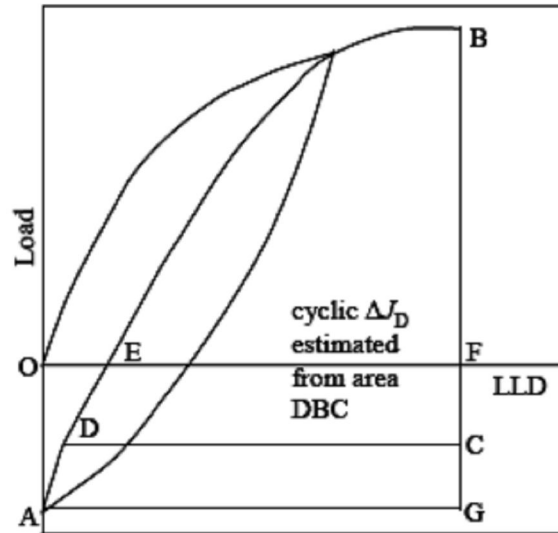


Fig. 2.2 Dowling's operational definition of cyclic J (Dowling and Begley, 1976)

Dowling's operational J has been denoted as ΔJ by Dowling and Begley (1976) and was followed by several other researchers. The ΔK in LEFM regime of FCGR is usually converted to ΔJ through the relation $\Delta J = (\Delta K)^2/E$, to obtain da/dN data in terms of ΔJ . The ΔJ as discussed by Dowling will henceforth be denoted as ΔJ_D in further discussion to avoid any confusion. Landes and McCabe (1983) have also analyzed the load-displacement data using Dowling's method. The results reported by these authors showed that da/dN vs. ΔJ_D data for HY130 steel do not fall on the extrapolated line of da/dN vs. ΔJ data converted from ΔK , as shown in Fig. 2.3. Crack growth is 5 to 15 times higher than the values of extrapolated fatigue data. The behaviour of HY130 steel was labelled as R-curve dominated crack growth. The da/dN vs. ΔJ_D plot for this steel falls within and near the da/dN vs. ΔJ data converted from ΔK as given in Fig. 2.4. This suggests that a majority of crack growth occurred due to cyclic component of loading rather than monotonic component, labelled as cyclic dominated crack growth. A strong cyclic crack growth effect was observed for A508 class 2 steel by Mogami *et al.* (1990). The difference in cyclic J - R curves of these two steels has been attributed

(Mogami *et al.*, 1990) to the differences in contribution of cyclic and monotonic components to the resultant crack growth.

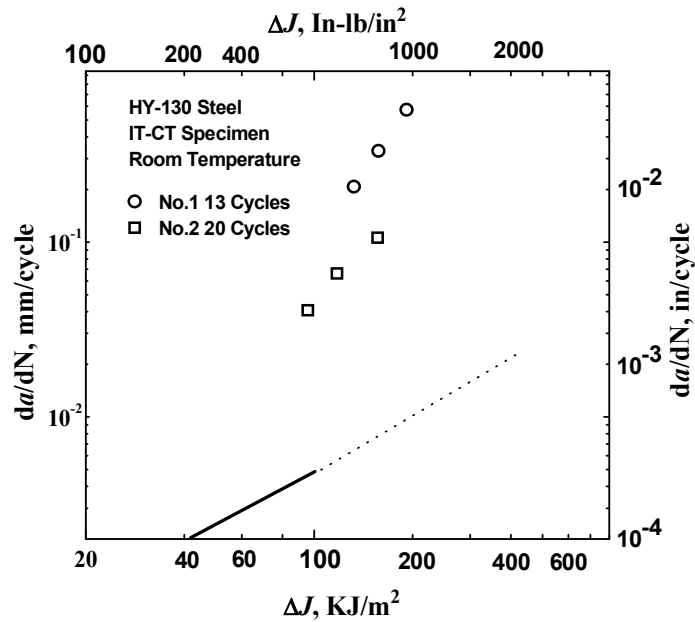


Fig. 2.3 da/dN vs. ΔJ for HY-130 steel loaded cyclically and compared with da/dN data on HY-140 (redrawn from the work of Landes and McCabe, 1983)

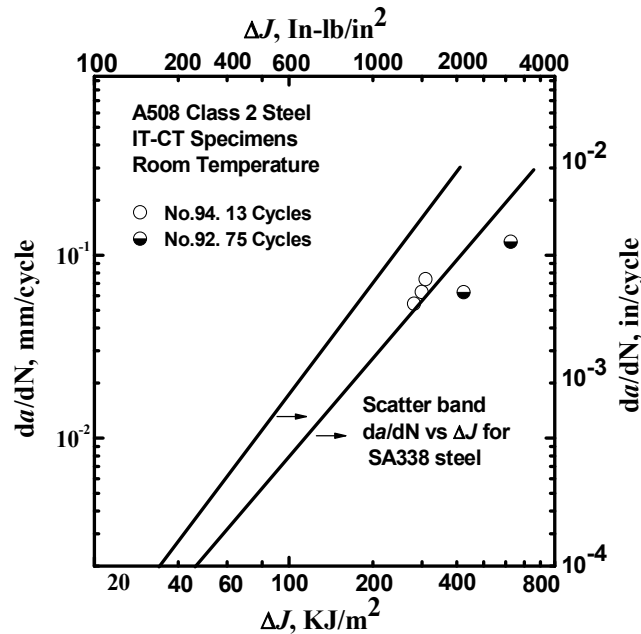


Fig. 2.4 da/dN vs. ΔJ for A508 Class 2 steel loaded cyclically and compared with da/dN data on A533B grade steel (redrawn from Mogami *et al.*, 1990)

Dowling's ΔJ_D analysis when applied to 4340 steel, Landes and Liaw (1987) have observed da/dN data to fall above the upper boundary of the extrapolated FCGR data obtained in LEFM regime. The crack growth rate is higher than what can be predicted from da/dN vs. ΔK plot. These investigators (Landes and Liaw, 1987) made an attempt to develop a model through a linear combination of monotonic and cyclic components of crack extension. It was observed that the summation rule works well in both the loading conditions for a few initial cycles. After that, the Δa obtained experimentally was reported to be larger than the Δa evaluated from linear summation of monotonic and cyclic components.

The cyclic crack growth resistance of a material depends significantly on the R ratio. The compatibility of cyclic and monotonic crack resistance is sensitive to test conditions. Attempts to obtain cyclic crack extension in terms of monotonic crack growth plus fatigue crack growth are shrouded with controversy.

2.3.2 Cyclic J - R curve for $R > 0$ and $R < 0$

The detailed review on cyclic J - R curve has been earlier carried out by Marshall and Wilkowski (1991) and later on by Prabha (2004). It has been observed that cyclic J - R curves of engineering materials may be divided broadly into two categories viz., tests conducted with a load ratio, $R \geq 0$ and $R < 0$. Clark et al. (1976) in their attempt to establish a single specimen partial unloading technique for fracture toughness determination imposed partial unloadings upto 10% of maximum load on CT specimens. These partial elastic unloadings were used for calculating (intermittently) crack lengths and J - R curves, developed for CT specimens of thickness ranging from 12.7 mm to 127 mm (0.5 to 5 inches). The J - R curves were observed to be identical for small crack extensions in all specimen sizes. The slopes of J - R curves change for different specimen sizes at large crack extensions. It was concluded by these authors that partial unloadings ($R > 0$) do not alter J - R -curves of materials as long as the process zone to plastic zone size ratio remains within a limit. Similar findings were also reported by Joyce (1988). He confirmed that unloading up to 50% of P_{max} during J - R tests on specimens of 3% Ni structural steel has no effect on fracture initiation toughness of the material. However, unloading upto 100% of P_{max} lowers the fracture toughness of the same material. Several other investigators

(Kaiser, 1983; Kobayashi *et al.*, 1992; Mogami *et al.*, 1990; Joyce, 1990) support the observations that the difference between J - R curves obtained at $R = 0.5$ and $R = 0$ (unloading of 50 and 100% of P_{\max} respectively) is insignificant.

Kaiser (1983) investigated two steels, one pressure vessel steel and another quenched and tempered structural steel, of yield strength 375 and 750 MPa respectively. The tests for crack growth resistance were carried out by Kaiser, in displacement control with constant increase in total displacement during each cycle. It was observed by the author that as the incremental displacement decreases, the slope of the J - R curve also decreases, and for the smallest displacement, the slope is minimum. For the large plastic displacements there were only 20 unloadings, whereas for smaller displacements there were more than 100 unloading cycles. The effect of cycling was very pronounced for small incremental displacement (0.74 μm) and the slope of J - R curve was only 5% of that of the monotonic J - R curve. This implies that certain amount of crack growth takes place in each cycle that can be estimated by Paris law given by eqn. (2.14). Assuming the total crack extension to be linear summation of “crack growth due to fatigue” and “monotonic crack extension”, it follows that:

$$\frac{da_{total}}{dN} = \frac{(da_{fatigue} + da_{tearing})}{dN} \quad \dots (2.15)$$

$$= \frac{da_{fatigue}}{dN} + \frac{da_{tearing}}{dN} \quad \dots (2.16)$$

we know that

$$\frac{dJ}{da} = \frac{T_J \sigma_{YS}^2}{E} \quad \dots (2.17)$$

where T_J = Tearing modulus,

Equation (2.17) can be written as,

$$da_{plastic} = \frac{EdJ}{T_J \sigma_{YS}^2} \quad \dots (2.18)$$

and $da_{fatigue}$ can be written as,

$$\frac{da}{dN} = C_1 (\Delta J_{fatigue})^{m_1} \quad \dots (2.19)$$

where, C_1 and m_1 are constants derived from Paris law;

Substituting this in equation (2.16) one can get,

$$\frac{da_{total}}{dN} = C_1 (\Delta J_{fatigue})^{m_1} + \frac{EdJ_{pl}}{T_J \sigma_{YS}^2} \quad \dots (2.20)$$

A comparison of values obtained from experimental data of a vs N curve and those calculated from eqn. (2.20) showed a good agreement. When the number of cycles imposed is of the order of 20, the unloadings up to 90 to 100% do not result in any apparent cyclic crack extension and the J - R curves remain unaltered. An exception to this observation was reported by Joyce and Culafic (1988) for ASTM designation A710 grade A class 3 steel having σ_{YS} and σ_{UTS} of 643 and 732.3 MPa, respectively. They concluded that if R ratio is small, the cyclic loading appeared to have little effect on the subsequent tearing resistance, but if R ratio was decreased the subsequent tearing resistance was also decreased.

Landes and MaCabe (1983) were the first to investigate the fracture behaviour under compressive cyclic loading. The investigations by Landes and MaCabe are on HY130 and A 508 steel using 1 inch thick compact tension (CT) specimens. A schematic representation of different load histories applied to the specimens by these workers is shown in Fig. 2.5. The study employed two methods of estimating J -integral. Landes and MaCabe (1983) determined J from the positive area under the load displacement curves and compared with the scatter band of the monotonic J - R curves of the material. In the case of HY-130 steel, the developed J - R curve remained well within the scatter band of the monotonic J - R curve for both the displacement levels. However, A508 steel exhibited different nature in comparison to HY-130 steel. The J - R curves of A508 steel is reported to lie well within the monotonic J - R curve scatter band for the case of larger incremental displacement. For smaller displacements, where the specimen is subjected to five times more number of cycles, J - R curve was reported to fall much below the monotonic J - R curve scatter band. The initiation toughness J_{IC} was reported lower for the specimen that

experienced more number of cycles for A508 steel. An attempt has been made to model the extent of crack growth by linear summation. No convincing explanation has been provided for the above observations by the investigators (Landes and MaCabe, 1983). In another report by Landes and Liaw (1987), the effect of cyclic loading under negative R ratio on fracture toughness of modified 4340 steel has been discussed. The material was quenched and tempered to yield strength of 1041 MPa (151 Ksi). Standard 1CT specimens were tested by these investigators for both ratcheting loads and elastic dominance loads (as shown in Fig. 2.5). In elastic dominance loading a progressively increasing maximum displacement is provided during each cycle and unloaded to zero displacement levels. This type of tests simulated the case where the elastic boundary had such a large effect that the material always returns to starting strain level upon unloading. It has been observed by the authors (Landes and Liaw, 1987) that the resistance to crack propagation is inferior in the case of cyclic loading in comparison to monotonic loading. The linear summation model of cyclic crack growth did not hold good for compressive cyclic loading in the case of modified 4340 steel.

Mogami *et al.* (1990) also investigated the effect of complete cyclic reversal load on ASTM A508 class 2 and STS 42 steels. The authors have commented that cyclic J_{max} -R curve is lower than monotonic J -R curve but falls back on monotonic J -R curve for large crack extensions. They observed that cyclic J -R curve for a cyclic load of a high level, in which fatigue crack growth rate was around 0.1mm/cycle, nearly coincided with monotonic J -R curve. But cyclic J -R curve is reported to be placed lower than the monotonic J -R curve if unloading is started at lower J level, when fatigue crack growth rate was less than 0.1mm/cycle. To characterize fatigue crack growth aspects, the authors proposed an equation as given below

$$\frac{da}{dN} = C \left(\frac{\sqrt{\Delta J}}{\left(B - \sqrt{\Delta J_{\max}} \right)} \right)^m \quad \dots(2.21)$$

Joyce and Culafic (1988) concluded that the cyclic J -R curve tests under COD control do not show significant effect on the ductile tearing toughness for A710 grade A steel. It was also shown (Joyce and Culafic, 1988) that increasing the ductile tearing step in each cycle

improves the resistance but this is always lower than the base line monotonic J - R curve for the steel investigated. Kobayashi *et al.* (1992) have observed in the case of a 2.5Cr-Mo steel, that the J - R curve for R ratio of -1.5 falls below monotonic J - R curve and exhibits increased crack extensions.

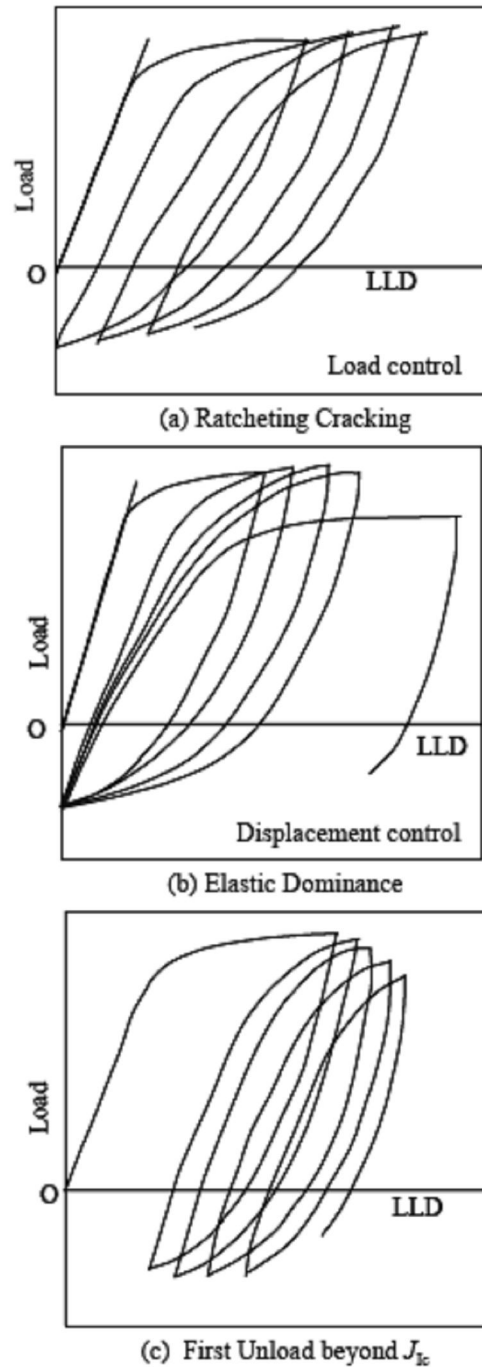


Fig. 2.5 Type of load histories used for developing cyclic R -curves by (Landes and MaCabe, 1983)

Rudland *et al.* (1996) have reported, for AISI 304 SS and A106 grade. B plain carbon steel, that the fracture initiation toughness and the resistance to crack propagation decrease with decrease in stress ratio as well as decrease in plastic displacement. The effect of cyclic loading on J - R curve saturates at a stress ratio of -0.8 and -1.0 for A106 steel and 304 SS, respectively. Seok *et al.* (1999, 2000) investigated the effect of reversed loading on the fracture resistance of SA 516 grade 70 steel. They also reported that cyclic J - R curves fall below the monotonic J - R curve. Pronounced effect of decreasing R and decreasing incremental plastic displacement on lowering J - R curve are similar to the conclusions drawn by Joyce (1990). On the basis of stress analysis, it was reasoned by Seok and Murty (2000) that considerable amount of residual tensile stress remains ahead of the crack tip when the load becomes zero (at position 4, as shown in Fig. 2.6) at the end of each cycle. Thus in the next cycle when the specimen is being loaded, crack tip opens up at a lower load level due to the additional residual tensile stress resulting in lowering of J - R curves. It was also shown that the stresses at the end of loading (position 3 in Fig. 2.6) are compressive in nature and at position 4 only tensile residual stresses prevail. So there must be some point in between positions 3 and 4 where residual stress is zero. It is reasoned that the particular load level at which the residual stresses are zero should be taken for calculating operational J .

2.4 Load-controlled cyclic fracture tests

The fracture analysis of nuclear power plant pipes considers the seismic loading as a one time applied load of magnitude equal to peak load at the postulated flaw location during the earthquake event. The assessment of pipe with flaw (or crack) is based on the monotonic tearing instability or net section collapse (NSC). There is no explicit consideration of the cyclic damage or the number of applied load cycles. During a typical earthquake event, nuclear power plant piping experiences around 10–20 cycles of large amplitude reversible loads. It is a well-known fact that the reversible cyclic loading significantly accelerates the fracture process due to the cumulative damage by the compressive plasticity (i.e., void flattening and crack tip resharping) and low cycle fatigue crack growth (fatigue crack growth under large scale yielding). As a result of

combined damage, there is a significant decrease in the apparent fracture resistance of the material under reversible cyclic loading when compared to monotonic loading. Unlike monotonic fracture, in cyclic fracture the instability depends on the full load history and parameters such as loading ratio, loading range, and number of load cycles. A cracked component, which is safe under monotonic load, may fail in a limited number of reversible cyclic loads of the same amplitude. Hence, for a realistic assessment of LBB, cyclic tearing should be considered.

There are limited experimental investigations on the fracture behaviour of steel under superimposed cyclic loading with the use of load control mode. Unlike displacement control test, one examines the number of cycles to failure in load-control test to understand the fracture behaviour of structural materials. Miura *et al.* (1994) were pioneers to examine the effect of loading pattern during crack growth rate on circumferential through-wall cracked pipes. He made three different kinds of tests under load control; (a) constant cyclic loading tests, (b) incremental-cyclic-loading tests and (c) random-cycle-loading tests.

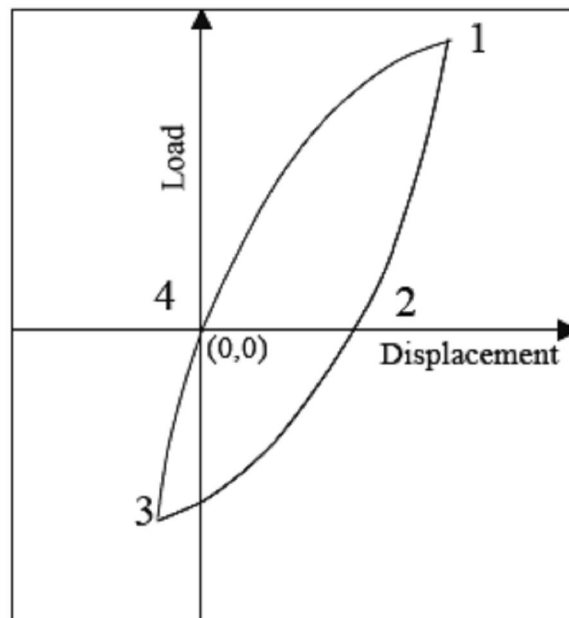


Fig. 2.6 Hysteresis loop during cyclic loading (Seok and Murthy, 2000)

Schematic plots of these load controlled tests are shown in Fig. 2.7. For the constant-cyclic-loading tests, the load amplitude is controlled to about 60-100% of the plastic collapse load predicted by using the flow stress in the quasi-static tensile tests. For the incremental-cyclic-loading tests, the load amplitude is controlled so that it increases cycle by cycle at a rate of 19.6 and 1.96 kN cycle⁻¹ (Miura *et al.*, 1994). For the random-cycle-loading tests, the load amplitude is controlled so as to be proportional to the seismic acceleration record; the maximum peak load is controlled to be 90% of the predicted plastic collapse load.

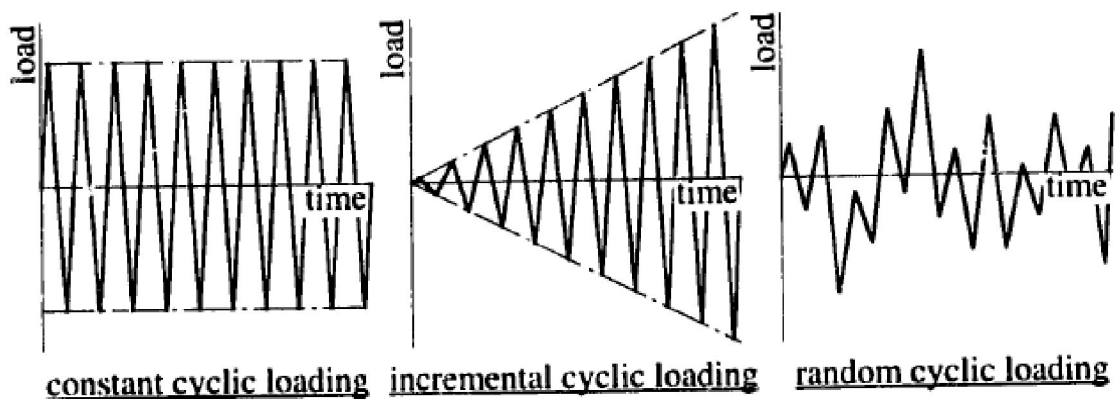


Fig 2.7 Schematic plots of various load controlled cyclic fracture tests (Miura *et al.*, 1994)

Gupta *et al.* (2007) have carried out both displacement and load control cyclic tests on SA333 Grade 6 steel during full scale pipe testing. These investigators have reported that the number of cycles for failure in load control tests depends on load amplitude, load ratio and initial crack length like that in tests related to fatigue crack growth rate (FCGR); but in displacement control mode the number of cycles to attain the peak load is dependent on displacement increment in each cycle. The state of the art related to fracture behaviour of steel under superimposed cyclic loading unambiguously indicates the deleterious effect due to imposition of compressive load cycles. The extent of such deleterious effects depends up on the magnitude of the compressive load and the frequency of load cycle. Thus to understand the seismic effect on structural components, one must examine fracture behaviour of materials under both load and displacement controlled modes, a discipline of current interest with extremely limited information.

2.5 Acoustic emission signal characterization

A large number of international standards on determining fracture toughness of structural materials are currently available, some of which have been discussed in earlier sections. These standards suggest procedures for estimating fracture resistance of materials using analysis of load–displacement plots. Acoustic emission (AE), on the other hand, is capable of indicating directly the crack initiation point during loading of a specimen. For exploiting this potential of AE, several investigators have carried out conventional fracture toughness tests in liaison with AE technique; but so far no generalized guideline has emerged out from this type of ‘combined’ experiments. The primary objective of this section is to review all the major investigations related to fracture toughness values of ductile materials estimated by these ‘combined type’ experiments in order to suggest a guideline.

2.5.1 Principles and sources of acoustic emission

Acoustic emission or stress wave emission is defined as the class of phenomenon where transient elastic waves are generated by rapid release of energy from localized sources within a material. Such emission occurs as a release of a series of short impulsive energy packets. The energy thus released travels as spherical wave front and causes minute atomic displacement as it reaches the surface of the material. Highly sensitive transducers detect this mechanical displacement and convert it into electrical signals. The electrical signal which on amplification, and subjected to suitable processing and analysis can reveal valuable information about the source causing the energy release. A schematic diagram of AE generation due to change in force field that causes the field to propagate as a mechanical disturbance throughout the structure is shown in Fig. 2.8.

The sources of AE may include various mechanisms of deformation and fracture. The major sources that have been identified in metals and alloys include movement of dislocations and grain boundaries (Heiple and Carpenter, 1983; Wadley and Mehrabian, 1984), formation and growth of twins (Heiple and Carpenter, 1987), decohesion and fracture of inclusions (Heiple *et al.*, 1990), corrosion (Mazille, 1995) and phase transformation (Speich and Schwoeble, 1975). There are also secondary or pseudo sources of AE, which includes leaks and cavitations, friction, realignment and growth of

magnetic domains (Berkhausen effect), solidification and solid-solid phase transformations.

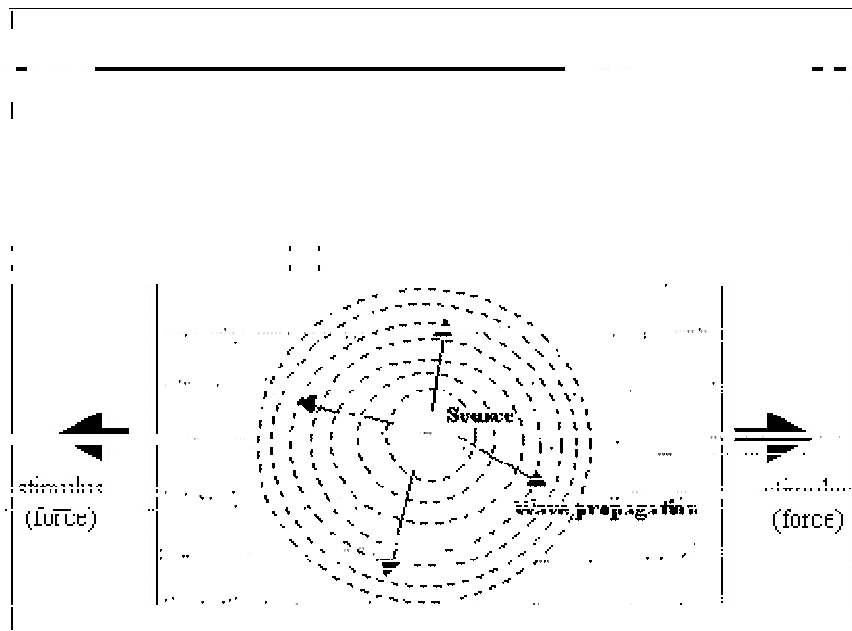


Fig. 2.8 Schematic diagram of AE generation due to force field change in a structure

2.5.2 Types of acoustic emission signals

Acoustic emission signals have been conventionally separated into burst-type and continuous-type emission. If the signal consists of pulses detectable from background noise and well separated in time so that there is not much of overlapping, then the emission is called burst-type emission. This is shown in Fig. 2.9. If resolution of individual pulses is not possible, then the emission is called continuous emission. A typical continuous emission signal has been shown in Fig. 2.10. "Burst" type refers to nature of signals which depicts fast rise /slow decay. The formation and propagation process of cleavage microcracks and intergranular microcracks in metals and alloys are the sources of burst-type of acoustic emission. It is in contrast to the continuous emission signals from leaks and plastic deformation in metals.

2.5.3 Acoustic emission during ductile fracture

The relationship between the growth of ductile cracks and acoustic emission has been studied extensively over the years. It has been shown that in some circumstances

(Takahashi *et al.*, 1981; Clarke and Knott, 1977) it is possible to detect the initiation of ductile cracking in laboratory specimens. Clark and Knott (1977) have used acoustic emission to detect the initiation of ductile cracks in a pressure vessel material using commercially available acoustic emission equipment.

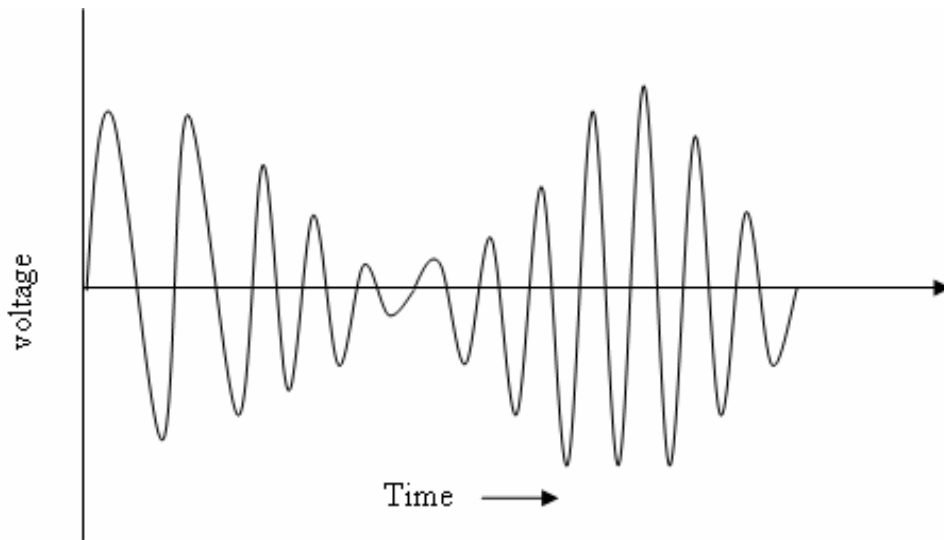


Fig. 2.9 Schematic diagram of a burst type emission

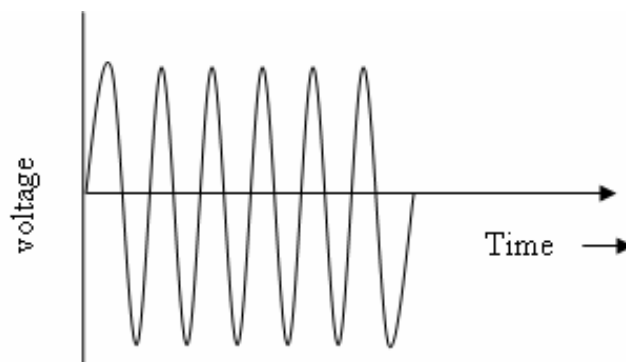


Fig. 2.10 Schematic diagram of a continuous type emission

The first appearance of high amplitude signals were attributed to the crack extension processes involving the rapid shear linkage of growing voids. A study of the acoustic emission behaviour of A516-70 steel (Blanchette *et al.*, 1983) has shown that acoustic emission is well suited to the detection of general yielding. It was found that the major

acoustic emission activity occurs during the process of formation of the plastic zone and ends at the load corresponding to general yielding of the untorn ligament. Figure 2.11 shows typical acoustic emission count rate curves from both tensile and fracture tests as a function of strain and displacement respectively for A516-70 steel. In the tensile test acoustic emission activity reaches a maximum at about the yield strength of the material. The plastic zone, especially after the Luders strain, is characterized by a lack of strong acoustic activity. In the fracture test, the acoustic emission count rate reaches a maximum near the point of deviation from linearity on the load-load point displacement curve, and is followed by a decrease in emission before the load reaches a maximum value. Similarly, acoustic emission technique has been used to detect the initiation of ductile crack extension in AISI 4340 and SA533B steels (Takahashi *et al.*, 1981). A clear indication of the onset of a stable crack extension is provided by a significant change in slope of the summation of acoustic emission energy vs. J curve. Experimental results for AISI 4340 and SA533B steels demonstrate that acoustic emission method is capable of providing quantitative information on the relative size of the cracks that extend beyond the size of those initially detected. Arii *et al.*, (1975) has monitored acoustic emission during the COD test of different steels. The relation between the total acoustic emission (AE) counts, N , and the crack opening displacement, δ which represents the deformation behaviour of a notched specimen, was studied and the following relation obtained

$$N = c\delta^n, n=2 \quad \dots (2.34)$$

following the model proposed by Dunegan *et al.* (1968). C and n in this equation are material constants. The AE counts, N as a function of COD, δ have been shown in Fig. 2.12. The results in Fig. 2.12 show that there are two distinct region; region I with small exponent, n and region II with considerably larger n . The plot shows that $COD(\delta_{AE})$, defined above corresponds to the COD at the point of transition from region I to II. In another instance (Camerini *et al.*, 1992) crack tip opening displacement (CTOD) tests were conducted and the acoustic emission were simultaneously monitored which enabled a correlation to be established at any moment between the acoustic behaviour ahead of the crack tip and its CTOD value. It was found that the CTOD value corresponding to the first detectable acoustic emission from the loaded crack tip is lower than the CTOD for initiation of stable crack propagation. Acoustic emission was also

monitored during J -integral tests of SA333 steel (Parida *et al.*, 1999) using single edge notch bend (SENB) specimens in L-T orientation. The results of Parida *et al.* (1999) show that three AE parameters, namely the peak amplitude, the energy rate and the count rate, are required to be used in a combined manner to study the fracture processes in steel. Acoustic emission during fracture toughness tests of high toughness Ni-Cr-Mo-V steel has been studied by Dal Re (1986) and it has been reported that AE generated during early stage of deformation is due to the formation of plastic zone at the crack tip; reduced AE activity at intermediate deformation regions and high AE activity during macro crack propagation are reported. Masounave *et al.* (1976) have suggested a correspondence amongst the acoustic emission, formation of contraction zone at the crack tip and deviation from linearity in the load-load point displacement curve of a notched specimen. The relationship between N and K_I proposed by these investigators also takes into account the plastic deformation and is of the form given by Dunegan *et al.* (1968). It has been reported by these investigators that their formulation predicts a value of 11 for m when K is not corrected for plasticity at the crack tip and is equal to 7 after correcting K . Masounave *et al.* (1976) have examined the AE counts generated during deformation of fatigue pre-cracked specimens of a tool steel and have found good agreement between their theoretical and experimental results. Mashino *et al.* (1996) have also obtained good correlation between fracture toughness values obtained from acoustic emission and that obtained from conventional ASTM procedure for Ti-8Al-1Mo-1V.

In brief it can be concluded that acoustic emission (AE) technique can provide a more reliable detection process for the load at which crack initiation occurs. The AE technique is well matured as a system for continuously monitoring structures in service as a NDE tool, but this method has limited applications in measuring crack initiation during fracture of ductile materials; the limitation is primarily due to the fact that initiation and growth of cracks in elastic plastic materials are found to be a relatively silent process (Blanchette *et al.*, 1983).

2.6 AISI 304LN stainless steel used in nuclear power plant

304LN stainless steel is an austenitic grade in the family of stainless steels. These steels have become versatile because of combination of the following properties: (a) good corrosion and oxidation resistance, (b) good creep strength, (c) high ductility and

formability, (d) high resistance to scaling and oxidation at elevated temperatures, (e) wide range of strength and hardness, (f) good weldability and machinability and (g) good low temperature properties as austenitic stainless steels do not undergo ductile/brittle transition.

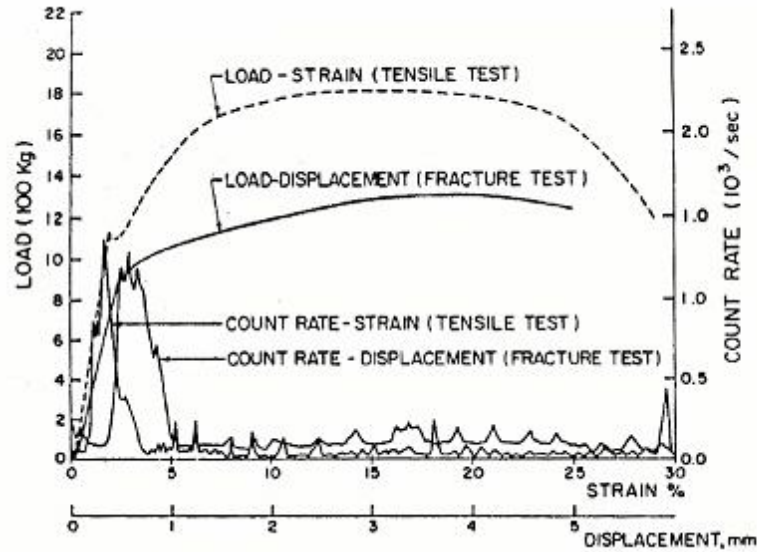


Fig. 2.11 Acoustic emission count rate from both tensile test and fracture test in A516-70 steel (Blanchette et al., 1983)

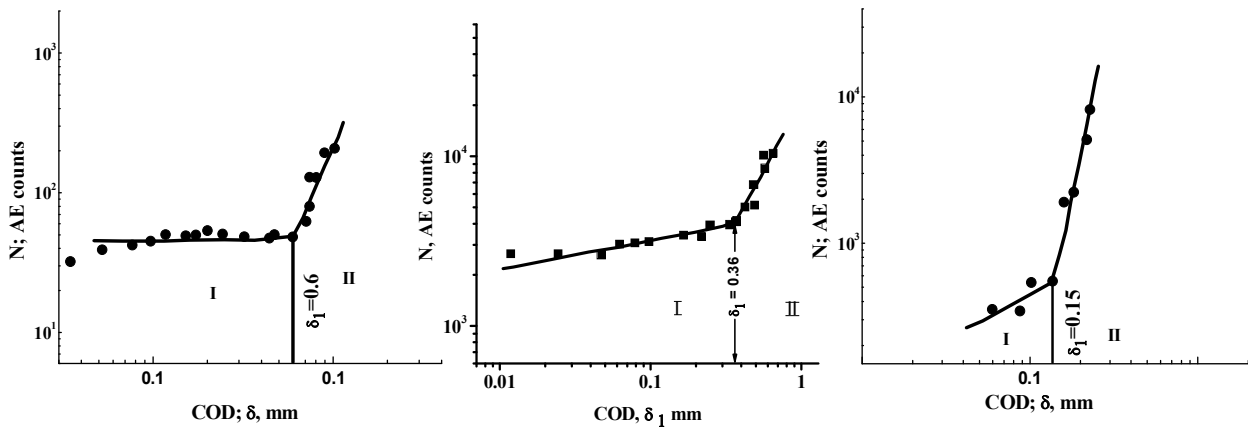


Fig. 2.12 AE counts, N vs. COD, δ (redrawn from the work of Arii *et al.*, 1975)

The numerous varieties of currently available stainless steels have been broadly classified into five categories: (a) Ferritic stainless steels, (b) Austenitic stainless steels, (c) Martensitic stainless steels, (d) duplex stainless steels and (e) Precipitation hardenable stainless steels. Austenitic stainless steels are 300 series steels having a face centered cubic (FCC) structure. This structure is attained through a liberal use of austenizing

elements such as nickel, manganese and nitrogen. These steels are essentially non-magnetic in the annealed condition and can be hardened only by cold working. These possess excellent cryogenic properties and good high temperature strength. The application of these steels in corrosive and high temperature environments is numerous. AISI 304LN stainless steel is a class of austenitic stainless steel as it comes from 300 series family. It is having a unified numbering system (UNS) No. S30453. Figure 2.13 shows the relationship with the other grades (Pickering, 1976). As the name suggests, 304LN SS have lower carbon content which avoids intergranular corrosion even on welded pieces and have specific nitrogen additions to increase strength. The alloy exhibits an austenitic microstructure free of deleterious carbide precipitations at grain boundaries. The density of 304LN SS is approximately 7.9 gm/cc.

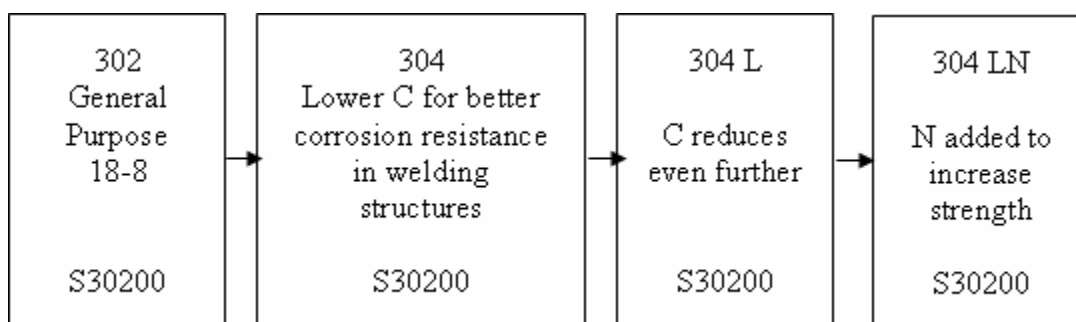


Fig. 2.13 Relationship of 304 LN stainless steels with other grades (Pickering, 1976)

These steels are almost free from of impurities and possess high fracture toughness properties. These are used in fabricating critical components like primary heat transfer pipings of advanced heavy water reactors (AHWR) in the nuclear power plants. The design philosophy of these components is "leak before break (LBB)". In high risk containment vessels LBB design concepts ensure that any damage due to accidents or natural calamities like earthquake etc leakage of fluid precedes burst/ rupture of the component. Section II A: Ferrous Materials' of the Boiler and Pressure vessel code has various material specifications that are employed in fabrication of nuclear power plant components. The corresponding ASTM specifications are given in the Annual book of ASTM Standards vol.1.01 "Steel-Piping, Tubing, Fittings".

The selected AISI 304LN stainless steel under investigation is obtained as courtesy of Bhabha Atomic Research Centre, Mumbai, India; the composition of the material is as per

ASME standards and the composition specified for advanced heavy water reactors are shown in Table 2.1. It can be seen from Table 2.1 that according to ASME the composition of nitrogen is in the range of 0.10-0.16 wt%, but for AHWR, nitrogen content is limited to 0.1 wt% (max) for improving weldability and for minimizing scatter in mechanical properties (McClintock and Irwin, 1965).

Table 2.1 Composition of 304LN SS in wt % according to ASTM A 240 and comparison with AHWR specification (Single value denote maximum permissible, Ns- Not specified) (McClintock and Irwin, 1965)

Element	C	Cr	Ni	Mo	N	Mn	Si	P	S	Ti	Nb	Cu	Co	B
ASTM 304 LN	0.03	18-20	8-12	Ns	0.1-0.16	2.0	1.0	0.045	0.03	Ns	Ns	Ns	Ns	Ns
AHWR 304 LN	0.024-0.03	18.5-20	8-10	0.5	0.06-0.08	1.6-2.0	0.5	0.03	0.01	0.05	0.05	1.0	0.25	0.002

2.7 Appraisal of the problem

The components such as heat transport pipes are designed on the concepts of leak before break (LBB). The LBB approach implies the application of fracture mechanics principles to demonstrate that the pipes are highly unlikely to experience sudden catastrophic rupture without prior indication of detectable leakage. The assessment of structural integrity of the pipes requires the knowledge of the fracture initiation toughness and resistance to crack propagation of the material. This necessitates detailed understanding of fracture behaviour of the pipe material. However, the effects of different factors like R ratio, extent of plastic displacement and the crack plane orientations on fracture resistance are also pertinent for the steel under consideration. For conservative design limits in the flaw assessment, there is a need to understand the crack initiation and propagation behaviour of this material under various cyclic loading situations and to establish suitable lower bound fracture mechanics parameters that can be used safely and confidently for LBB analysis. Moreover, acoustic emission technique can be sought for to accurately estimate the crack initiation process and to eliminate uncertainties associated with identification of the point of departure of the tearing curve from the blunting line.

This investigation has been directed to understand the process of crack initiation and its detection in AISI 304LN SS and its weldment under various types of loading

situations. Generation and analysis of data related to (a) effect of strain rate on tensile properties, (b) monotonic fracture behaviour of base metal and weldment (c) nature of cyclic J - R curve at different test conditions and (d) acoustic emission signal characterization during fracture toughness tests, are essential to bring forward such understanding.

The selected steel and its characteristics

3.1 Introduction

The material selected for this investigation is a nuclear grade AISI 304LN stainless steel and its weldment. It is used in the fabrication of primary heat transport (PHT) piping of the advanced heavy water reactors (AHWR) of Indian nuclear power plants. These components usually operate in the temperature range of 301-553 K and are used as circuit pipings of AHWR to carry the heavy water (D₂O) coming from the core channels. In order to ensure the structural integrity of 304LN piping components in service and to employ leak before break (LBB) concepts in their design, the materials of interest have to be rigorously characterized in terms of their mechanical properties with emphasis on its response to deformation and fracture behaviour. Moreover 304LN SS is known to be strain rate sensitive even at ambient temperature (Talonen *et al.*, 2005). It is thus necessary to understand the influence of strain rate on tensile properties of the selected steel and its weldment at ambient temperature apart from determining their strength, ductility and the flow behaviour (strain hardening exponent) before any elaborate investigation is attempted to examine its fracture toughness.

The major aims of the investigation reported in this chapter are: (i) to generate information about the microstructure of the selected steel and its weldment and (ii) to determine their conventional mechanical behaviour like hardness and tensile properties at ambient temperature at different strain rates.

3.2 Experimental procedure

The procedural details for obtaining the chemistry, microstructural features and that for determining hardness and tensile properties are described in different sub-sections below; the procedure for examining fractographic features of broken tensile specimens is given at the end of the section.

3.2.1 Chemical analysis

The AISI 304LN SS and its weldment used in this investigation were obtained as courtesy of Bhabha Atomic Research Centre, Mumbai, India. The steel was obtained in the form of sections of a pipe having external diameter of 320 mm and wall thickness of 25mm. Small pieces (of dimension 25 mm x 25 mm x 5 mm) were cut from the as received material and their longitudinal and transverse surfaces with respect to pipe section were made parallel by grinding. These samples were used for determining chemical composition of the steel with the help of an Optical Emission Spectrograph (make: Shimadzu, Japan, model: GVM 1014P). The analysis of nitrogen was done using a series of cylindrical samples of 3 mm diameter having 10 mm length with the help of a N₂ determinator (make: Leco, Michigan, USA model: TC436). The chemical composition (weight %) of the steel and its weldment are given in Table 3.1.

Table 1: Chemical composition of the investigated steels (in wt %)

Steels	C	Si	Mn	P	S	Cr	Ni	Fe
304LN Base	0.03	0.54	1.80	0.028	0.014	18.55	9.50	Bal.
304LN Weld	0.06	0.11	1.35	0.013	0.009	18.02	10.05	Bal.

Both the steel contain 0.08 (wt %) nitrogen

3.2.2 Metallographic specimen preparation

Small sample blanks of approximately 10 mm x 10 mm x 10 mm size were cut from the as received material for metallographic examinations. These specimens were first ground successively on silicon carbide abrasive papers having grit sizes from 80 to 1200. The specimens were then polished on Texemet cloth using diamond paste successively with particle sizes of 1 μ m and 0.25 μ m. Samples were finally etched with freshly prepared aqua regia (3 part HCl and 1 part HNO₃) solution.

3.2.3 Metallographic examination

The polished and etched metallographic specimens of AISI 304LN SS base metal and its weldment were examined using an optical microscope (make: M/s Meizi Techno, Saitama, Japan, model: MT7530F). These examinations were carried out for both CL and

LC planes of the pipe (Fig. 3.1) at different magnifications and several representative microstructures of the specimens were recorded. In addition to examining the phases in the microstructures, grain size of austenite in the base metal and the volume fraction of δ -ferrite in the weldment were also determined.

The austenite grain size was determined at 400x using random linear intercept method following ASTM standard E112-09 (2009). In this method a linear test grid is superimposed on the microstructure and the numbers of austenite grains intercepted by the test line were counted. A total number of 30 such random test lines were considered for obtaining the average austenite grains. The mean austenite grain size was calculated using the equation (ASTM E112-09, 2009):

$$L = \frac{V_f \cdot L_T}{N} \quad \dots(3.1)$$

where L = mean austenite grain size

V_f = volume fraction of austenite phase

L_t = total no. of superimposed grid lines

N = total no. of austenite grains intercepting the test line.

The volume fraction of the phases was determined manually by point counting technique following the ASTM standard E 562-09 (2009). A 20x20 grid was superimposed on a microstructure viewed at 500x magnification. Random counting was done on 30 fields of observations to estimate the mean volume fractions of the phases. The volume fraction, V_f , of a phase has been calculated using the following expression (ASTM E 562-09, 2009):

$$V_f = \frac{P}{nP_0} \quad \dots(3.2)$$

where, P = total number of points on a phase

P_0 = number of grid points

n = number of fields of observations

The amount of δ -ferrite (V_f^δ) was estimated and the volume fraction of austenite (V_f^a) was calculated as $(1 - V_f^\delta)$.

3.2.4 Hardness evaluation

Hardness values were determined on both CL and LC (Fig. 3.1) surfaces of the specimens with the help of a vickers hardness tester (make: Instron, model: Tukon 2500) using a load of 10 kgf. The specimen surfaces used for hardness studies were ground up to 1200 grade emery paper following the procedure described in section 3.2.2 other than chemical etching prior to hardness examination. At least ten indentations were taken to estimate the average value of hardness.

3.2.5 Tensile testing

Round specimens of diameter 5 mm and gauge length 25 mm were fabricated for tensile tests following the ASTM standard E 8M-09 (2009) from the as received pipe section. The nominal dimensions of the tensile specimens and their orientation in the pipe section are shown in Fig. 3.2 and in Fig. 3.1 respectively. All tensile tests were performed with the help of a universal testing machine (make: Instron, UK, model: 8562); this was an electromechanical dynamic testing system fitted with a 100kN capacity load cell. The machine was equipped with digital controller (model: 8500) interfaced to a computer through IEEE 488/GPIB protocols. The tests were conducted using Flaps 5; a software supplied by M/s Instron Ltd, UK. The software has provision for controlling test conditions like displacement rate, and data acquisition for load, displacement and strain in different channels. The strain was measured through an extensometer of 25 mm gauge length, attached to the middle of the specimen length. About 2500~3000 data points of load and displacement were acquired in each test for post processing. The tests were conducted at five different strain rates of 0.0001 s^{-1} , 0.001 s^{-1} , 0.01 s^{-1} , 0.1 s^{-1} and 1 s^{-1} at the ambient temperature of 301 K. The variations of strength, ductility and strain hardening capacity of the materials at different strain rates have been analyzed for both base metal and weldment.

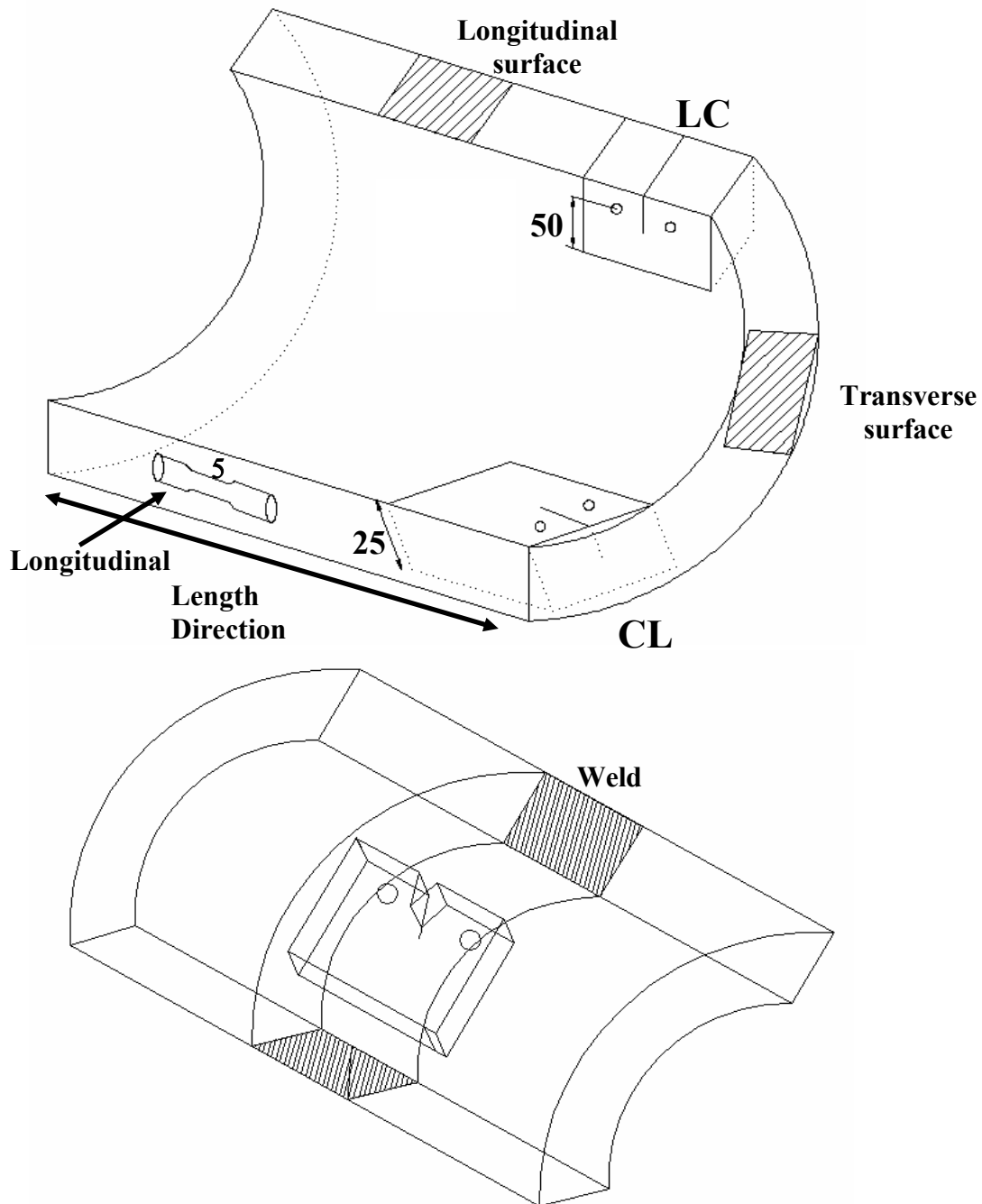


Fig. 3.1 Typical sketch showing samples fabricated from longitudinal and transverse sections of the as received pipe for metallography (shaded), tensile and fracture tests

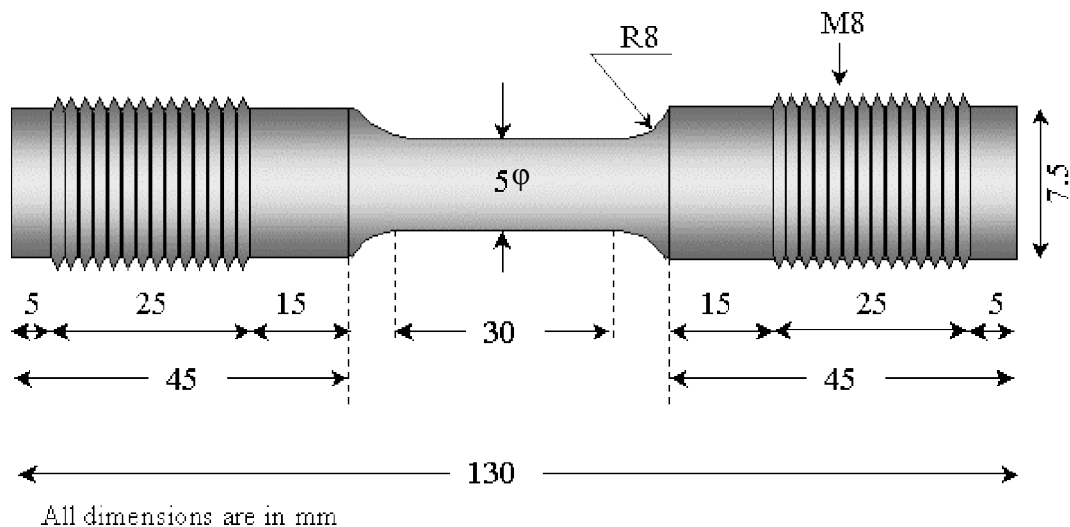


Fig. 3.2 Dimension of tensile specimen

3.2.6 Fractographic examination

The fractured surfaces were cut out carefully from the broken tensile specimens and were ultrasonically cleaned prior to their examination under a scanning electron microscope (make: M/s Hitachi, Japan, model: S-3000N). A series of representative fractographs were recorded during such examinations.

3.3 Results and discussion

3.3.1 Chemistry, microstructure and hardness

The chemical compositions of the base metal and its weldment are given in Table 3.1. Repeated analyses did not show variations of more than two units on the last significant decimal place of each elemental composition as given in Table 3.1 and hence the obtained analyses are considered reliable. The composition of the steel indicates that the amounts of carbon, manganese, phosphorous, sulphur, chromium, nickel and silicon are in accordance with the AISI 304L grade of stainless steel. However, the base metal has 0.08 % nitrogen; the investigated steel would therefore fall under the corresponding ASME specification SA 312 type 304LN, specified for AHWR materials (Sandusky *et al.*, 1990). The pipes were commercially welded (manually) using most widely and versatile welding process, gas tungsten arc welding (GTAW) as root pass and submerged metal arc welding (SMAW) as filling passes. Welding was done using ER

308L filler electrode by gas tungsten arc welding process in inert argon atmosphere. These welding processes are currently being followed in Indian nuclear power plants. The welded region was approximately 20 mm in the crown and about 3 mm in the root.

Representative optical micrographs of base metal and the weldment taken from the longitudinal (CL) and the transverse (LC) sections of the pipe are shown in Fig. 3.3 and Fig. 3.4, respectively. These micrographs of the base metal reveal austenite grains associated with some annealing twins, whereas that of the weldment exhibit uniformly distributed δ -ferrite in austenite matrix. The average austenite grain size in the base metal, the estimated volume fractions of δ -ferrite in weldment, and average hardness values of the base metal and the weldment along CL and LC orientations are summarized in Table 3.2. The average austenite grain size was found to be of the order of $83\ \mu\text{m}$, whereas the microstructure of the weldment reveals almost $12.3 \pm 2\%$ δ -ferrite in austenite matrix. The hardness of the base metal is $195\ \text{H}_\text{V}$ whereas that of weldments is $210\ \text{H}_\text{V}$. The detailed results as given in Table 3.2 indicate that microstructural anisotropy in the selected steel and its weldment is not significant.

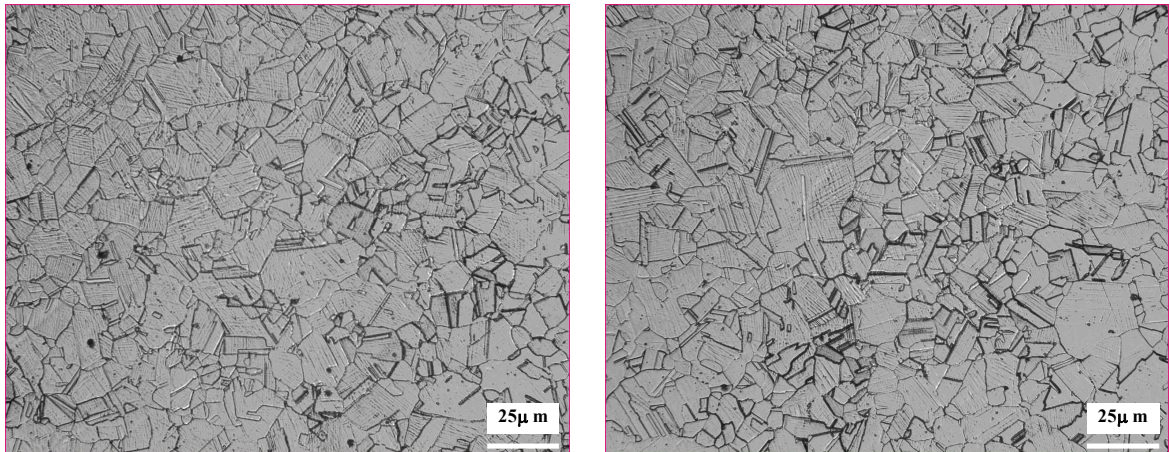
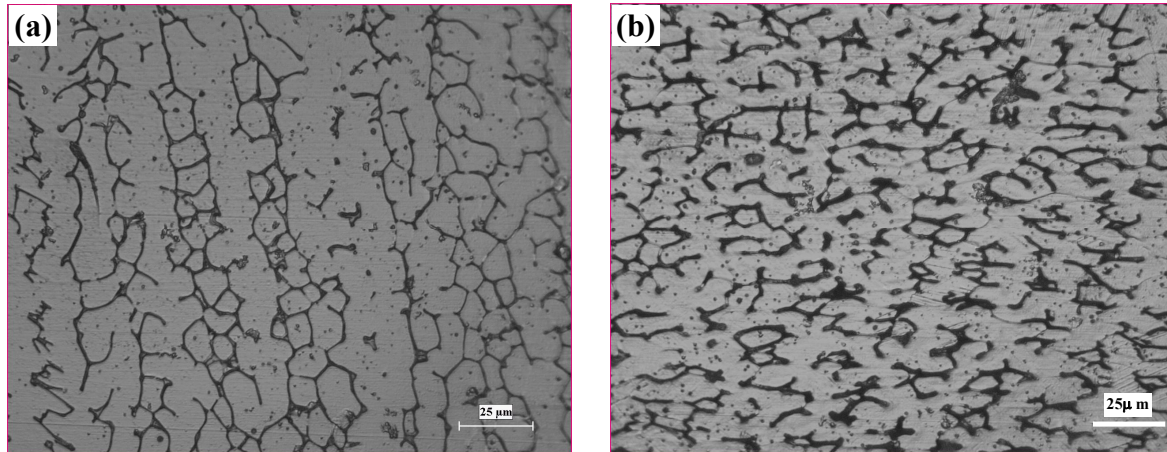


Fig. 3.3 Optical photomicrographs of the base metal at (a) longitudinal and (b) transverse sections of the pipe



3.4 Optical photomicrographs of the weldment at (a) longitudinal and (b) transverse sections of the pipe

Table 3.2 Details of microstructural and hardness characterization in CL and LC planes

Material	Orientation	Avg. austenite grain size (μm)	Avg vol. fraction of δ ferrite (%)	Hardness (VHN)
AISI 304LN SS Base Metal	CL (Longitudinal)	83 \pm 5	-	195 \pm 8
	LC (Transverse)	85 \pm 5	-	197 \pm 8
Weldment	CL (Longitudinal)	-	12	210 \pm 20
	LC (Transverse)	-	15	214 \pm 20

3.3.2 Tensile deformation behaviour

The tensile stress-strain data were analyzed to estimate the yield strength (YS), ultimate tensile strength (UTS), true uniform elongation (e_u), and total elongation (e_t), whereas % reduction in area (% RA) was estimated from the initial and final diameters of the specimens. Typical engineering stress-strain plots of AISI 304LN base material at different strain rates are shown in Fig. 3.5. For a number of tests (corresponding to various strain rates), the values of % elongation were also calculated from the cross-head position of the test machine and compared with the elongation obtained from the extensometer. This was required since for higher strain rate experiments, the extensometer could not be used and the deformation of material had to be calculated from cross-head displacement. A close agreement has been observed in all the cases as can be seen in Fig. 3.6 indicating that cross-head position is reliable obtaining deformation of

material. Elongation measurements from cross-head positions have been adopted later wherever use of extensometer is found to be difficult (such as high strain rate tests at 1 s^{-1}). The strain hardening exponent (n) was computed from the stress-strain data following ASTM standard E 646-93 (1993) which is based on the Hollomon relation, $\sigma = k\epsilon^n$. The average tensile parameters evaluated for AISI 304LN stainless steel and its weldments are summarized in Table 3.3. The estimated values of YS, UTS and % elongation for AISI 304LN SS base metal at a nominal strain rate of 0.0001 s^{-1} were found to be 340 MPa, 680 MPa and 69% respectively. These values are in close agreement with that given in ASME specification SA312 type 304LN, specified for AHWR materials (Sandusky *et al.*; 1990, ASM Material Handbook; 1990).

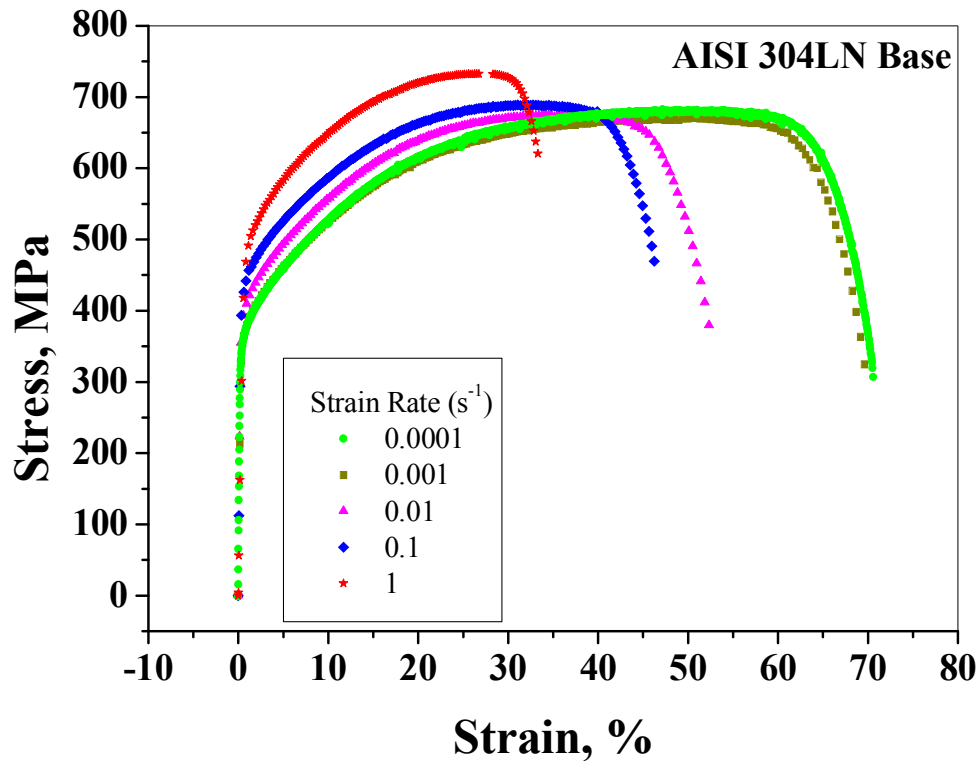


Fig. 3.5 Plots of engineering stress versus strain at different strain rates for AISI 304LN base metal

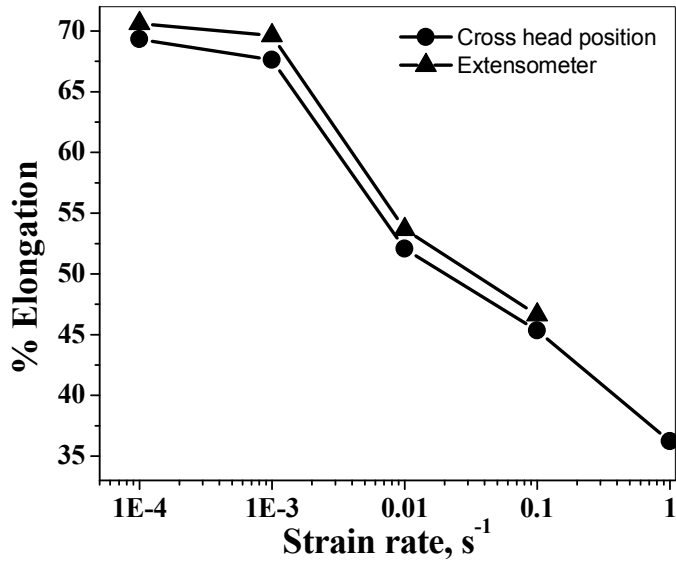


Fig. 3.6 Comparison of measurement of % elongation using cross head position with that of extensometer

Table 3.3: Variation in tensile properties of 304LN SS base metal and weldment at different strain rates

#	Test Temp °C	Strain rate (s^{-1})	YS _{0.2} (MPa)	UTS (MPa)	%El	%RA	%Uni.Elong	$n^{\#}$
Base Metal								
1.	26	1E-4	340	680	69.31	87.64	49.78	0.359
2.	26	1E-3	353	671	67.61	88.20	50.83	0.366
3.	26	1E-2	382	675	52.07	85.84	36.90	0.33
4.	26	1E-1	418	688	45.33	82.20	31.56	0.297
5.	26	1E0	464	734	36.22	66.88	26.92	0.255
Weldment								
1.	26	1E-4	560	682	35.69	74.55	28.45	0.156
2.	26	1E-3	594	700	37.10	62.95	26.46	0.153
3.	26	1E-2	549	638	30.25	59.50	20.50	0.137
4.	26	1E-1	563	656	19.32	53.97	11.68	0.087
5.	26	1E0	627	734	15.8	42.62	11.25	0.107

$n^{\#}$ = strain hardening exponent using Hollomon's equation

An attempt has been made to study the effect of strain rate on the tensile properties of AISI 304LN stainless steel and its weldment, and the obtained results are compiled in Table 3.3. The results related to the variation of strength (YS, UTS), ductility (% elongation and % RA) and strain hardening exponent (n) with strain rate are shown in Fig.3.7 to Fig. 3.9. The results indicate that both yield and ultimate tensile strength increase with increase in strain rate (Fig. 3.7); however, the rate of change of YS and UTS are different at lower strain rate unlike their close resemblance at higher strain rates. The magnitudes of % elongation and % RA are found to decrease with increasing strain rate (Fig. 3.8), opposite to the nature of variations of strength with strain rate. The estimated values of strain hardening exponent (Fig. 3.9) for the base metal at different strain rates are found to be between 0.255 and 0.366.

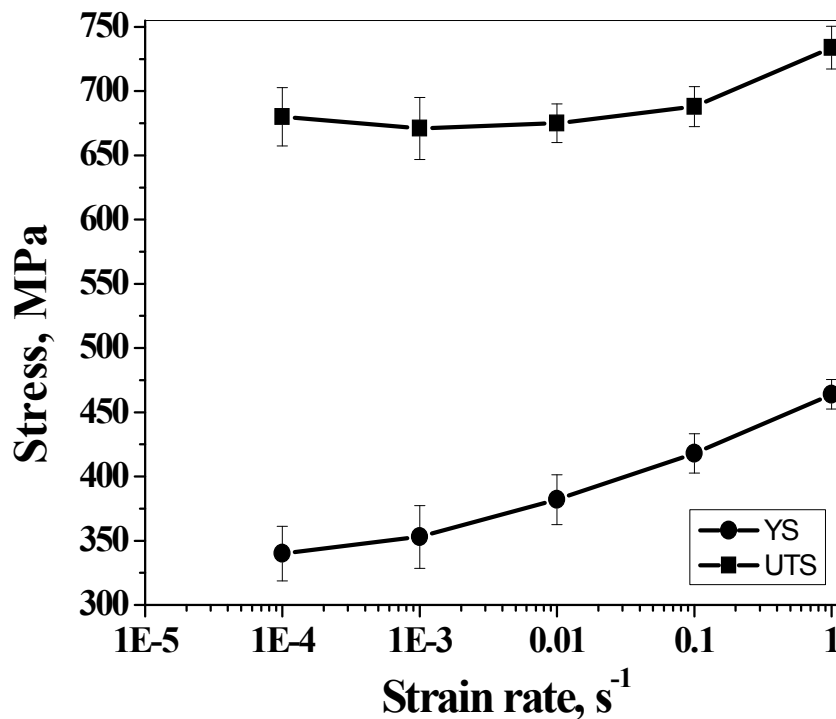


Fig. 3.7 Variation of YS and UTS with strain rate for AISI 304LN base metal

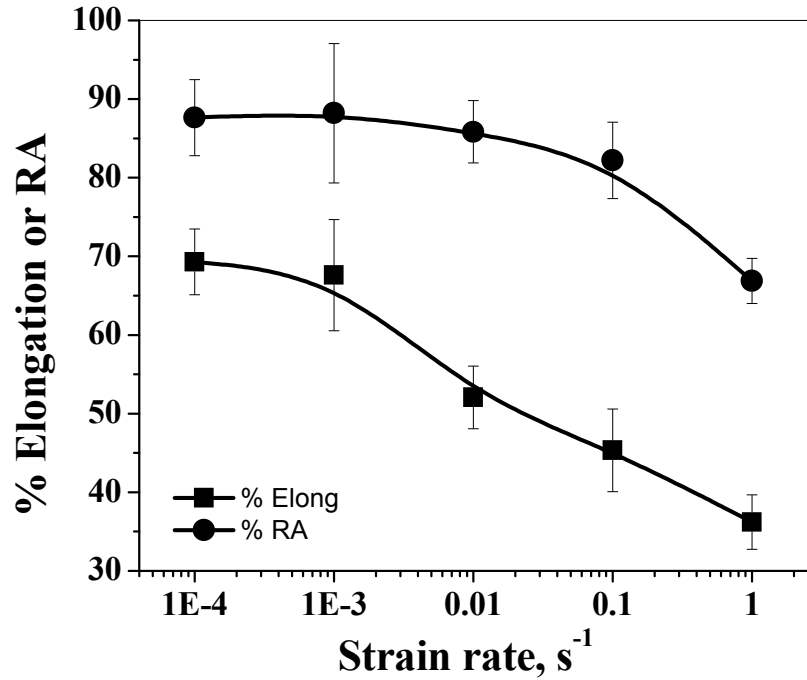


Fig. 3.8 Variation of percentage elongation and percentage reduction in area (RA) with strain rate for AISI 304LN base metal

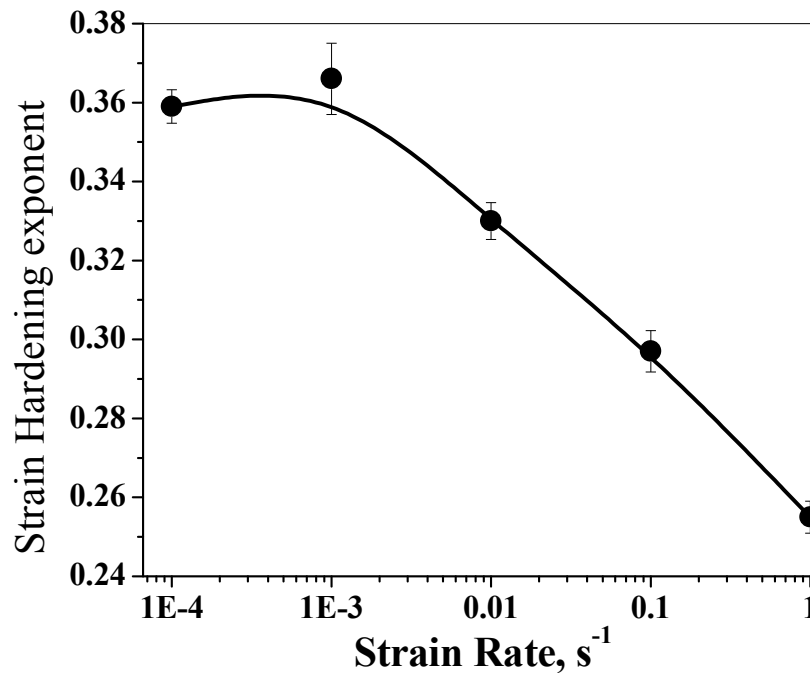


Fig. 3.9 Variation of strain hardening exponent (n) with strain rate for AISI 304LN base metal

Typical true stress-true strain plots for the base metal at different strain rates are shown in Fig. 3.10, whereas the variations of true stress with strain rate (in log-log plot) at different values of true strain are depicted in Fig. 3.11. The results in these figures show that magnitudes of true stress increase significantly from lower to higher strain rates at a specific strain indicating considerable strain rate sensitivity of the material. The slope of log (true stress) versus log (strain rate) is used to obtain the strain rate sensitivity parameter β , following the expression:

$$\sigma = k (\dot{\varepsilon})^\beta \quad \dots (3.3)$$

where σ is the true stress and $\dot{\varepsilon}$ is the nominal strain rate. The results presented in Fig. 3.11 show that there is marginal change in the magnitude of σ when strain rates lie in the range $0.0001-0.001 \text{ s}^{-1}$, whereas increase in σ is significant when strain rates lie in the range $0.001-1 \text{ s}^{-1}$. Considering this observation, the magnitude of β has been calculated by linear regression analyses of $\log \sigma - \log \dot{\varepsilon}$ for the range of strain rate in the domain $0.001-1 \text{ s}^{-1}$. The variation of β with true strain is shown in Fig. 3.12, which indicates decrease in strain rate sensitivity with increase in true strain. Similar variation of β with increase in strain rate is reported by Huang *et al.*, (1995) for AISI 304 grade stainless steel sheet. The obtained results are thus in suitable accordance with similar results in the literature.

Lee and Lin (2001) have earlier shown the variation of strain rate sensitivity of AISI 304L in discrete steps using the expression (3.4):

$$\beta = \ln(\sigma_2 - \sigma_1) / \ln(\dot{\varepsilon}_2 / \dot{\varepsilon}_1) \text{ at a particular strain value} \quad \dots (3.4)$$

Following the work of Lee and Lin (2001), the strain rate sensitivity (β) has also been calculated for adjacent strain rate values and the results are shown in Fig. 3.13. It is obvious from Fig. 3.13 that at a constant strain, strain rate sensitivity decreases with decreasing strain rate for AISI 304LN base metal. The obtained results are in close agreement with the results of Lee and Lin (2001). The nature of variation of β with strain rate has been discussed later.

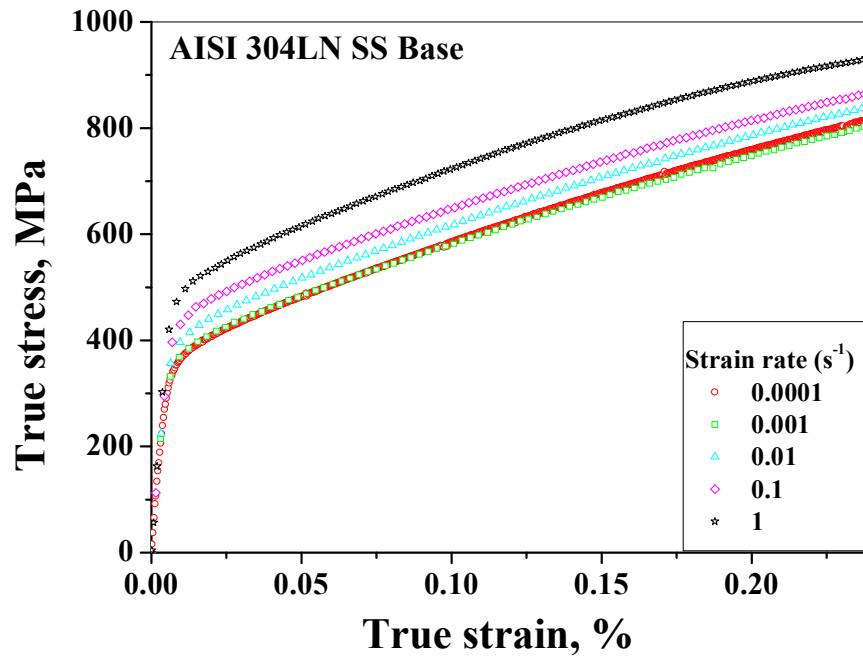


Fig. 3.10 True stress-true strain plots of AISI 304LN base metal at different strain rates

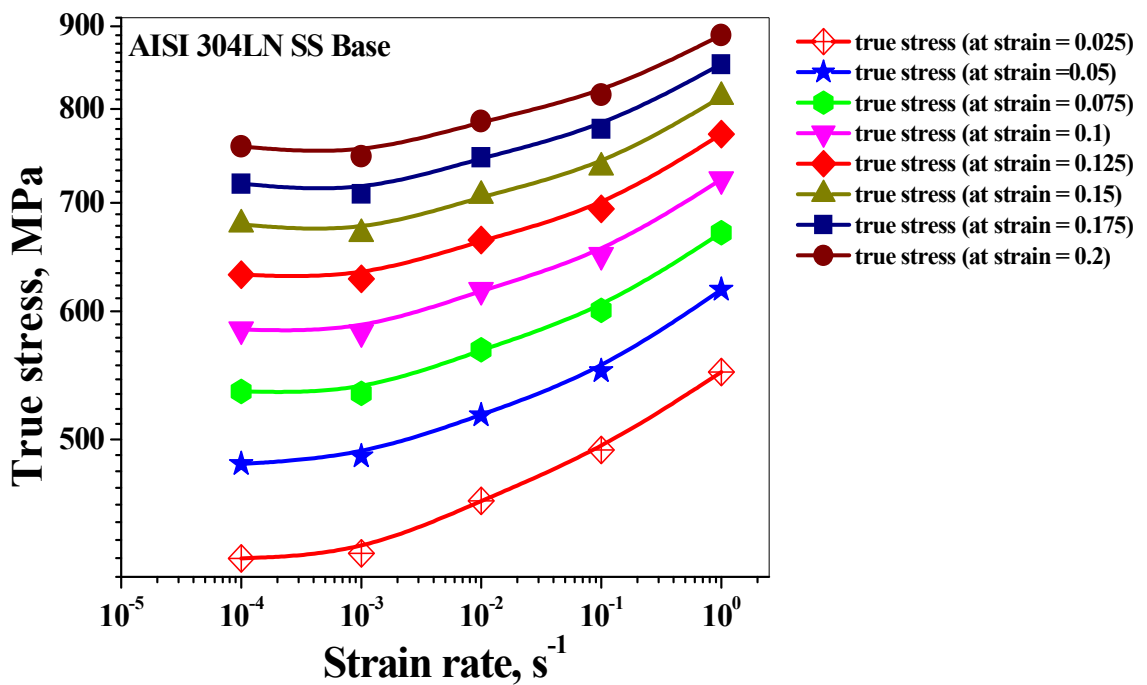


Fig. 3.11 Variation of true stress with strain rate (at different true strain values) for AISI 304LN stainless steel base metal

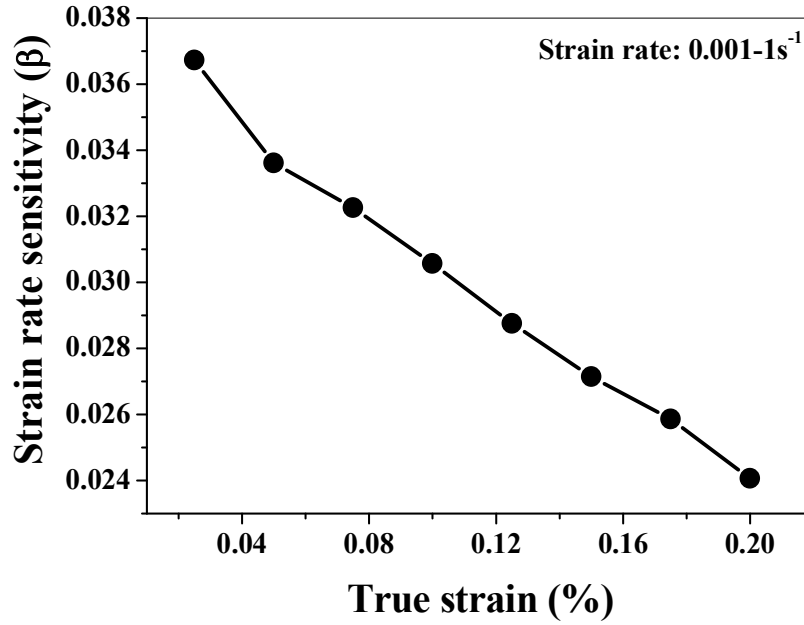


Fig. 3.12 Variation of strain rate sensitivity as a function of true strain for AISI 304LN base metal

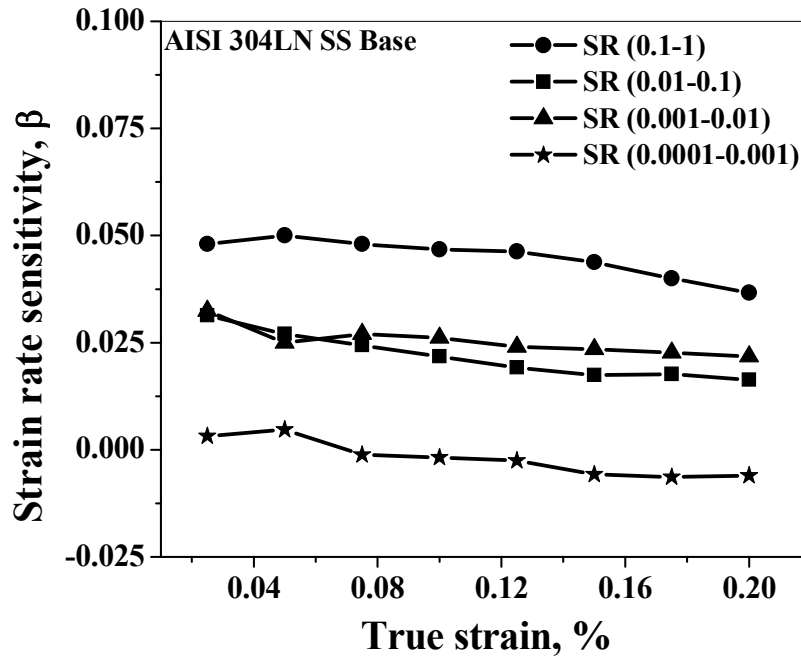


Fig. 3.13 Variation of strain rate sensitivity as a function of plastic strain for AISI 304LN base metal

Tensile properties of the weldment, obtained in a similar manner are given in Table 3.3 and in Fig. 3.14-3.20. The nature of variation of % elongation and % RA for the weldment are similar to the base metal; however, YS, UTS and strain hardening exponent (n) shows non-monotonic variation with an inflection at a strain rate of 0.01 s^{-1} . Comparison of tensile properties of base metal and weldment is shown in Fig. 3.21 at two extreme strain rates of 0.0001 s^{-1} and 1 s^{-1} . The results in Fig. 3.21 reveal that YS of the weldment is higher, whereas the % elongation, % RA and strain hardening exponent are lower compared to its base metal. The change in tensile properties of base metal and of its weldment is attributed to arise from the fact that weldments exhibit composite structures with $12.3 \pm 2\%$ δ -ferrite in austenite matrix. The interfaces of δ -ferrite interact with dislocations generated during tensile deformation but the nature of interaction varies differently depending on amount of δ -ferrite interfaces (Rho *et al.*, 2000); and this interface interaction with dislocations is considered to play a significant role in bulk deformation behaviour of the weldments.

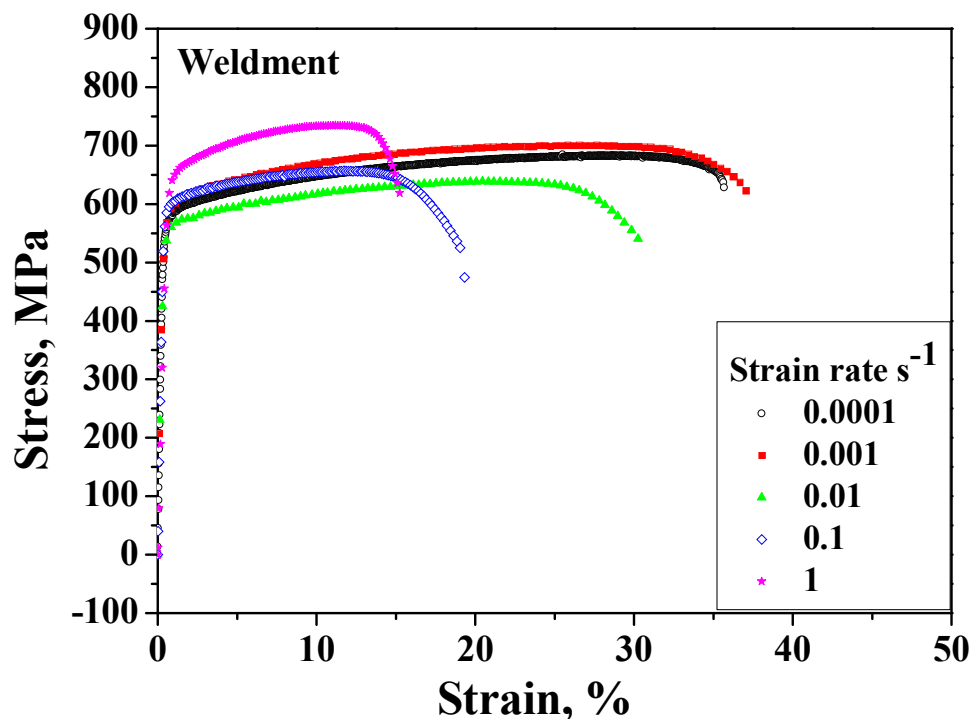


Fig. 3.14 Engineering stress versus strain at different strain rates for AISI 304LN weldment

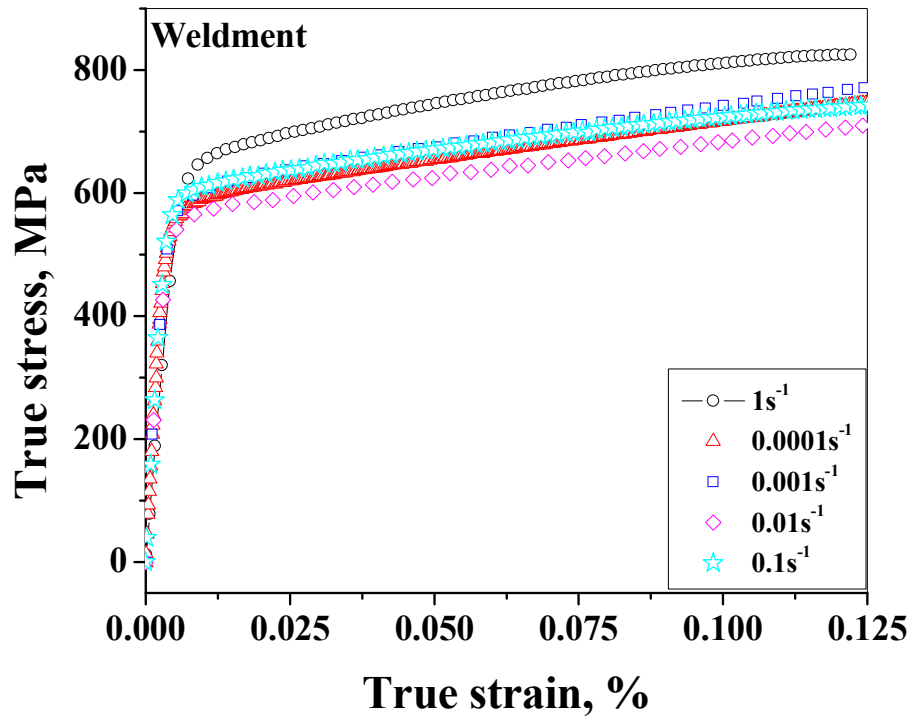


Fig. 3.15 Variation of true stress and true strain (at different true strain values) for the weldment

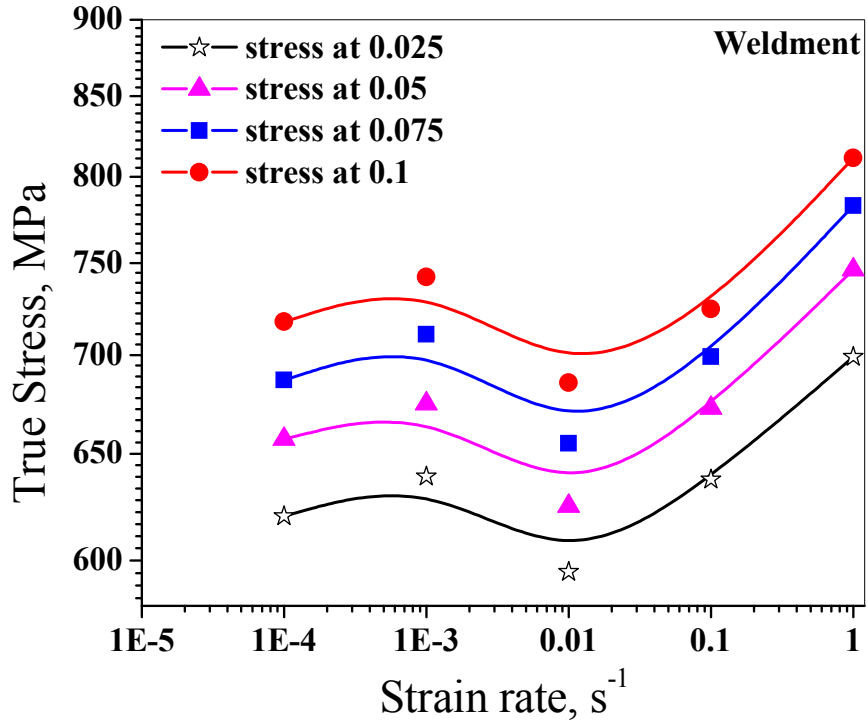


Fig. 3.16 Variation of true stress with strain rate (at different true strain values) for the weldment

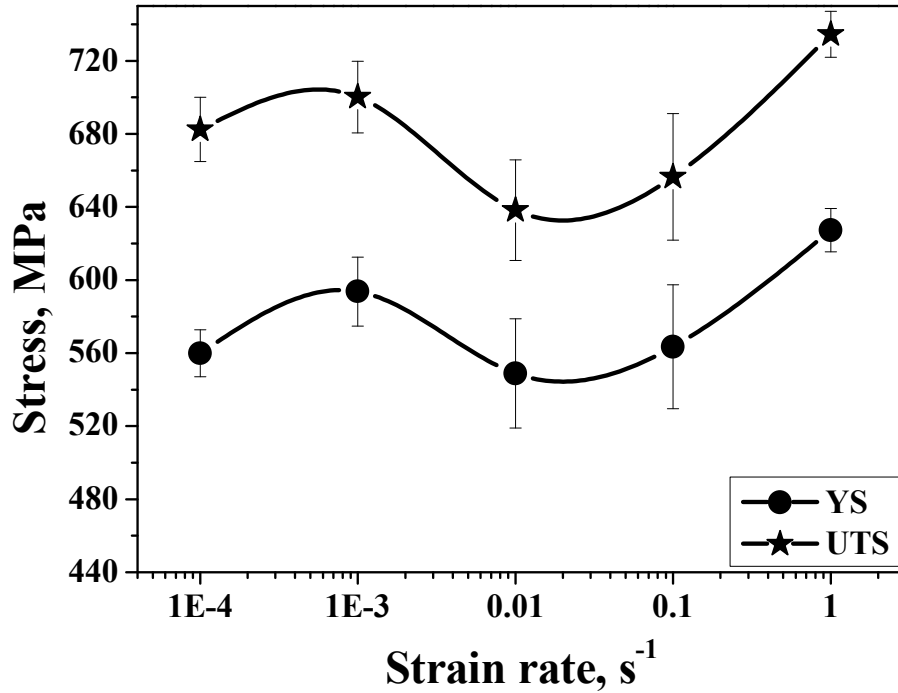


Fig. 3.17 Variation of YS and UTS with strain rate for AISI 304LN weldment

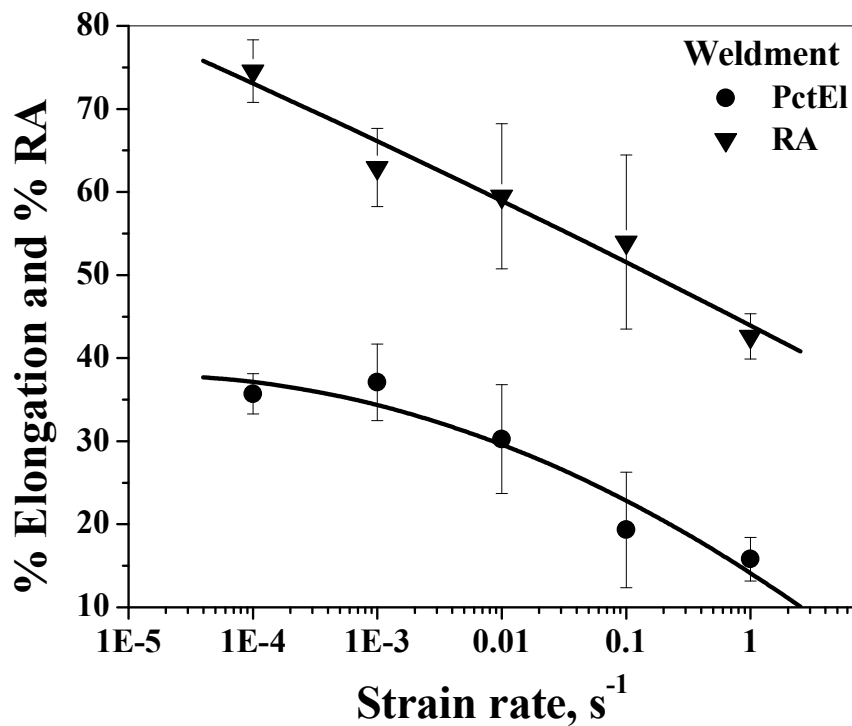


Fig. 3.18 Typical variation of ductility properties (% elongation and % RA) showing a decreasing trend with increase in strain rate

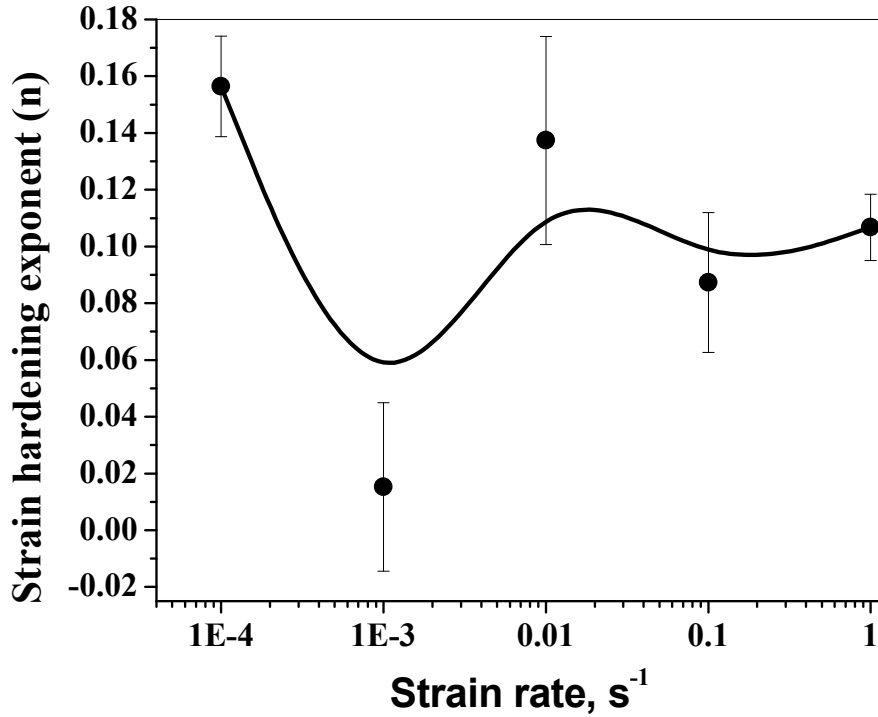


Fig. 3.19 Variation of strain hardening exponent with strain rate for weldment

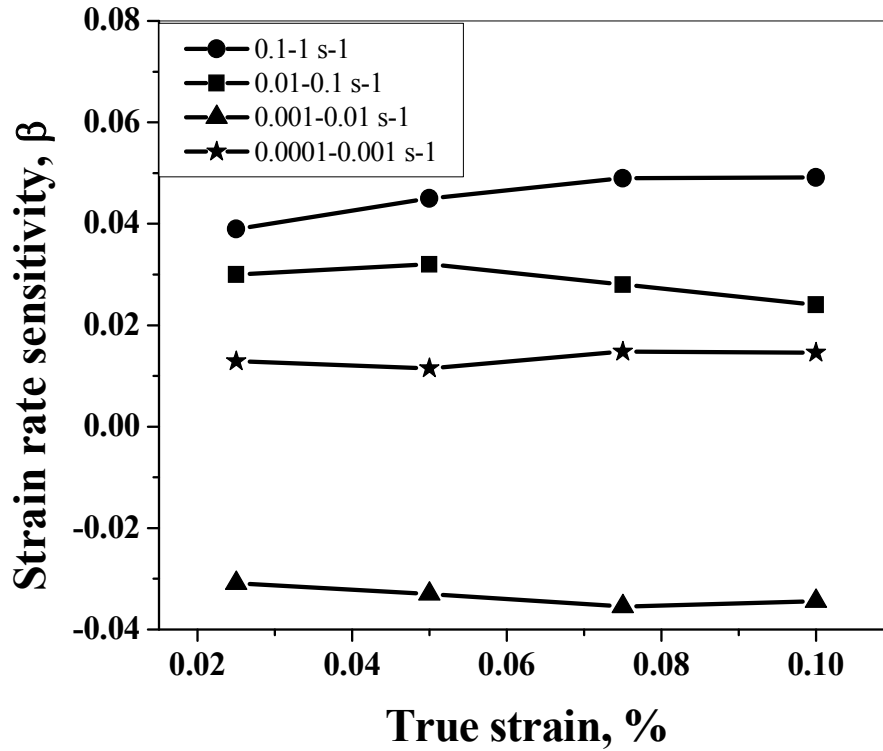


Fig. 3.20 Variation of strain rate sensitivity as a function of plastic strain for weldment

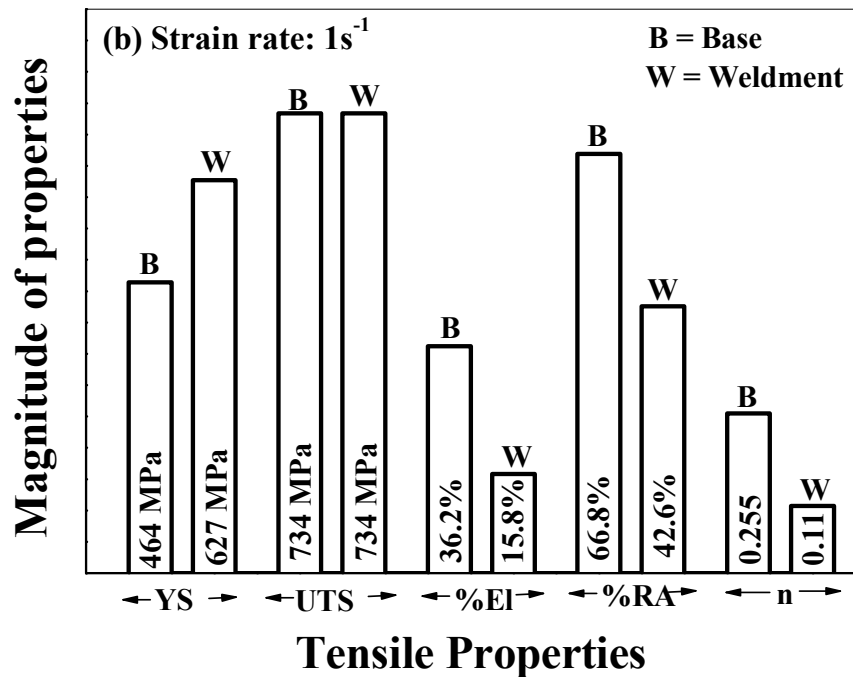
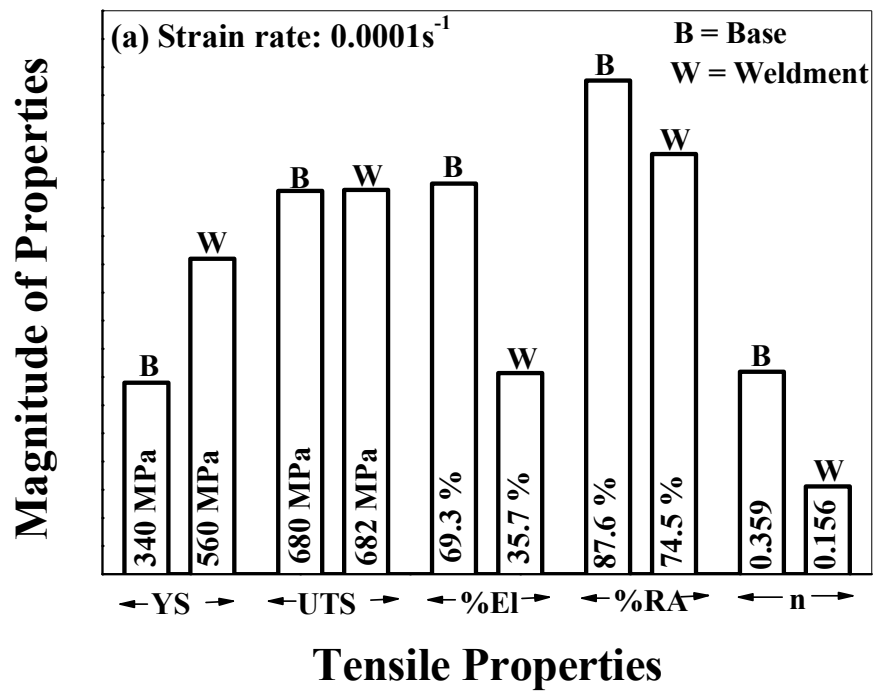


Fig. 3.21 Comparison of tensile properties between base metal and weldment of AISI 304LN stainless steel at two extreme strain rates of (a) 0.0001s^{-1} and (b) 1s^{-1}

The observed decrease of β with decreasing strain rate in AISI 304LN base metal has earlier been explained by a few other investigators (Huang *et al.*, 1989; Ayres, 1985) considering increase in temperature of the specimen due to adiabatic heating and due to deformation induced phase transformation during testing. The adiabatic increase in temperature with increase in strain rate can be calculated using the following expression (Lee and Lin, 2001):

$$\Delta T = \left(\frac{1}{\rho C_p} \right) \int_0^\epsilon \sigma d\epsilon \quad \dots(3.5)$$

where ΔT is the temperature rise, ρ is the density (7.9 gm/cm^3), C_p is the heat capacity ($477 \text{ JKg}^{-1} \text{ K}^{-1}$), σ is the stress and $d\epsilon$ is the interval of strain. The estimated ΔT values at different strain rates are shown in Fig. 3.22.

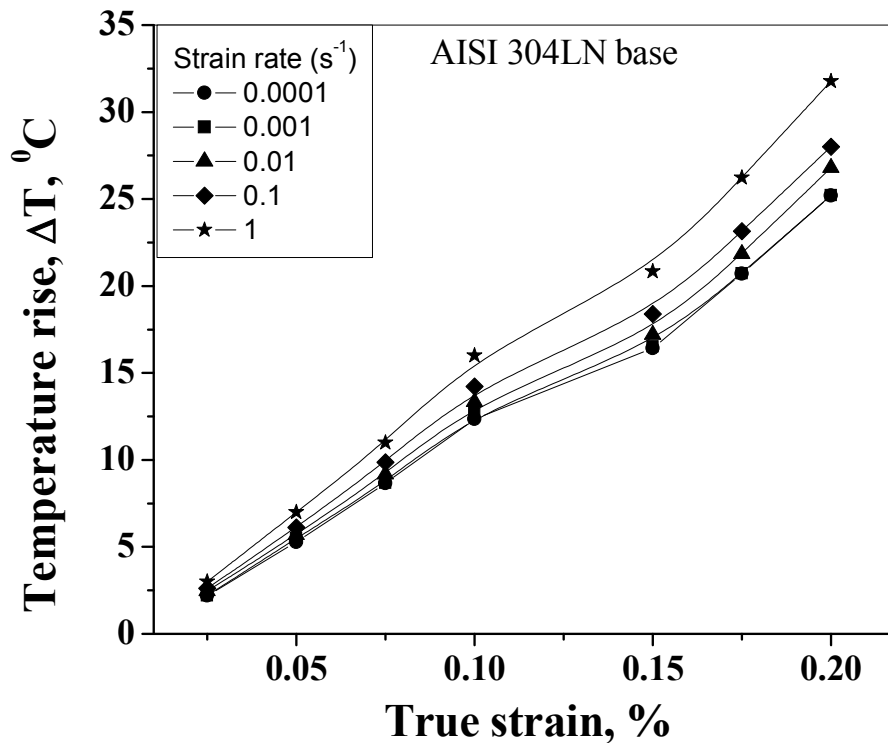


Fig. 3.22 Variation of rise in temperature (ΔT) as a function of strain and strain rate for AISI 304LN base metal

Similar strain rate dependency of mechanical properties for 301LN and 304LN stainless steels was observed by Talonen *et al.* (2005). It is well documented that strain rate is related to the mobile dislocation velocity (Dieter, 1993; Lee, 2006; Zhang, 2007) and therefore increasing strain rate is liable to alter the dislocation dynamics and

consequently the mechanical behaviour of a material. Substantial changes in the mechanical property of 304L stainless steel has been reported by Lee and Lin (2001) in whose work strain rate is increased from 10^{-3} to 4800 s^{-1} . However, five-order variation of nominal strain rate used in this work is not expected to produce large variation in tensile deformation behaviour since the dislocation dynamics is not expected to get significantly affected. It is surprising to note that even this limited variation in strain rate during tensile tests produces substantial change in the mechanical behaviour of 304LN stainless steel. There must, therefore, be factors other than the intrinsic influence of strain rate on dislocation velocity that are responsible for the substantial variation in the mechanical properties observed here. The 304 series of stainless steels exhibit metastable austenite microstructures and the latter is easily transformed into martensite during plastic deformation. Martensite transformation is thus one of the important factors which affect the deformation behaviour of metastable austenitic steels and the extent of this transformation is influenced by changes of strain rate, stress state and strain. A few investigators (Hecker *et al.*; 1982, Huang *et al.*; 1989, Murr *et al.*; 1982, Das *et al.*; 2008a, Das *et al.*; 2008b, Erdogen and Tekli; 2002) have reported that formation of deformation induced martensite (DIM) contribute significantly towards the alteration in the deformation behaviour of stainless steels. The microstructures of a few deformed samples were examined to reveal presence of DIM, if any. The microstructures indeed revealed fine platelets of martensite (Fig. 3.23); this phase transformation is also confirmed by X-ray diffraction analysis (Fig. 3.24).

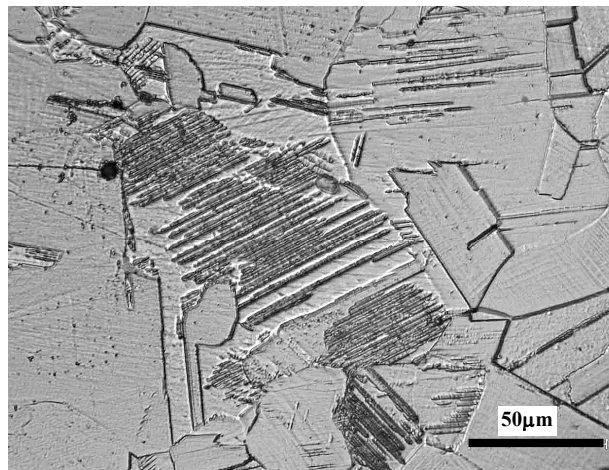


Fig. 3.23 Typical microstructure of a deformed tensile sample revealing platelets of martensite

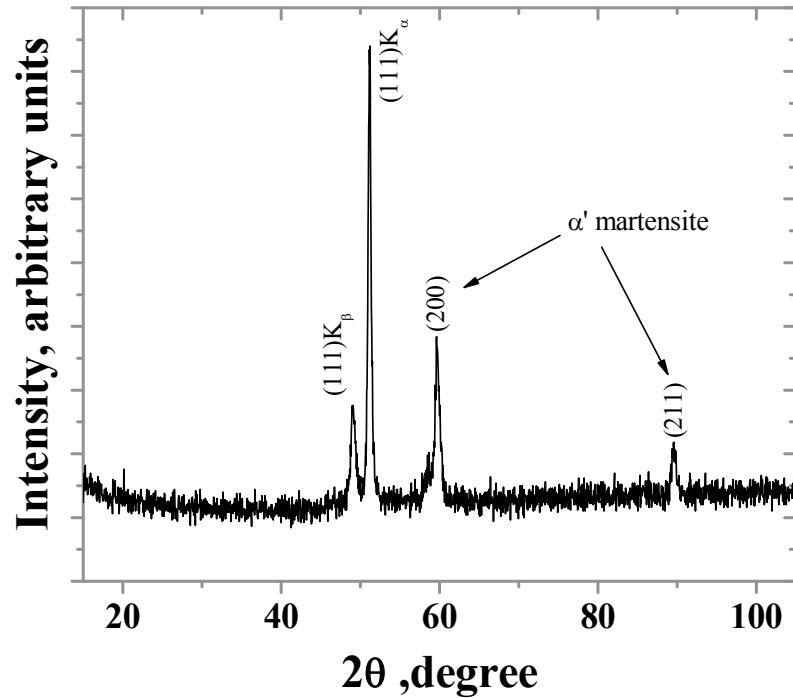


Fig. 3.24 XRD analysis of one deformed sample showing presence of α' -martensite

Typical fractographs of tensile fracture surfaces generated at different strain rates for base metal and weldment are shown in Fig. 3.25 and Fig. 3.26, respectively. The fractographs depict typical dimple fracture and exhibit bimodal distribution of voids. The smaller voids can be thought to be parts of void sheets that form within the interacting strain fields of larger voids at relatively advanced stages of deformation (Garrison, 1984). The void size is found to increase while the density of smaller voids is found to decrease with increase in strain rate for the base metal. It is, therefore, evident from these fractographs that systematic variation in the appearance of fracture surfaces occurs with increasing strain rate. The fractographs of the weldments however show non-uniform variation of void size and density with variation in strain rates.

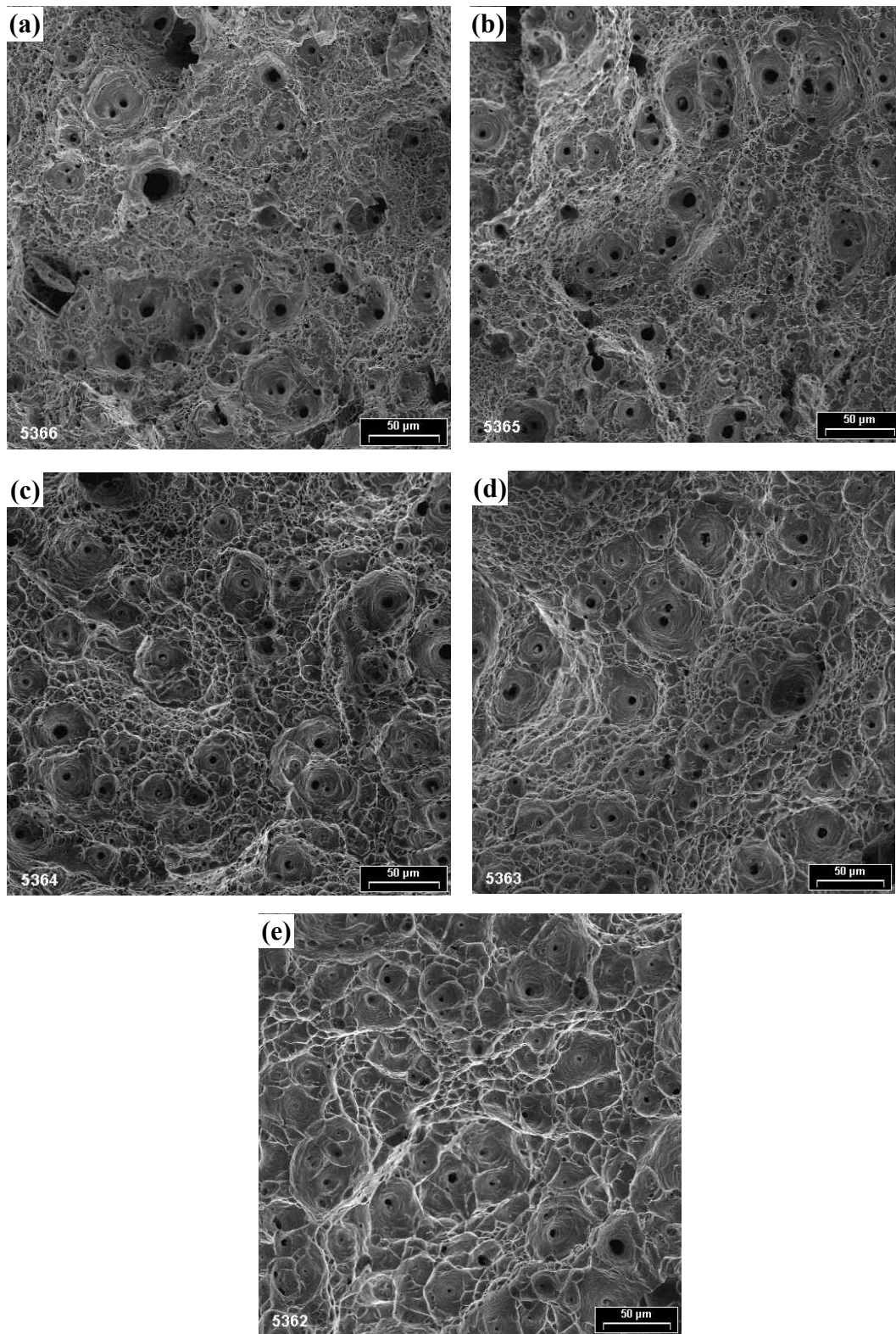


Fig. 3.25 Fracture surface of tensile specimens of AISI 304LN base metal at strain rates of (a) 0.0001, (b) 0.001, (c) 0.01, (d) 0.1 and (e) 1.0 s⁻¹

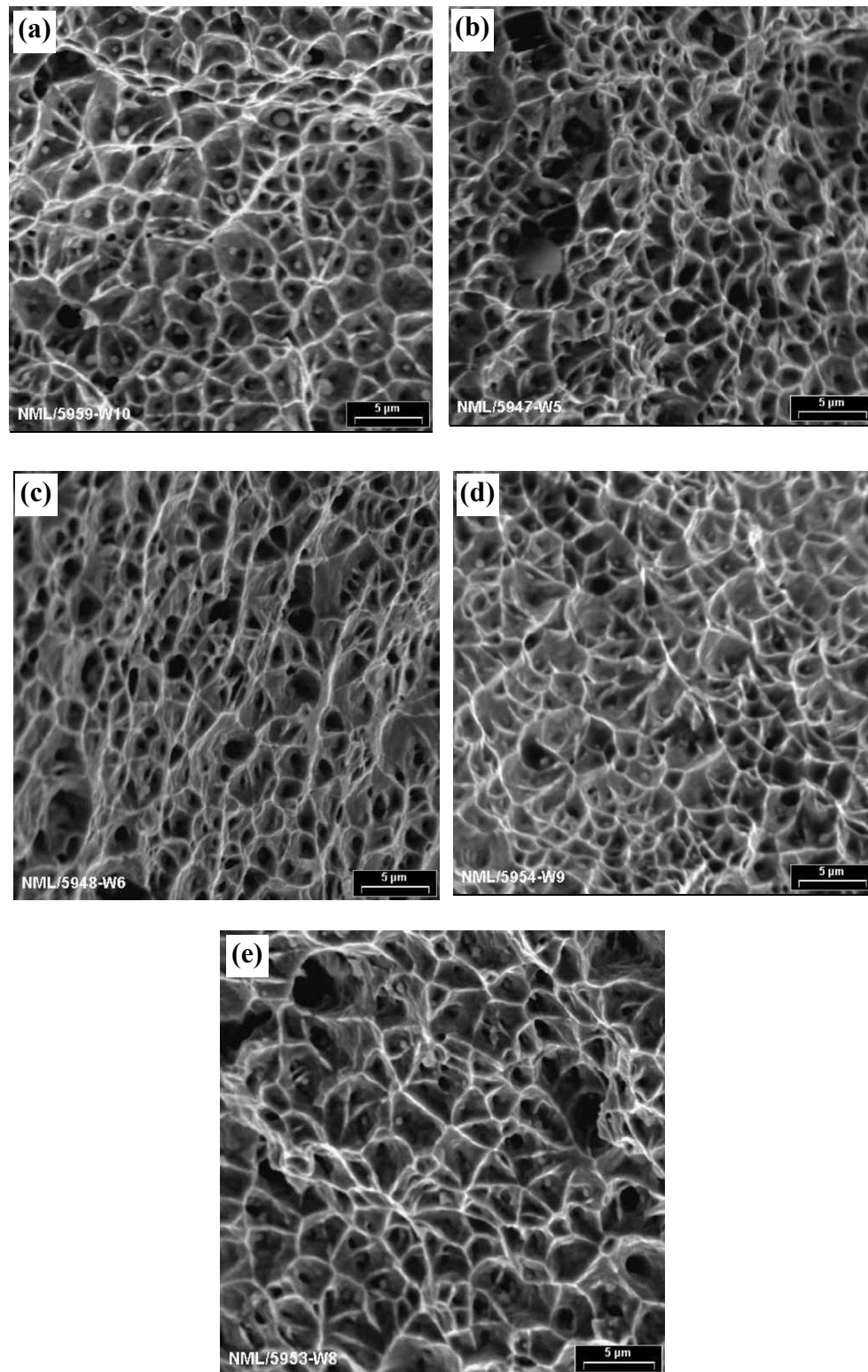


Fig. 3.26 Fracture surface of tensile specimens of AISI 304LN weldments at strain rates of (a) 0.0001, (b) 0.001, (c) 0.01, (d) 0.1 and (e) 1.0 s⁻¹

The mechanism of ductile fracture is well established and known to be constituted of three distinct events: void nucleation, growth and coalescence (Gurson, 1977; Thomason, 1990; Benzerga *et al.*, 2004; Bandstra *et al.*, 2004). The nucleation of voids in AISI 304LN SS base metal has been considered to be governed by dislocation-dislocation interaction, dislocation-twin boundary interaction, shear band interaction, interaction between deformation induced martensite (DIM) and dislocations (Gurson, 1977; Tvergaard, 1981; Tvergaard and Needleman, 1984; Anderson, 1995; Christy *et al.*, 1986). In addition, it is suggested that for weldments the nucleation of voids may also arise from interaction between dislocation and δ -ferrite interfaces. Some investigators (Das *et al.*, 2008; Lee and Lin, 2002) have ascribed the phenomenon of decrease in void density with increase in strain rate for AISI 304LN SS due to the formation of DIM. These investigators have shown that the majority of the voids have nucleated preferentially from these martensitic colonies. At low strain rates, both volume fraction of martensite and (small) void number density have been reported to be higher, but at higher strain rates, since martensitic transformation is suppressed (Das *et al.*, 2008), void number density is reported to be lower.

The observed variation of fractographic features with increasing strain rate is considered to be primarily governed by the amount of DIM generated at different strain rate.

3.4 Summary

The chemical analysis, microstructure, hardness, and tensile properties of the selected steel and its weldment have been studied prior to examination of their fracture behaviour. The obtained results can be summarized as follows:

- The selected steel as per its composition corresponds to ASME specification SA312 type 304LN stainless steel.
- The microstructure of the AISI 304LN SS base metal is completely austenitic whereas that of its weldment shows $12.3 \pm 2\%$ δ -ferrite in austenitic matrix.

- Microstructural and hardness characterizations on longitudinal (CL) and the transverse (LC) sections reveal that the materials under investigation are isotropic in nature.
- The strength (YS and UTS) increases whereas the ductility (% Elongation and % RA) decreases with strain rate for AISI 304LN SS base metal as expected. The nature of variation of % elongation and % RA for the weldment are similar to the base metal; but, YS, UTS and strain hardening exponent (n) shows non-monotonic variation with an inflexion at a strain rate of 0.01 s^{-1} .
- Comparison of tensile properties of base metal and weldment reveals that the YS of the weldment is higher, whereas the % elongation, % RA and strain hardening exponent are lower than the base metal.
- The selected materials are found to be strain rate sensitive; the strain rate sensitivity parameter (β) decreases with decrease in strain rate.
- The fractographs of the base metal and weldment reveal systematic variation in appearance of fracture surface with strain rate. The void size increases but the void density decreases with increase in strain rate.

Displacement controlled fracture behaviour of AISI 304LN stainless steel and its weldment

4.1 Introduction

Design of primary heat transport (PHT) piping of nuclear reactors has to ensure implementation of leak-before-break (LBB) concepts. In order to fulfill this requirement, fracture characteristics of PHT piping material has to be quantified. The LBB approach based on fracture mechanics principles attempts to ensure that no catastrophic failure occurs in an engineering component without prior indication of detectable leakage of fluids. In component integrity program for PHT piping one thus requires information and understanding about the fracture behaviour of the material under different experimental conditions. This chapter deals with studies related to crack initiation toughness of the selected AISI 304LN stainless steel and its weldment used for PHT piping under displacement controlled mode.

Plane strain fracture toughness (K_{IC}) cannot be used for characterizing crack initiation resistance of the selected AISI 304LN SS having moderate strength and high ductility, because the maximum thickness of CT specimens that can be fabricated from the available component stock is only ~ 20 mm. A rough estimate based on reported fracture toughness and yield strength, reveals that the thickness required for AISI 304LN SS base metal and weldment would be approximately 220 mm and 72 mm respectively to determine valid K_{IC} values. To estimate fracture toughness criteria for such materials, one has to consider the approach of elastic plastic fracture mechanics such as J -integral or CTOD (Meguid, 1989; Broek, 1976). The J -integral fracture criterion is currently popular and is used for the LBB analysis of the piping systems. Hence in the present investigation, attempts have been directed to study fracture behaviour of AISI 304LN SS and its weldment using J -integral approach.

Ensuring integrity of components during seismic events is one of the critical issues in the design of nuclear power plants. The load fluctuations during seismic activity

may be random, with postulated cracks and flaws often experiencing high tensile as well as compressive load amplitudes leading to their extension or growth to critical levels. In order to incorporate seismic factors in design, the existing design codes and practices (Scott, 2003) demand understanding the deleterious effects of load reversals on fracture resistance (J - R) curves that are determined conventionally. Although a standard experimental procedure is yet to be recommended for such investigations, periodic load reversals during conventional tests have been employed at times to simulate the load excursions during seismic events. Such conventional J tests with significant load reversals are often termed as "cyclic J - R tests" and the same terminology is used here to differentiate these modified experiments from the conventional J - R tests. The concept of cyclic J - R behaviour is of recent origin. Only a few international laboratories have worked on this problem and the available literature on cyclic J - R behaviour of materials is scanty. Mogami *et al.* (1990) have first proposed cyclic J -integral tests to simulate the deleterious effects of periodic load reversals. But there exists controversy over the applicability of the J -integral approach to compressive crack tip load-excursions that take place in such tests because the definition of J through crack extension is theoretically considered violated even for the standard J -integral tests; but periodic partial unloading has been accepted only in favour of an engineering solution by consensus (Landes *et al.*, 1979). Similar consensus can be considered for cyclic J -integral tests which is likely to bring forth understanding related to J - R behaviour of materials (Taraferder *et al.*, 2003). A few earlier research works (Marschall and Wilkowski, 1989; Rudland *et al.*, 1996; Seok *et al.*, 1999; Seok and Murthy, 2000; Taraferder *et al.*, 2003) indicate that fracture behaviour of a material is deleteriously altered due to imposition of compressive load cycles. However, the extent of such deleterious effect seems to depend up on the magnitude of the compressive load and the frequency of load cycle. Accordingly, attempts have been made in this chapter to unfold the monotonic fracture behaviour of AISI 304LN SS and its weldment with significant emphasis on cyclic J - R behaviour of the materials at various extents of cyclic unloading and plastic displacement. The results of cyclic J -integral tests have been compared with their monotonic fracture resistance behaviour. The mechanism associated with the cyclic fracture behaviour in AISI 304LN SS and its weldments has also been addressed.

The major objectives in this part of the investigation in brief are: (i) to determine the monotonic and cyclic fracture toughness of the selected steels (ii) to examine the effect of R ratio and plastic displacement on cyclic J - R curve, and (iii) to understand the damage mechanisms under monotonic and cyclic fracture toughness tests.

4.2 Experimental procedure

4.2.1 Specimen preparation and fatigue pre-cracking

The fracture toughness tests in this investigation were carried out using compact tension specimens of two different orientations. Considering the available form of the material, standard CT specimens with a maximum of 20 mm thickness were possible; however, other dimensions were as per ASTM E1820 were machined following the guidelines of ASTM E1820-09 (2009), in two orientations, LC and CL with respect to pipe geometry. Typical diagram of a CT specimen is shown in Fig.4.1. The exact dimensions of the specimens used in this investigation are shown in Table 4.1. A set of commercially welded pipes of similar dimensions were used to examine the fracture behaviour of the weldments. The welding was done using ER 308L filler electrode by gas tungsten arc welding (GTAW) process in inert argon atmosphere. The welded region was approximately 20 mm in the crown and about 3 mm in the root. It must be noted that the welded pipe specimens employed in this investigation are part of actual components which are used in service as in the case of base metal.

Fatigue pre-cracking of the CT specimens are carried out at room temperature using a decreasing ΔK envelope as described in ASTM standard E647 (ASTM E647-07, 2007) employing a commercial software (Advanced Fatigue Crack Propagation, AFCP) supplied by INSTRON Ltd U.K. The crack lengths were measured by unloading compliance technique using a crack opening displacement (COD) fitted to the integral knife edge machined at the load line of the specimen. The software permitted on-line monitoring of the crack length (a), stress intensity factor range (ΔK) and the crack growth rate per cycle (da/dN). All pre-cracking experiments were carried out at a stress ratio of $R = 0.1$ using a cyclic frequency of 15 Hz and with a starting ΔK (termed as ΔK_0) between 25 and 28 $\text{MPa}\sqrt{\text{m}}$. The magnitude of ΔK was continuously decreased with

crack growth as per the expression $\Delta K = \Delta K_0 \exp\{c(a - a_0)\}$, where the value of 'c' was taken as -0.08, 'a' is the instantaneous crack length and 'a₀' is the notch length. All specimens were pre-cracked to achieve a total crack length of approximately 25 mm, which corresponds to $a/W \approx 0.5$. Details of the actual pre-crack lengths were presented in Table 4.1. The magnitude of ΔK at the end of pre-cracking was kept between 16~18 MPa $\sqrt{\text{m}}$ in all the specimens.

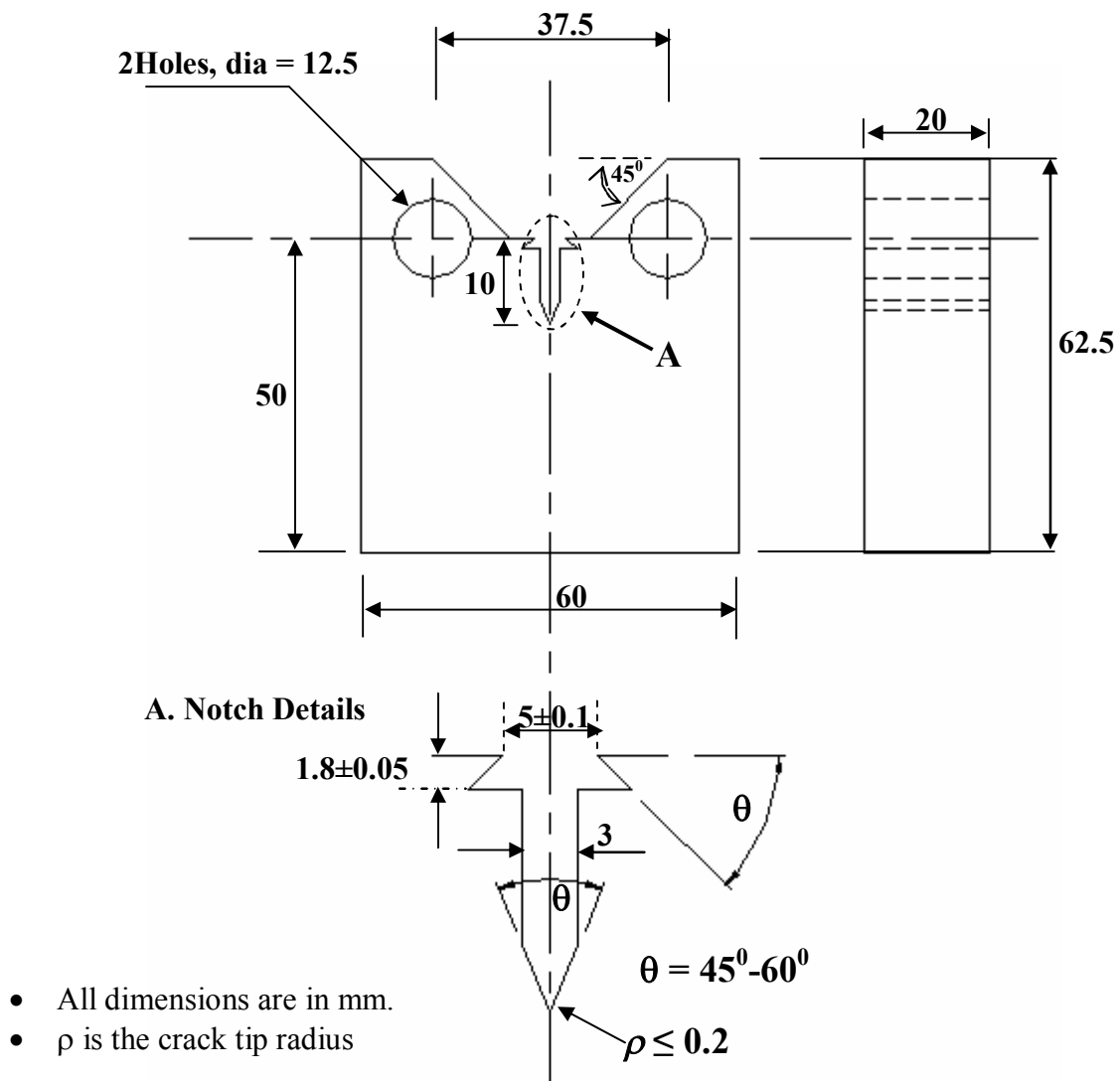


Fig. 4.1 Dimension of the CT specimen

Table 4.1 Details of the tested specimen dimensions

Sl. No.	Specimen Code	Specimen Dimensions			a_0 (mm)
		W (mm)	B (mm)	a_N (mm)	
Monotonic tests					
1	LC1	49.86	19.87	10.01	24.87
2	LC2	50.01	19.92	10.02	25.12
3	LC3	49.97	20.01	10.01	24.83
4	CL1	50.18	20.03	10.02	24.35
5	CL2	50.13	19.96	9.99	25.01
6	CL3	49.96	19.92	10.03	24.88
7	WLC1	49.98	19.95	9.97	25.13
8	WLC2	50.12	20.10	10.10	25.12
9	WLC3	50.01	19.88	10.01	25.01
10	WLC4	50.04	19.96	10.02	24.80
Cyclic Tests					
1	LC4	50.04	19.87	10.03	24.89
2	LC5	50.11	19.90	9.97	25.10
3	LC6	49.98	19.88	10.02	25.02
4	LC7	50.10	20.03	10.01	24.78
5	LC8	49.89	19.78	10.03	25.10
6	LC9	50.01	20.05	10.04	24.78
7	LC10	49.89	19.86	10.01	25.12
8	LC11	50.13	20.01	10.03	25.13
9	WLC5	50.08	19.94	10.01	24.98
10	WLC6	50.12	20.13	9.98	25.01
11	WLC7	50.09	19.98	10.02	24.97
12	WLC8	49.91	20.01	10.01	24.63

W= Width, B= Thickness, a_N = notch length, a_0 = initial crack length

4.2.2 Monotonic J -integral test

Estimation of monotonic J - R curves of the materials was carried out using an INSTRON (model: 8562) servo-electric based machine. Single specimen unloading compliance technique has been used for evaluation of J -integral fracture toughness. In this method the crack lengths are determined from elastic unloading compliance measurements. This is done by carrying out a series of sequential loading, unloading and reloading to predetermined displacement levels during a test. The loading-unloading extents were selected in a manner that the loading cycles are almost equally spaced along the load

versus displacement record. These experiments were carried out following ASTM E1820-09 (2009). In the single specimen J -integral tests, unloading should not exceed more than 50% (ASTM E1820-09, 2009) of the current load value, thus design and control of the test procedure is important. Some initial trial experiments indicated that a specific actuator displacement control for the selected steel could lead to the desired test procedure. This control consisted of loading a specimen to a level of 0.3 mm, unloading through 0.15 mm, reloading through 0.15 mm and then repeating the sequence till an appreciable load drop was noticed on the load displacement plot. A schematic representation of the variation of displacement with time used for the present tests is shown in Fig. 4.2. The displacement cycles were carried out using a crosshead ramp velocity of 0.003 mm/sec at room temperature. The tests were controlled through a computer attached to the machine. The actuator displacement, load and the load line displacement (LLD), were recorded continuously at a frequency of 1 Hz. The magnitude of LLD was monitored by a crack opening displacement (COD) gauge attached to the specimen. A minimum of approximately 50 data points of load-LLD was collected from the unloading part of the loading sequence for crack length calculations. Typical load-LLD plots for AISI 304LN SS base metal and weldment tested at room temperature are shown in Fig. 4.3.

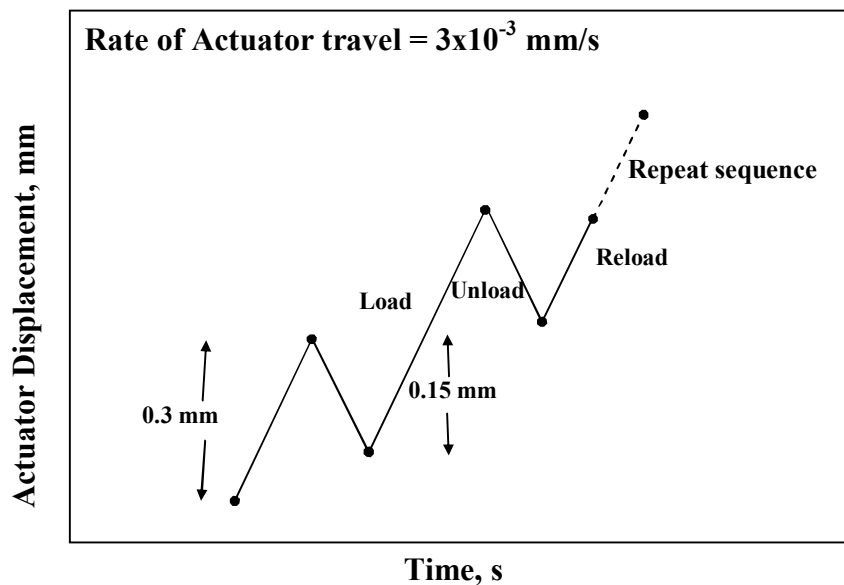


Fig. 4.2 Loading sequence used for constructing monotonic J -R curve

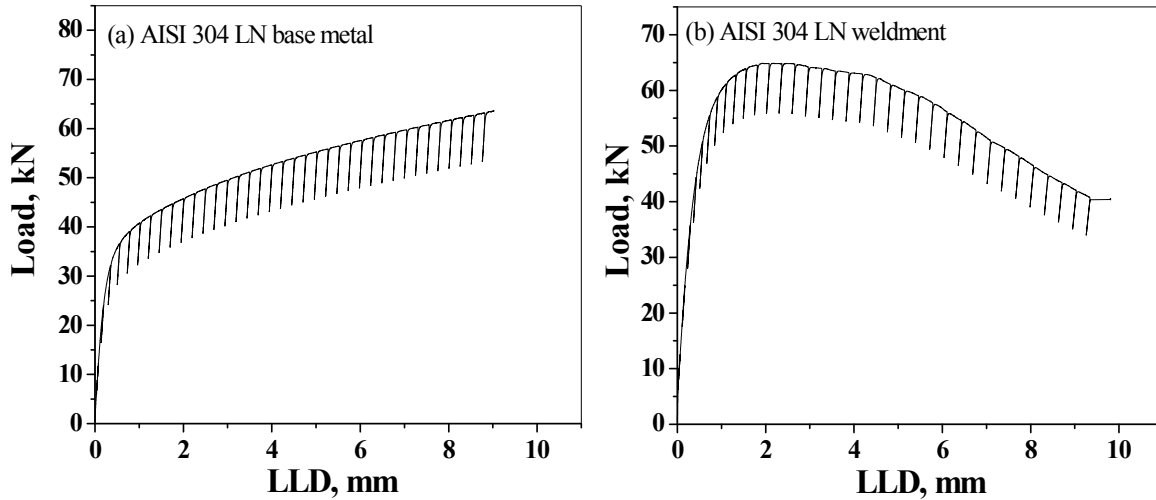


Fig. 4.3 Typical Load-LLD curves for AISI 304LN (a) base metal and (b) weldment recorded during a monotonic J -integral test

The specimens, after the J -integral tests, were post fatigue cracked to delineate the crack growth region. The initial and the final crack lengths were measured as recommended in the ASTM standard (ASTM E1820-09, 2009) using a traveling microscope and these values were then compared with the crack lengths estimated through unloading compliance technique. The magnitude of the crack lengths measured by the microscope are found to be within ± 0.05 mm of that calculated by compliance crack length (CCL) relation as discussed later in section 4.2.4. This procedure for estimating crack length was followed for all the tested specimens.

4.2.3 Cyclic J -integral test

The cyclic J - R tests on the fabricated specimens were estimated using an INSTRON (model: 8562) machine and with the use of a COD gauge. A series of these tests were carried out; the details of the specimen dimensions used for this test are shown in Table 4.1. An additional X-Y recorder was attached to the analog output ports of the machine to record the load displacement plot during a test, apart from recording the digital data in a computer for monitoring the inflection points as described below in the test sequence for these tests are being carried out in a semi-automated mode.

The loading sequence for the cyclic J - R test is given in Fig. 4.4 while the employed test variables are summarized in the Table 4.2. The cyclic J tests were carried

out using an actuator speed of 0.5 mm/min. Each test consisted of the following displacement steps as shown in Fig. 4.5.

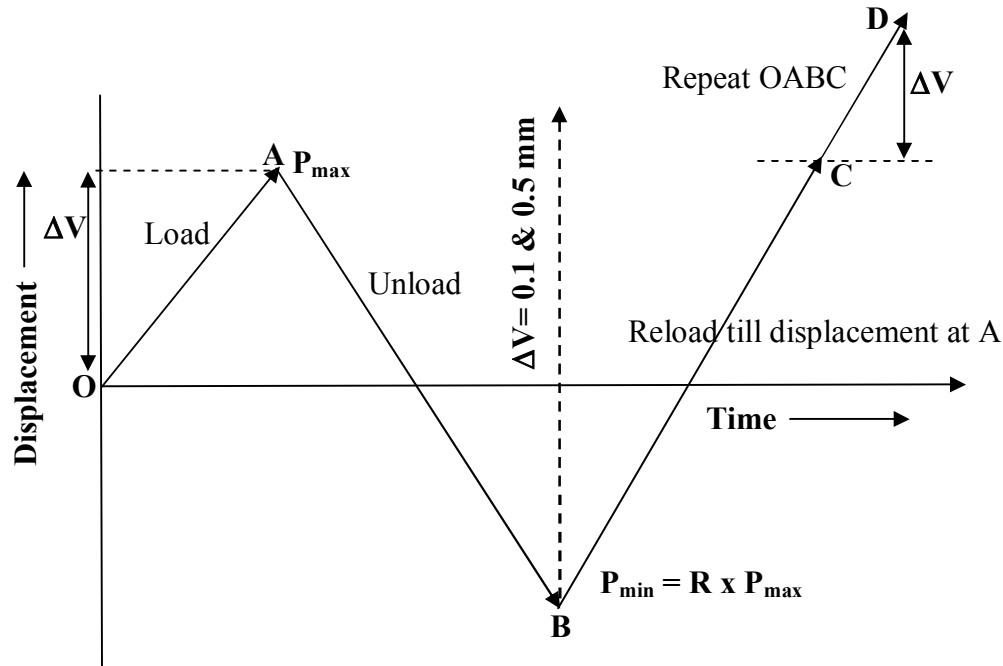


Fig. 4.4 Loading sequence in a cyclic *J-R* test

Table 4.2 Test variables for cyclic *J-R* tests

Specimen Type	Stress ratio (R)	Plastic displacement (ΔV), mm
Base Weld	-0.5	0.1
	-0.8	
	-1.0	0.5
	-1.2	

- (1) A specimen was loaded (segment OA in Fig. 4.5) to a desired plastic displacement level ΔV (0.1 or 0.5 mm).
- (2) This was then unloaded to the desired predetermined load P_{\min} ($= R \times P_{\max}$) where R is the stress ratio at which the test was being conducted and P_{\max} is the load achieved before start of unloading. The magnitude of R was varied in different tests (§ Table 4.2).
- (3) Next the specimen was reloaded till it achieved the displacement level corresponding to point C in the unloading path (as shown in Fig. 4.5).

- (4) The specimen was further loaded to the next desired plastic displacement level (as shown by point D in Fig. 4.4 as well as in Fig. 4.5) and the steps 2 to 4 were iterated. These iterations were continued till the maximum load-bearing capacity of the sample or to an extent corresponding to some significant crack growth in the specimen (as observed on the specimen surface).
- (5) After the completion of the cyclic J -integral test, the specimens were post fatigue cracked till failure.

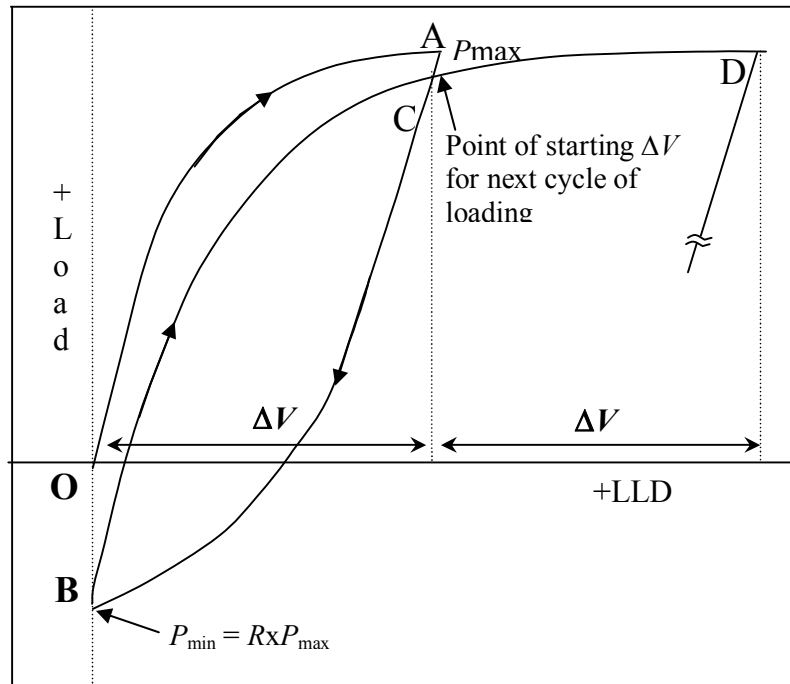


Fig. 4.5 Demonstration of loading sequence for negative stress ratio cyclic J -R tests

The digital data of load, position and LLD were collected through a computer attached to the machine. The initial and the final crack lengths were measured using a travelling microscope as described in section 4.2.2 on the broken fracture surfaces of specimens. The measured values of crack length were found to be within ± 0.05 mm of what have been estimated using CCL relations (eqn. 4.3 in section 4.2.4). Typical load-LLD data recorded during cyclic J -integral tests of AISI 304LN SS base metal and its weldment are shown in Fig. 4.6.

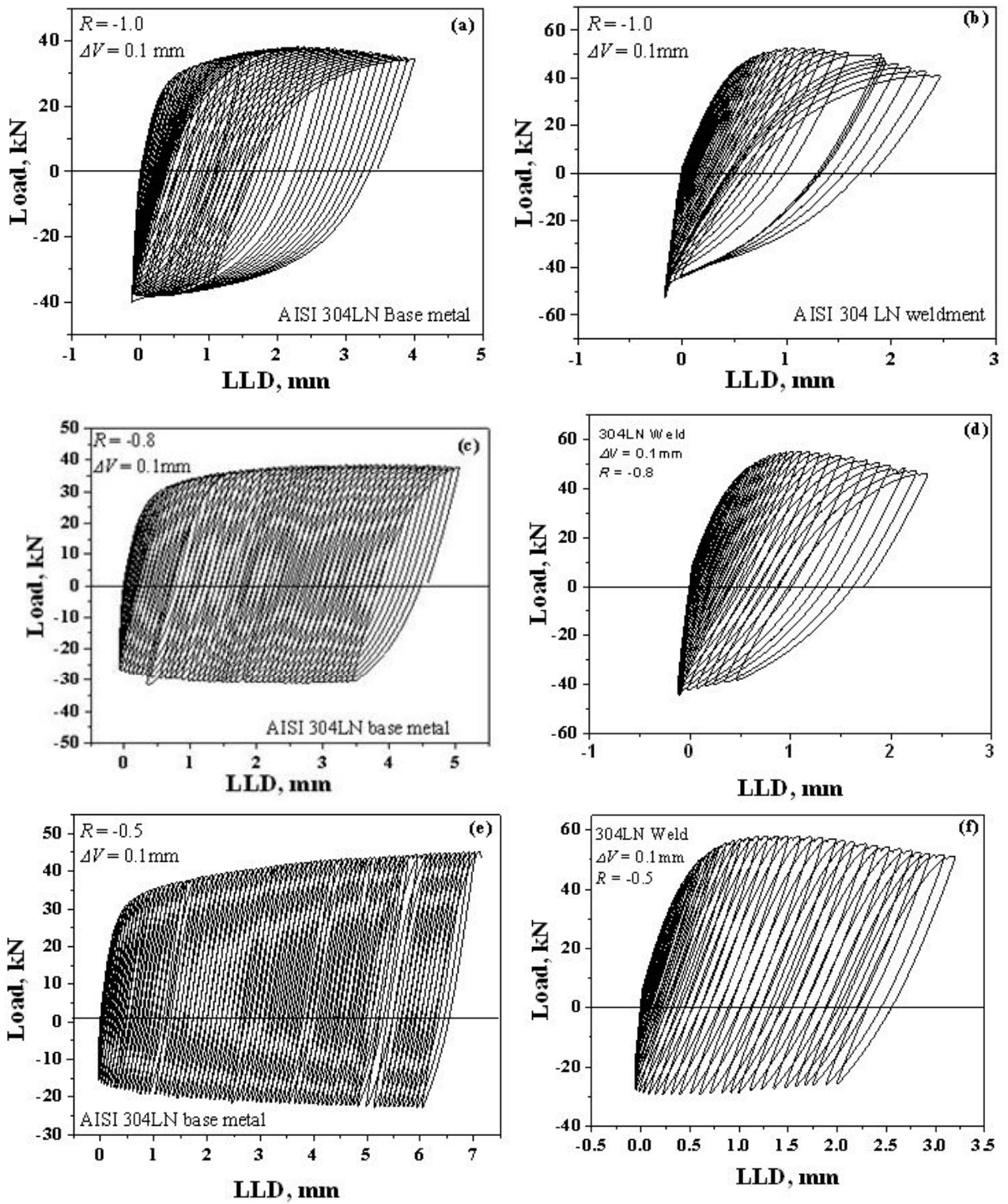


Fig. 4.6 Typical Load-LLD plots obtained during cyclic *J-R* test of base metal and weldment of 304LN steel

4.2.4 Generation of J - R curve under monotonic and cyclic J -integral test

The experimental data generated from the monotonic J -integral tests were analyzed following the recommendations of ASTM standard E1820-09 (2009). The load vs. LLD data obtained from the tests were analyzed to compute the magnitude of crack extension (Δa) and the corresponding J -integral value at each unloading sequence.

The slope of each unloading path of load vs. LLD data was calculated by linear regression analysis. The inverse of the slope yielded the compliance (C_i) of the specimen corresponding to the load from which the unloading has been carried out. The obtained C_i -values were corrected for the specimen rotation using the following expression to get the modified compliance (C_{ci}) of the specimen at that particular load (ASTM E1820-09, 2009).

$$C_{ci} = \frac{C_i}{\left(\frac{H^*}{R} \sin \theta - \cos \theta\right) \left(\frac{D}{R} \sin \theta - \cos \theta\right)} \quad \dots (4.1)$$

where H^* = initial half-span of the load points (centre of pin holes)

R = radius of rotation of the crack centre line, $(W+a)/2$

D = one half of the initial distance between the displacement measurement points

θ = angle of rotation of a rigid body element about the unbroken midsection line

usually expressed as $\sin^{-1}[(d_m/2+D)/(D^2+R^2)^{1/2}] - \tan^{-1}(D/R)$ in which

d_m = total measured load-line displacement.

The crack length (a_i) at the point of interest was next estimated using the expression suggested by Hudak and Saxena (1978) as:

$$\frac{a_i}{W} = 1.000196 - 4.06319U_x + 11.242U_x^2 - 106.043U_x^3 + 464.335U_x^4 - 650.677U_x^5 \quad \dots (4.2)$$

$$\text{where } U_x = \frac{1}{(B_e E' C_{ci})^{1/2} + 1} \quad \dots (4.3)$$

$$B_e = \text{Effective thickness of the specimen} = B - \left[\frac{(B - B_N)^2}{B} \right] \quad \dots (4.4)$$

$$E' = \frac{E}{(1 - \nu^2)} \quad \dots (4.5)$$

W = Width of the specimen

B = Total thickness of the specimen

B_N = Net thickness of the specimen

Δa = a_i - a₀ = magnitude of crack extension

The magnitude of *J* is the sum of its elastic and plastic component denoted by *J_e* and *J_{pl}*.

The elastic component of *J* was calculated using the equation:

$$J_e = \frac{K_i^2(1 - \nu^2)}{E} \quad \dots (4.6)$$

where *K_i* is the elastic stress intensity parameter evaluated using the expression:

$$K_i = \left[\frac{P_i}{(BB_N W)^{1/2}} \right] f \left(\frac{a_i}{W} \right) \quad \dots (4.7)$$

where,

$$f \left(\frac{a_i}{W} \right) = \frac{\left((2 + a_i/W)(0.886 + 4.64(a_i/W)) - 13.32(a_i/W)^2 + 14.72(a_i/W)^3 - 5.6(a_i/W)^4 \right)}{(1 - a_i/W)^{3/2}} \quad \dots (4.8)$$

The magnitude of *J_{pl}* was calculated by considering only load vs. plastic load line displacement. In order to obtain the latter, the elastic parts of displacements at different loads were first calculated using the slope of the initial load-LLD diagram. A simple subtraction of the elastic component from the total displacement yielded the plastic part of LLD. The area under the load vs. plastic LLD data from the start of the test to the load of interest was calculated to obtain the magnitude of *J_{pl}*. This was done by using the expression (ASTM E 1820-09, 2009):

$$J_{pl(i)} = \left(J_{pl(i-1)} + \frac{\eta_{i-1} (A_{pl(i)} - A_{pl(i-1)})}{b_{i-1} B_N} \right) \left(1 - \frac{\gamma_{i-1} (a_i - a_{i-1})}{b_{i-1}} \right) \quad \dots (4.9)$$

where

A_{pl(i)} - *A_{pl(i-1)}* = Incremental plastic area

η_(i-1) = 2.0 + 0.522(*b_{i-1}* / *W*)

$$\text{and } \gamma_{(i-1)} = 1.0 + 0.76(b_{i-1}/W)$$

The obtained values of J and the corresponding crack extension Δa were plotted to get the J - Δa curves of the material.

The crack lengths under cyclic J -integral tests were calculated using the unloading data falling between P_{\max} and 70% of P_{\max} . The selection of the unloading data range for estimating the crack length was based on its compatibility with that estimated by optical measurements. In case of cyclic J , the area under the envelope curve above the baseline (i.e. $P=0$ as shown in Fig. 4.7) has been used to measure J . The values of J_{eI} and J_{pI} were estimated by similar procedure as prescribed (ASTM E1820-09, 2009) for monotonic J -integral tests. Schematic representation of the procedure for estimating cyclic J - R curve is shown in Fig. 4.7.

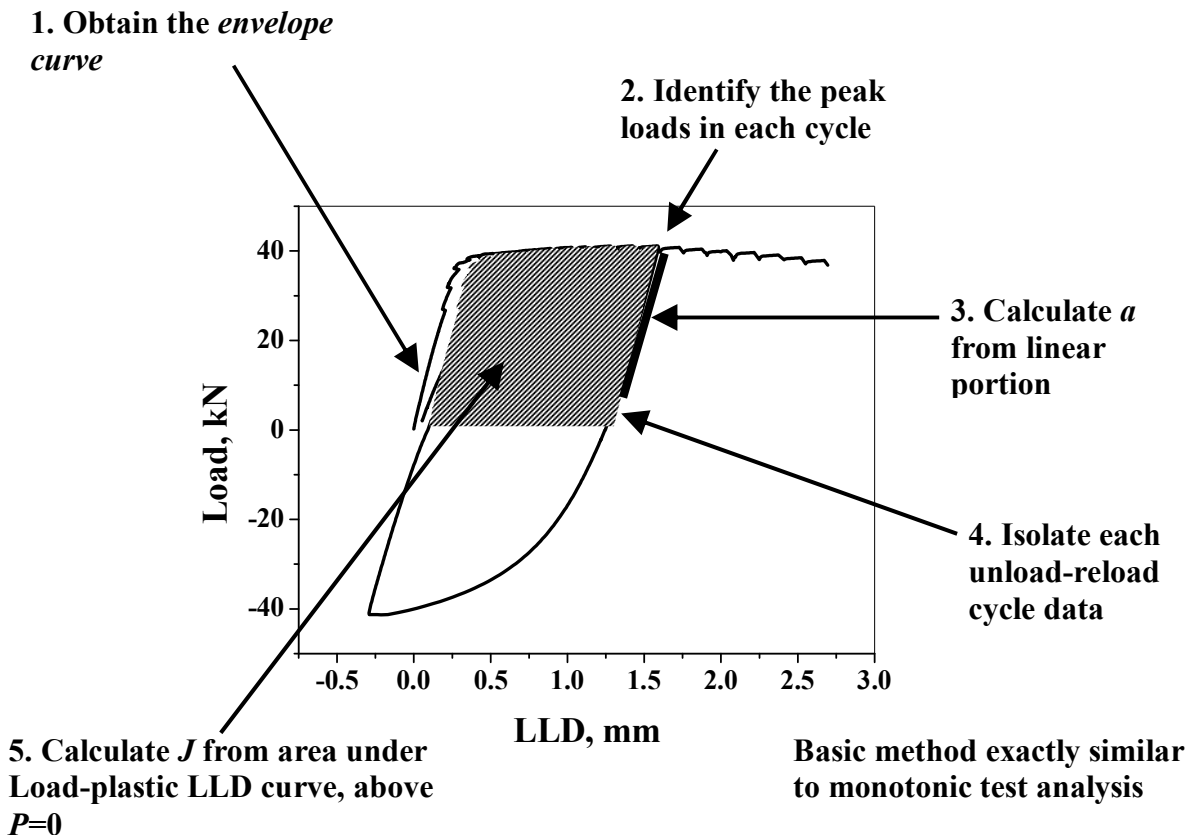


Fig. 4.7 Schematic representation of the procedure for estimating cyclic J - R curve

4.2.5 Fractography

The end of ductile crack extension during loading of the specimens, subjected to J -integral test, was delineated by post fatigue cracking, and then the specimens were over loaded to fracture. Approximately 15 mm x 15 mm long samples were cut from near the central plane of the fractured surface of each tested specimens for fractographic examinations. In addition, some fractured samples under cyclic J -integral tests were cut from near the notched region of the tested specimens and were polished up to 1 μ m diamond finish to examine the crack tip profile. The fractured surfaces were ultrasonically cleaned and examined using a scanning electron microscope [Model: S 3000-N, Hitachi, Japan]. This was done to examine the governing features of stable crack extension as well as to understand the mode of failure.

4.3 Results and discussion

In this section at the outset the procedures employed to evaluate critical values of J under monotonic and cyclic fracture toughness tests are presented followed by discussion on the effect of specimen orientation on monotonic J - R curves. The results related to cyclic J - R curves are discussed next with respect to (i) effect of stress ratios on cyclic J - R curve, (ii) effect of plastic displacement on cyclic J - R curve, (iii) monotonic fracture toughness vis-à-vis cyclic fracture toughness, and (iv) micro mechanisms of fracture under monotonic and cyclic loading.

4.3.1 Determination of monotonic J -integral fracture toughness

Typical J - R curves (plot of J vs. Δa) for specimens LC1 and WC1 representing base metal and weldment, respectively are shown in Fig. 4.8. Initially attempts were made to evaluate conditional fracture toughness J_Q , by conventional method, which consists of locating the intercept of a theoretical blunting line with the J - R curve. The equation of the blunting line as suggested in the ASTM standard E1820-09 (2009) is:

$$J = m\sigma_0\Delta a \quad \dots (4.10)$$

where, the value of m is the slope of blunting line and is taken as 2. The parameter σ_0 is the flow stress of the material at the test temperature and was taken as $(\sigma_{ys} + \sigma_{uts})/2$. The values of σ_{ys} and σ_{uts} are already reported in Table 3.3. The values of σ_{ys} and σ_{uts} were taken from the results of tensile tests carried out at nominal strain rate of 0.0001 s⁻¹.

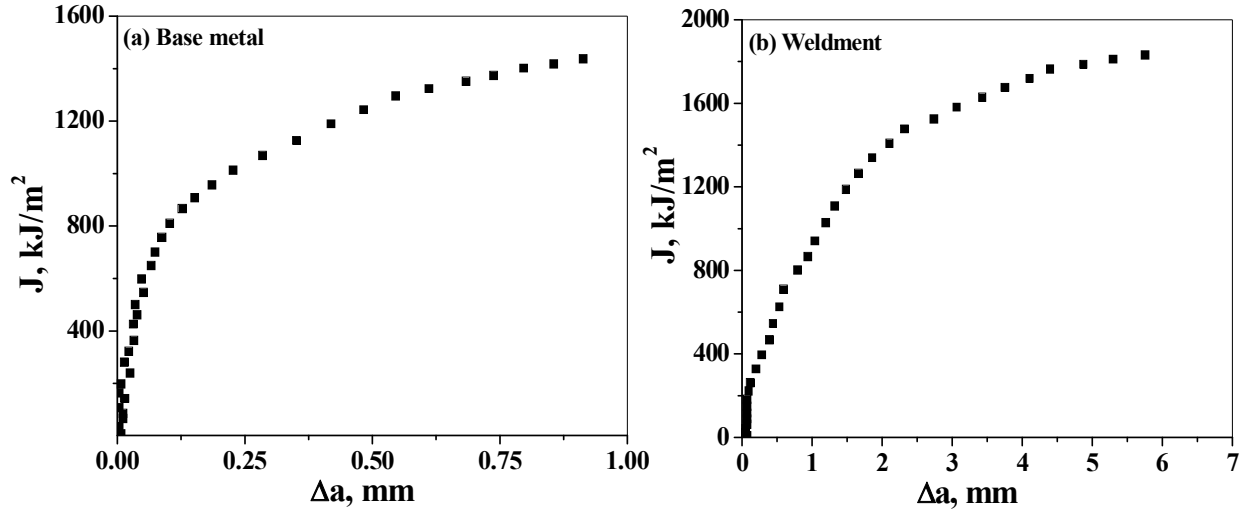


Fig. 4.8 Typical J - R curves for AISI 304LN (a) base metal and (b) weldment obtained during monotonic J -integral test

The ASTM blunting line for the specimen LC1 was estimated and is shown in Fig. 4.9. This line (in Fig. 4.9) does not intersect the experimental J - R curve. Similar observations were also made for the other tested specimens as listed in Table 4.1. These observations are in following the results reported by several earlier investigators on high toughness materials (O'Brien and Ferguson, 1982; Srinivas *et al.*, 1994; Heevens *et al.*, 1998). In order to estimate the J_Q values, an experimental blunting line was then drawn considering the initial linear portion of J vs. Δa data for each of the specimens. The magnitudes of slopes of such blunting lines were estimated, and the values of m were calculated from the slope values using the concerned value of σ_0 . A line parallel to the experimental blunting line at $\Delta a = 0.2$ mm was next constructed. The intersection of this offset line with the fitted J - R curve was considered as the critical value of J , i.e. J_Q . In order to fit the power law equation (eqn. 4.11) to J - R curve, the experimental points of J vs. Δa lying between two exclusion lines i.e 0.15 mm and 1.5 mm were considered. The exclusion lines were constructed parallel to the experimental blunting line at Δa -offset values of 0.15 mm and 1.5 mm following the ASTM standard E1820-09 (2009). The experimental results between two exclusion lines were then fitted using equation of the form (ASTM E1820-09, 2009):

$$J = C_1 (\Delta a)^{C_2} \quad \dots (4.11)$$

where C_1 and C_2 are material constants at the test conditions.

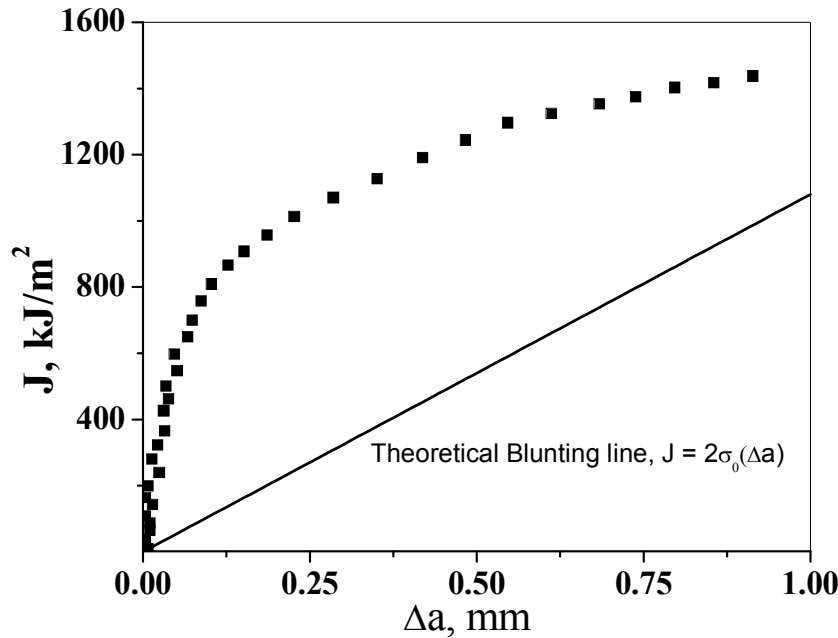


Fig. 4.9 Theoretical blunting line for AISI 304LN base metal

Typical plots showing the estimated values of J_Q for base metal specimens in LC and CL orientations are shown in Fig. 4.10. Estimations of J_Q for all specimens including those with weldments were also made in a similar manner. The estimated values of C_1 , C_2 , J_Q , m and dJ/da are shown in Table 4.3. The estimated J_Q values were next examined for the validity of referring these as J_{IC} as per ASTM standard E1820-09 (2009). The validity criterion states that thickness (B) and the remaining ligament (b_0) of a specimen should be greater than $10(J_Q/\sigma_{ys})$. A typical calculation indicates that thickness should be at least 34.42 mm for base metal specimens (LC1) considering $J_Q = 1155 \text{ kJ/m}^2$ and $\sigma_{ys} = 340 \text{ MPa}$ in order to refer J_Q as J_{IC} . Similarly, for a typical weldment sample (WC1) having $J_Q = 640 \text{ kJ/m}^2$ and $\sigma_{ys} = 560 \text{ MPa}$, the minimum thickness required for qualifying J_Q as J_{IC} is 11.44 mm. The calculated thickness values for base metal are therefore higher than the employed thickness of the tested specimens and even that of the available maximum thickness of the PHT pipe. Hence the evaluated J_Q values for base metal cannot be referred as J_{IC} as per ASTM standard E1820-09 (2009), whereas the same for the weldment can be referred as J_{IC} . Similar results (Table 4.3) were obtained when the J_Q values for the other specimens were also subjected to the validity test; the wall thickness of the PHT pipe does not permit to fabricate specimens of adequate thickness to get a valid J_{IC} of the base metal. The crack growth resistance parameter dJ/da has been

estimated as the slope of the linear regression line of J and Δa data points, lying between crack extension of 0.2 mm and 6.25 mm (i.e. 25% of the remaining ligament) following Newman *et al.* (1988). The magnitudes of dJ/da are also included in Table 4.3.

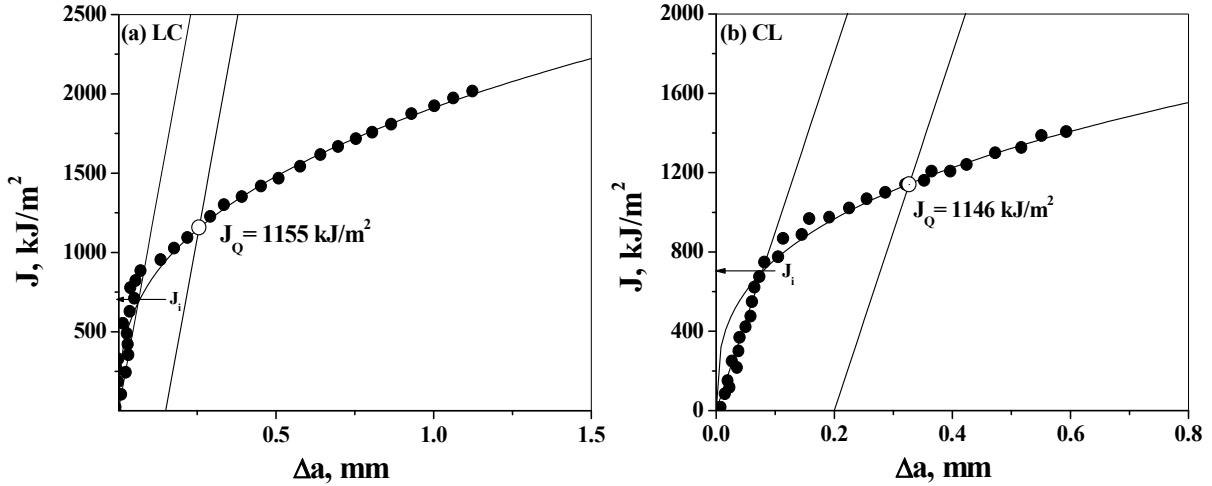


Fig. 4.10 Typical monotonic J - R curves for AISI 304LN SS base metal at (a) LC and (b) CL orientations

Table 4.3 J -integral fracture toughness parameters of the investigated steels

Specimen code	C_1	C_2	J_Q kJ/m ²	m	dJ/da MJ/m ³
LC1	1676.9	0.34	1076	16.67	4879.5
LC2	1912.6	0.37	1155	20.10	3975.4
LC3	1487.6	0.26	1092	19.98	4235.6
CL1	1267.2	0.533	915	12.69	3469.2
CL2	1481.4	0.456	1124	15.45	4245.1
CL3	1568.4	0.412	1146	17.79	3987.1
WLC1	914.3	0.63	550	7.13	1402.2
WLC2	1152.2	0.66	587	10.38	1116.7
WLC3	1012.5	0.54	640	8.39	1149.1

C_1 and C_2 = Constants in eqn. (4.11), m = slope of blunting line

The average monotonic fracture toughness of AISI 304LN SS and its weldments are calculated as 1107 ± 27 kJ/m² and 592 ± 45 kJ/m², respectively. The estimated monotonic fracture toughness values of AISI 304LN SS base metal and its weldment

when compared with some reported values of 1280 kJ/m² and 615 kJ/m² (Report No. MST/304IR-1), are found to be lower. The observed difference could be attributed to the variation in the specimen thickness considered in the two investigations; specimen thickness considered in the present study is 20 mm while that in the earlier report is 12.7 mm. Rudland *et al.* (1996) have also reported average fracture toughness values of AISI 304 SS base metal and weldment as 943 kJ/m² and 623 kJ/m². The obtained fracture toughness values of AISI 304LN SS base metal and its weldment are therefore in close agreement with the reported values of Rudland *et al.* (1996). The minor variations in the initiation toughness values could possibly have arisen due to minor variations in the material characteristics used in these two investigations.

The obtained results related to the fracture behaviour of LC and CL specimens for base metal (§ Table 4.3, Fig. 4.10) indicate that fracture toughness (J_Q) and crack growth resistance (dJ/da) do not get significantly influenced by orientation effect. However, the base metal indicates higher fracture resistance than its weldment as expected. Moreover, it is observed that the scatter associated with the weldment (± 45 kJ/m²) is relatively larger compared to that of the base metal (± 27 kJ/m²) of the investigated steel. Two reasons can be ascribed for the relatively high scatter associated with the average fracture toughness value of the weldments. First, the multi-pass welding, in general, is expected to produce microstructural heterogeneity which can be thought to be responsible for the larger scatter in the estimated values of fracture toughness of the weldments. Secondly, it is difficult to contain crack growth within the fusion zone during fracture testing. Extension of a crack into the heat affected zone is often unavoidable; this phenomenon would result in an average fracture toughness value of the different regimes which may not be the true representative of the fusion zone. It may be mentioned here that the V-shaped weld in the pipe from which the specimens were fabricated had the dimension of the crown as 20 mm and that of the root as 3 mm and, therefore, a portion of the crack extending to HAZ region could not be ruled out resulting in larger scatter associated with fracture toughness of the weldments.

4.3.2 Determination of the cyclic J -integral fracture toughness

Typical recorded load versus load line displacement (LLD) plots for AISI 304 LN base metal and its weldment, generated during cyclic J - R tests are shown in Fig. 4.6.

Comparison between displacement controlled cyclic fracture tests and corresponding quasi static monotonic tests in Fig. 4.11 reveal that cyclic loading reduces both load carrying capacity and energy absorbing ability of AISI 304LN SS. The J - R curves were constructed using load-LLD data as described in section 4.2.3. The magnitudes of J_e and J_{pl} were calculated using eqn. (4.6) and eqn. (4.9). The values of J_{pl} were estimated by considering only the area under the tensile loading part of the load-LLD data following several earlier reports (Marschall and Wilkowski, 1989; Rudland *et al.*, 1996; Seok *et al.*, 1999; Seok and Murthy, 2000). It is noted that the cyclic J - R curves vary with change in stress ratio (R) and plastic displacement (ΔV). In order to assess this phenomenon, systematic studies have been carried out to evaluate cyclic J - R curves for conditions of varied stress ratio and plastic displacement.

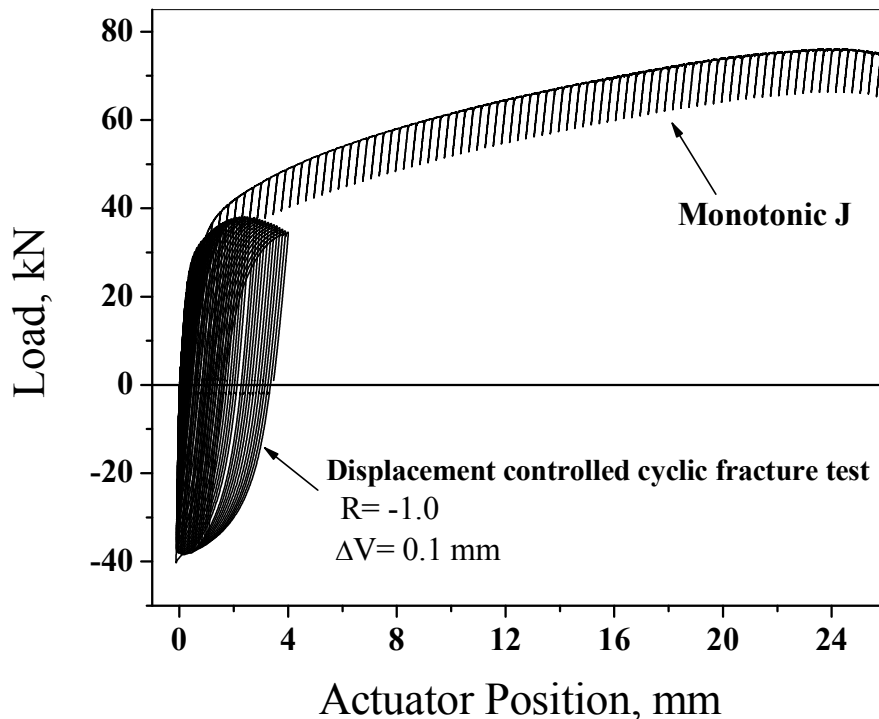


Fig. 4.11 Load-Position curves obtained from monotonic and cyclic fracture tests of AISI 304LN stainless steel

4.3.2.1 Effect of stress ratio on cyclic fracture toughness

Rudland *et al.* (1996) have shown that monotonic J - R curve at $R = 0.9$ is almost identical to the cyclic J - R curves at $R=0$ for three different levels of plastic displacements for

304 SS. Based on this information a series of tests with only negative R ratio have been made here in order to understand the effect of stress ratio on J_{QC} . Typical J - R curves generated using the experimental load-LLD data for AISI 304LN base metal and weldments with $R < 0$ is shown in Fig. 4.12. The J - R curves are found to lie systematically below each other with decrease in stress ratio. It is obvious from Fig. 4.13 that the estimated cyclic fracture toughness values (J_{QC}), decrease with decreasing stress ratio (R) up to $R = -1.0$, thereafter it indicates a marginal increasing trend. Information related to cyclic J - R curves under tension-compression load cycle is limited (Landes and McCabe, 1983; Landes and Liaw, 1987; Seok and Murthy, 2000; Rudland *et al.*, 1996; Marschall and Wilkowski, 1989); Seok *et al.*, 2000). Seok *et al.* (1998, 2000) have observed that the resistance to crack propagation for SA516 steel decreases as it is subjected to increased compressive loads; the minimum resistance to crack propagation being encountered by these authors was at stress ratio $R = -1.0$. Rudland *et al.* (1996) have made similar observation for AISI 304 and SA 106 B steels; but the minimum resistance to crack initiation is reported to be at $R = -0.8$ and at -1.0 for SA 106 B steel and 304LN SS respectively. A comparison of the present results related to estimated J_{QC} values (Fig.4.13) with those reported by earlier investigators (Prabha, 2004; Singh *et al.*, 2003; Roy *et al.*, 2009) indicate a general trend. It can be inferred that resistance to crack initiation in cyclic loading of structural materials deteriorates with increased magnitude of the compressive load cycle up to about $R = -1.0$, below which there is no further deterioration in the resistance to crack propagation. Rudland *et al.* (1996) have explained the trend of variation of fracture toughness with stress ratio in terms of re-sharpening of the blunted crack tip and the voids formed ahead of it. It has been observed in this investigation that both the crack tip and the voids ahead of it get compressed during the compressive load cycle and leads to the formation of a sharp crack tip, which needs less amount of energy to open up in the next cycle of tensile load. This phenomenon causes decrease in resistance to crack propagation in specimens tested at $R < 0$. The occurrence of the saturation of cyclic unloading at high negative R ratios is presumably due to complete closure of the crack, leading to the transfer of load through the crack faces in preference to the compressive deformation at the crack tip (Kobayashi *et al.*, 1992).

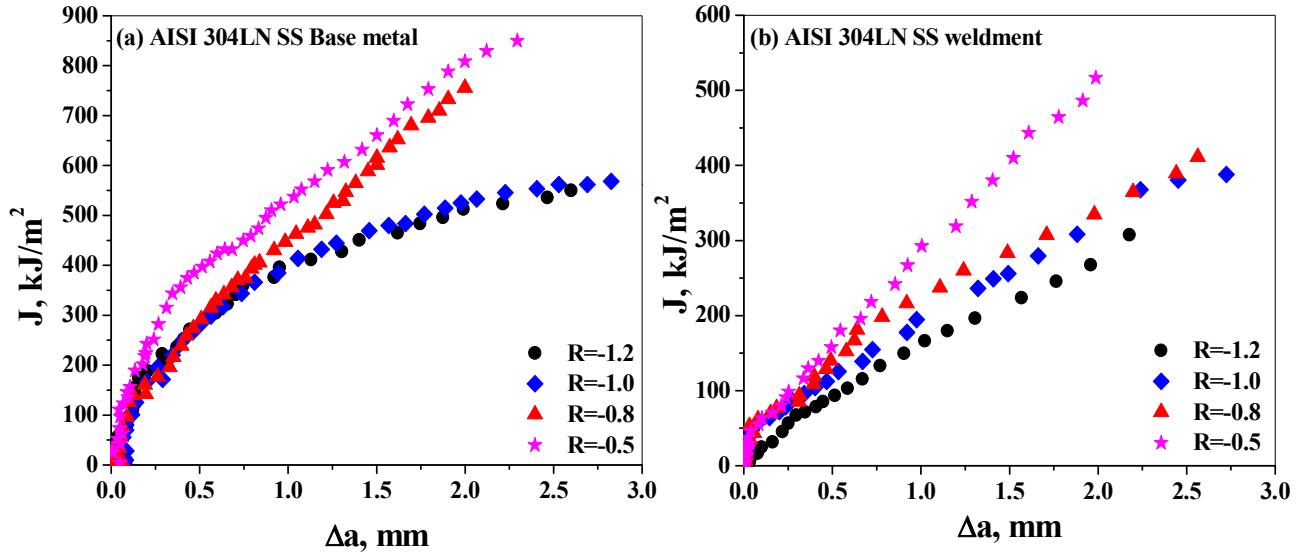


Fig. 4.12 Typical cyclic J - R curves for AISI 304LN (a) base metal (b) weldment

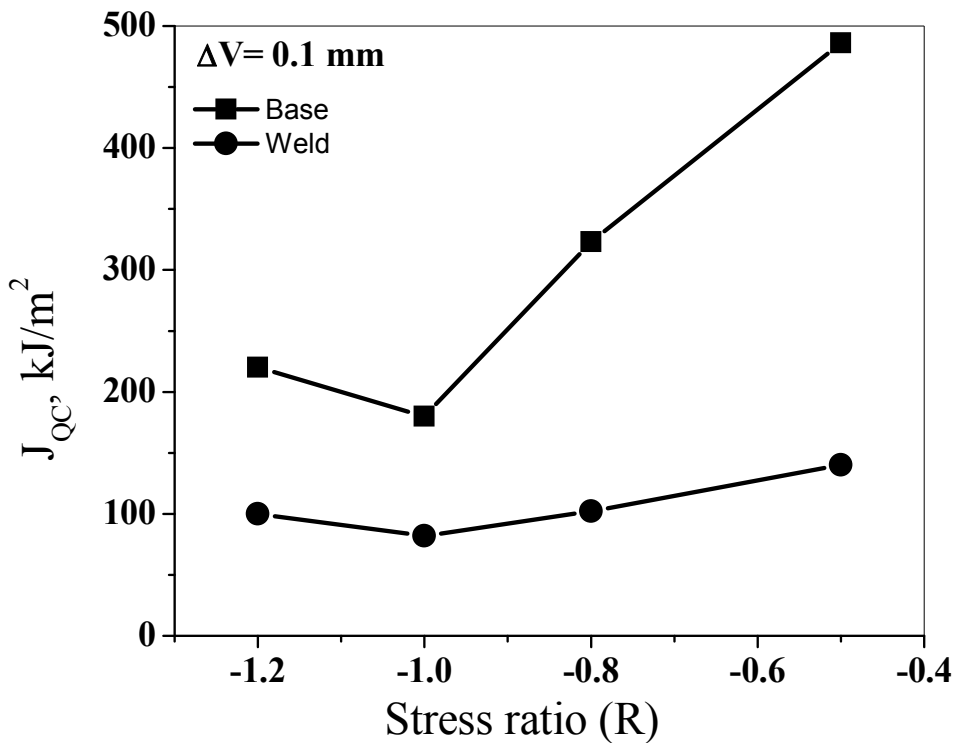


Fig. 4.13 Typical variation of cyclic fracture toughness (J_{QC}) with stress ratio (R) for AISI 304LN base metal and its weldment

4.3.2.2 Effect of plastic displacement on cyclic fracture toughness

The effect of the extent of plastic displacement on cyclic J - R curves is illustrated in Fig. 4.14 for stress ratios of -0.5 , -0.8 , -1.0 and -1.2 . At negative stress ratio, lower extents of plastic displacement lead to enhanced degradation of the resistance to crack propagation. This is obvious from the results shown in Fig. 4.14 where one can notice that cyclic J - R curve at $\Delta V = 0.1$ mm lies quite below that at $\Delta V = 0.5$ mm. The cyclic fracture toughness (J_{QC}) values determined using $\Delta V = 0.5$ mm are higher compared to that determined from similar tests carried out at $\Delta V = 0.1$ mm (Fig. 4.15). Prabha (2004) has reported similar results for SA333 Grade-6 steel. So it can be inferred that at negative stress ratio, lower plastic displacement leads to higher degradation to crack propagation resistance in structural materials.

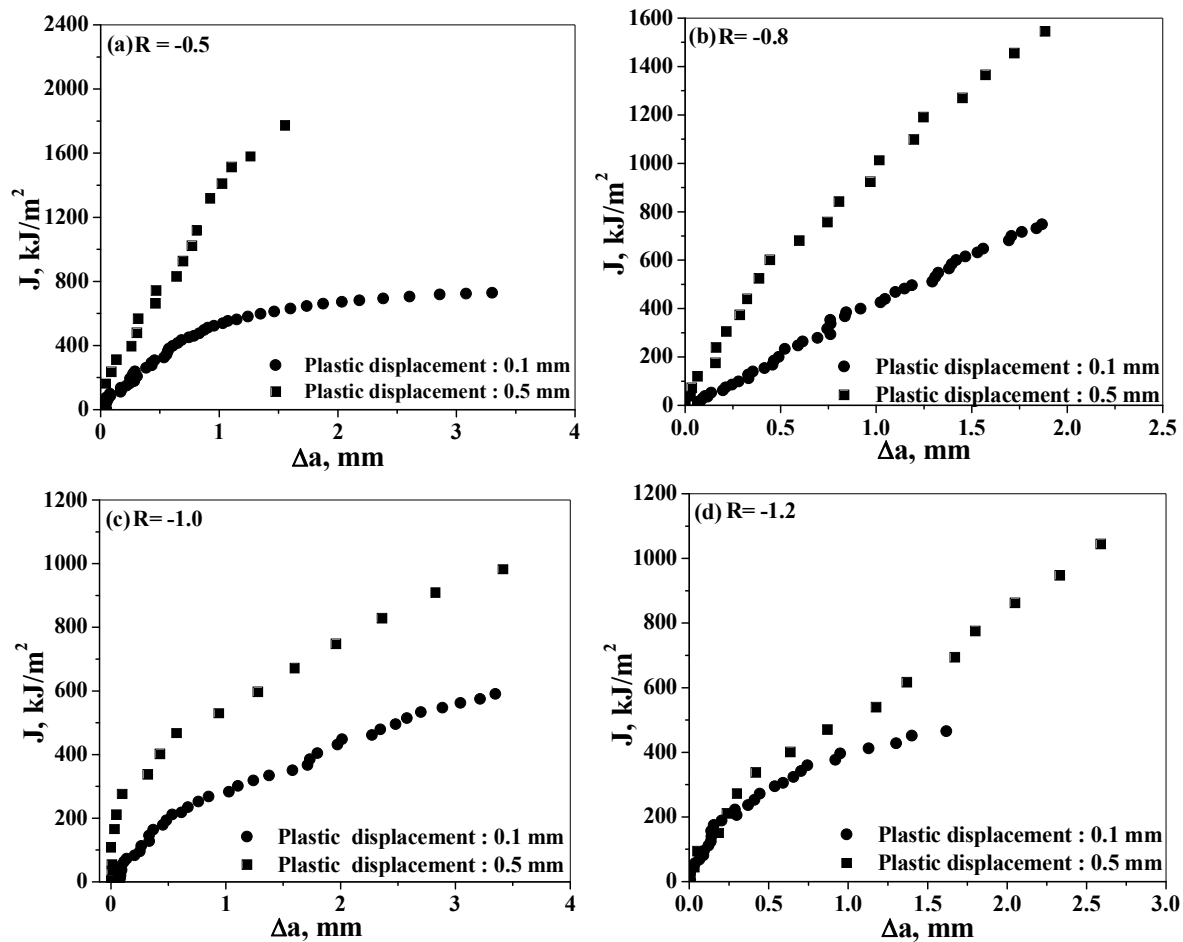


Fig. 4.14 Effect of plastic displacement (ΔV) on cyclic J - R curves of AISI 304LN base metal for (a) $R = -0.5$, (b) $R = -0.8$, (c) $R = -1.0$ and (d) $R = -1.2$

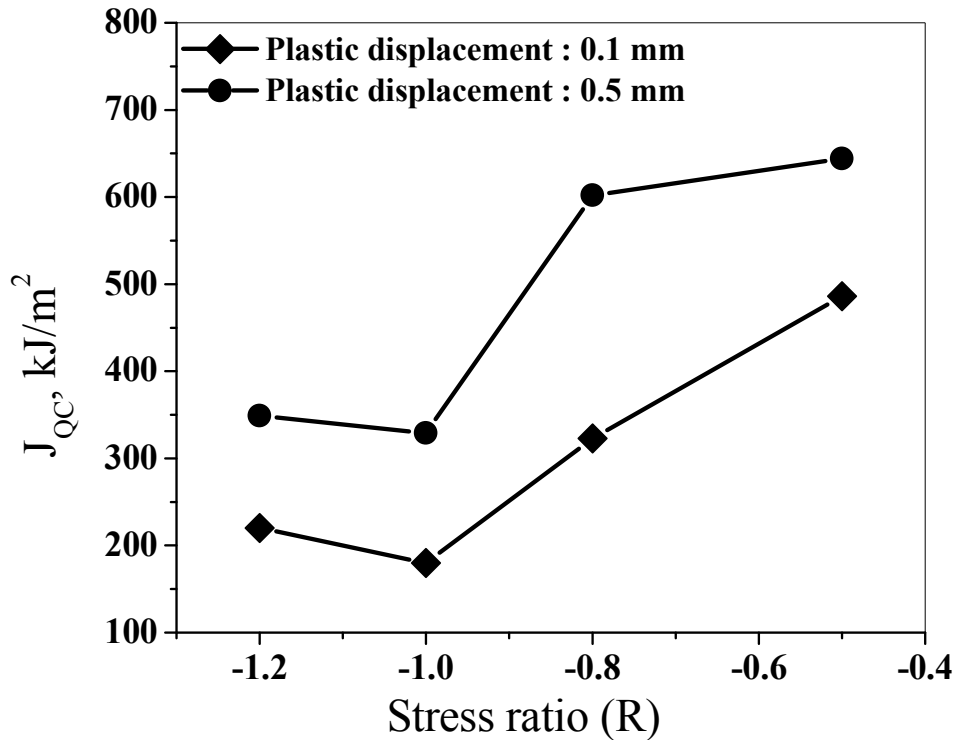


Fig. 4.15 Typical variation of cyclic fracture toughness (J_{QC}) with stress ratio (R) for AISI 304LN base metal at different extents of plastic displacement (ΔV)

Any decrease in plastic displacement during cyclic J - R tests means imposition of more number of cycles to generate appropriate variation between J and Δa . Alternately, when more number of cycles is imposed on a structural steel at negative stress ratio, the resistance to crack propagation degrades in comparison to its magnitude determined at lower number of cycles. The decrease in the amplitude of cyclic J - R curves with increase in number of cycles is considered to be due to increased residual tensile stress at the crack tip. Seok *et al.* (1999, 2000) have shown that when a specimen passes through zero load from compressive load, some amount of tensile residual stress is left at the crack tip at zero load, and increased number of cycles increases the magnitude of this residual stress. This observation gets supported by stress analysis carried out by Seok *et al.* (1999, 2000). Thus, the crack tip is subjected to more number of cycles at lower ΔV than that at higher ΔV . Since higher magnitude of tensile residual stress builds up at the crack tip in experiments conducted with lower magnitude of ΔV , the applied stress in conjunction with this results in inferior resistance to crack propagation.

4.3.2.3 Determination of critical J and dJ/da under cyclic J -integral tests

There is presently no standard for evaluating fracture initiation toughness by J -integral test with superimposed cyclic loading (termed here as cyclic J - R test) to estimate J_{QC} unlike that for monotonic determination of J_Q . An attempt has been made here to evaluate J_{QC} from the cyclic J - R curves following the guidelines for evaluating J_Q in monotonic tests. The crack lengths under cyclic J -integral tests were calculated using the unloading data falling between P_{max} and 70% of P_{max} . In case of cyclic J , the area under the envelope curve above the baseline (i.e. $P=0$ as shown in Fig. 4.8) has been used to measure J . The $(J, \Delta a)$ data points falling between 0.15 mm to $0.3 \times (W-a_i)$ mm of crack extension were fitted to eqn. (4.11). An experimental blunting line was thereafter constructed from the initial linear region of the obtained cyclic J - R curve. The intercept of the fitted curve with a line parallel to the experimental blunting line offset at 0.2 mm crack extension was considered as critical J_{QC} . A typical example illustrating the procedure for the evaluation of J_{QC} is illustrated in Fig. 4.16. This method is in following the recommendations of European Structural Integrity Society (ESIS P2-92). The evaluated values of J_{QC} , the relevant experimental conditions and the magnitudes of C_1 and C_2 obtained through eqn. (4.11) are reported in Table 4.4.

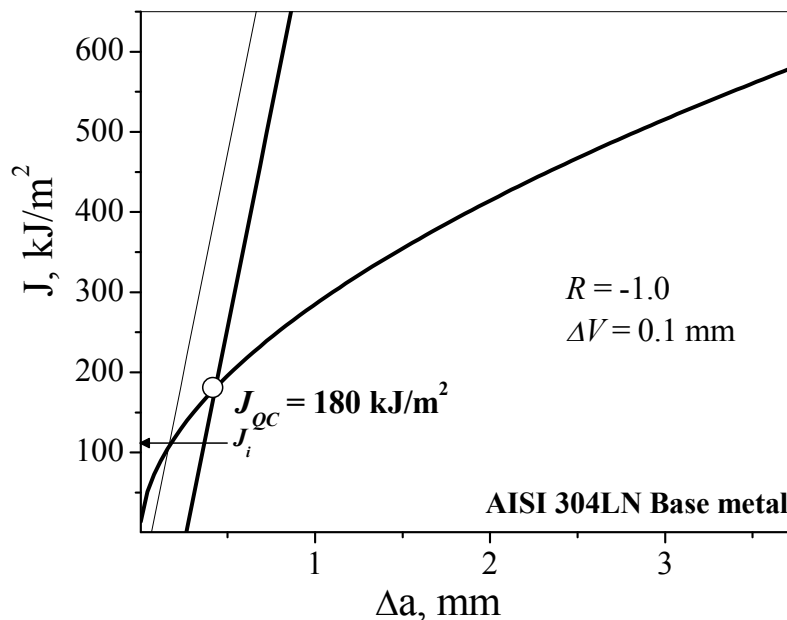


Fig. 4.16 Evaluation of conditional fracture toughness J_{QC} for cyclic J - R test of AISI 304LN SS base metal at $R=-1.0$ and $\Delta V=0.1$ mm

Table 4.4 Fracture toughness parameters of the investigated steel under cyclic J - R tests

Specimen code	ΔV (mm)	Stress Ratio (R)	C_1	C_2	J_{QC} kJ/m ²	dJ/da MJ/m ³
LC4	0.1	-0.5	524.214	0.36	486	771.2
LC5	0.1	-0.8	420.313	0.93	323	657.8
LC6	0.1	-1.0	284.911	0.54	180	555.4
LC7	0.1	-1.2	389.124	0.47	220	639.3
LC8	0.5	-0.5	1311.16	0.84	644	792.7
LC9	0.5	-0.8	974.768	0.72	602	687.4
LC10	0.5	-1.0	564.590	0.43	329	573.7
LC11	0.5	-1.2	515.017	0.69	349	692.2
WLC5	0.1	-0.5	286.08	0.84	140	981.1
WLC6	0.1	-0.8	221.052	0.70	102	717.2
WLC7	0.1	-1.0	193.83	0.67	82	651.8
WLC8	0.1	-1.2	127.43	0.76	100	667.7

It is clear from Table 4.3 and Table 4.4 that fracture toughness of AISI 304LN SS base metal and its weldment under cyclic loading condition is lower than that estimated from conventional tests under monotonic loading. The average fracture toughness values for AISI 304LN SS base metal and its weldment obtained under monotonic J -integral tests are found to be 1107 ± 27 kJ/m² and 592 ± 45 kJ/m², whereas the lowest observed fracture toughness value for base metal under cyclic loading condition (at $R = -1.0$, $\Delta V = 0.1$ mm) is found to be 180 kJ/m². Therefore, it is found that for AISI 304LN SS, the fracture toughness under superimposed cyclic loading deteriorates almost 1/5th of its corresponding monotonic fracture toughness values. However, cyclic J - R curve is sensitive to R ratio and ΔV ; this fact suggests that it is not a true material characteristic curve; it just portrays the extent of deterioration in the monotonic fracture resistance when cyclic load reversals are superimposed. This information is required for engineering analysis as required in new regulatory guide for leak before break applications (Scott, 2003). The fracture toughness values estimated from both monotonic and cyclic fracture tests of AISI 304LN SS base metal are higher compared to its weldments.

The average fracture toughness value of the base metal is almost twice than that of its weldments when it is determined using monotonic tests; but under cyclic loading condition at a constant plastic displacement of 0.1 mm the fracture toughness value of the weldment at $R = -1.2$ is almost 60% lower compared to that of the base metal.

The resistance to crack propagation (dJ/da) for cyclic J - R curves was next evaluated following the procedure described in section 4.3.1. The magnitudes of dJ/da for base metal and weldments are found to decrease with decreasing stress ratio from 0 to -1.0 as shown in Fig. 4.17. The magnitude of dJ/da is found to be minimum at the condition $R = -1.0$ and $\Delta V = 0.1$ mm. The lowest dJ/da values for AISI 304LN SS base metal and its weldment at $R = -1.0$ for plastic displacement 0.1 mm are about 10% and 40% of their monotonic fracture resistance values. The resistance to crack propagation is found to be higher for $\Delta V = 0.5$ mm compared to $\Delta V = 0.1$ mm as shown in Fig. 4.18. Cyclic loading through compressive load excursions has thus significant deleterious effects on the fracture initiation toughness and the resistance to crack propagation behaviour of AISI 304LN SS base metal and its weldments. The observed degradation of dJ/da in the investigated steel is in agreement with similar observations made by Rudland *et al.* (1996) for 304 stainless steel and SA 106B steel. The comparative analysis of J_{QC} and dJ/da in cyclic and monotonic loading thus lead to the conclusion that fracture initiation toughness and the resistance to crack propagation of materials degrade considerably under compressive cyclic loading.

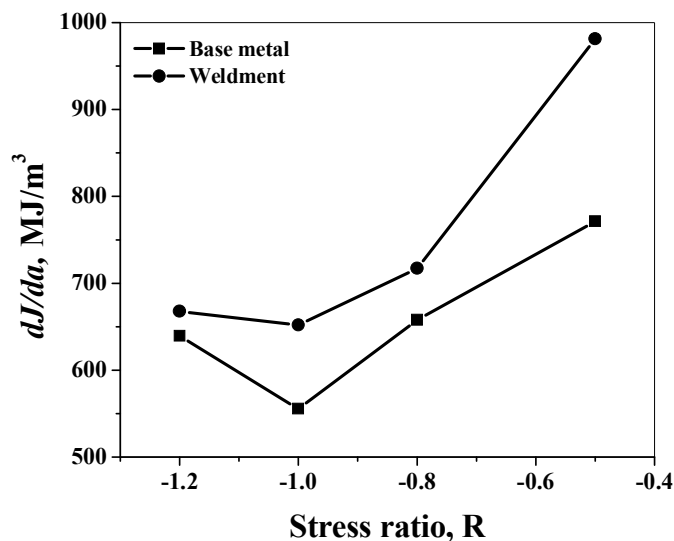


Fig. 4.17 Typical variation of cyclic crack growth resistance (dJ/da) with stress ratio (R) for AISI 304LN SS base metal and its weldment

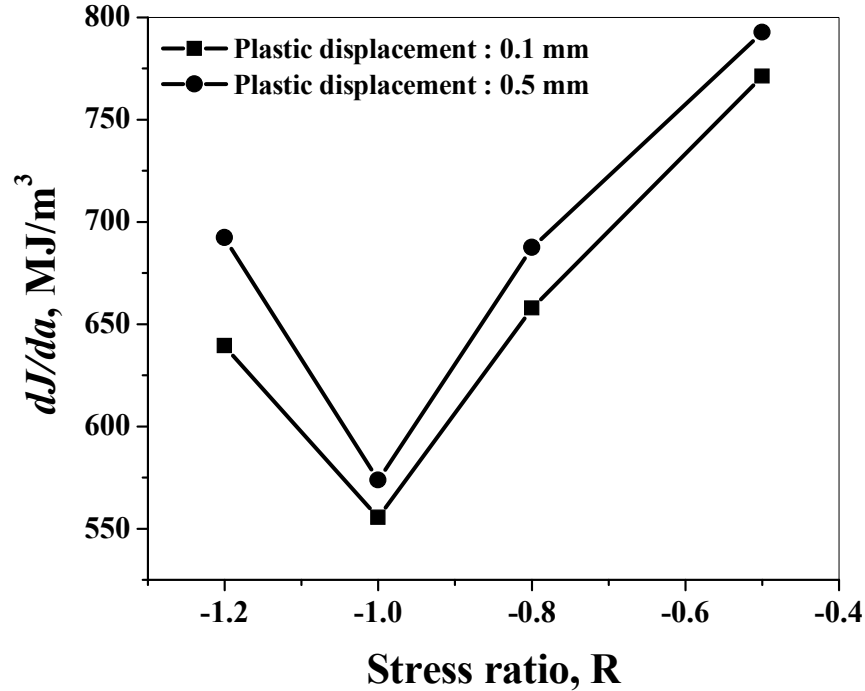


Fig. 4.18 Typical variation of cyclic crack growth resistance (dJ/da) with stress ratio (R) for AISI 304LN SS base metal at two different plastic displacement levels of 0.1 mm and 0.5 mm

4.3.3 Micro mechanisms of fracture in the investigated steel

The differences in the fracture behaviour of the stainless steel specimens subjected to monotonic and cyclic loading are evident from the J - R curves and the estimated fracture toughness values. An attempt is made here to search for the physical causes behind the above phenomenon using fractographic examinations. The crack front in specimens subjected to monotonic loading exhibits a thumbnail shape, whereas this shape gets warped on the crack front in specimens tested under cyclic loading as shown in Fig. 4.19. These observations are attributed to the difference in the stress conditions on the surface and within the interior of the specimens subjected to monotonic and cyclic loading. In monotonic loading, free deformation occurs along the crack tip, while the deformation is constrained in specimens subjected to cyclic loading. The changes in the mode and magnitude of plastic deformation in specimens subjected to cyclic loading are considered to occur due to the occurrence of crack closure. Similar suggestions have been forwarded by Kobayashi *et al.* (1992) for 2.5Cr-1 Mo steel.

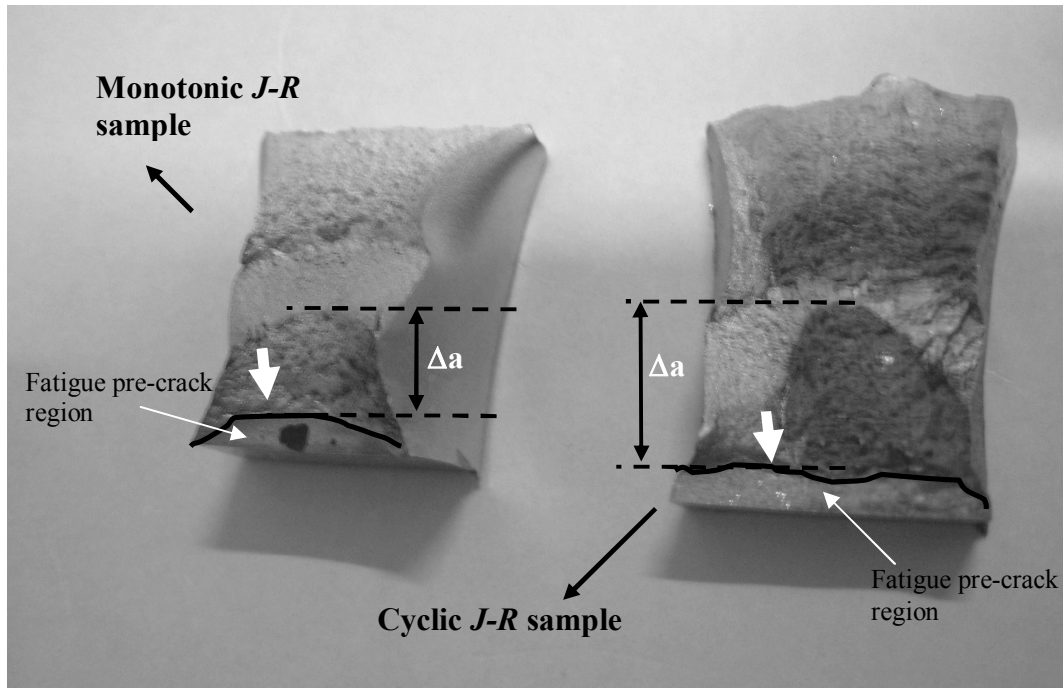


Fig. 4.19 Typical fractured surfaces of base metal specimens of AISI 304LN SS subjected to monotonic and cyclic J - R tests. Monotonic J - R specimens show a thumbnail shape (shown by an arrow) whereas cyclic J - R specimens depict warped thumbnail type shape ahead of the fatigue crack. The crack extension (Δa) has been marked in the photograph.

Typical fractographs of AISI 304LN SS base metal subjected to monotonic and cyclic loading are shown in Fig. 4.20 and Fig. 4.21. The fracture surfaces of monotonic loading show dimples (Fig. 4.20a), which confirms that void nucleation and growth is the predominant mechanism of fracture. In addition, these samples exhibit pronounced stretch zone (Fig. 4.20b) ahead of the fatigue pre-crack region. The fractographs of specimens subjected to cyclic loading, on the other hand, reveal smeared and smashed voids due to rubbing of crack surfaces along with fissure cracks (Fig. 4.21). Striation marks are also observed on fracture surfaces tested at lower R ratio ($R = -0.5$ and -0.8) as shown in Fig. 4.22. The existence of fissure cracks on the fracture surfaces of specimens at negative R ratio can be considered to be the characteristics of compressive load cycles (Kobayashi *et al.*, 1992). Thus it can be inferred that formation of dimples, their smearing and formation of fissure cracks govern the mechanism of crack growth in cyclic J - R specimens. It is considered that the damage produced in the fracture process zone at the crack tip by each cyclic unloading is quite extensive to result in ready crack extension on

resumption of tensile loading (Tarafder *et al.*, 2003). Apart from that, crack extension is facilitated in AISI 304LN SS and its weldments by the re-sharpening of the blunted crack tip by compressive excursion of load during cyclic unloading (Roy *et al.*, 2009). The compressive load excursion leaves behind some residual tensile stress ahead of the crack tip (Seok *et al.*, 1999) and this assists easy opening of the crack in the subsequent tensile load. In addition, resharpenering of the crack and smearing of the void increases the stress intensity factor (Rudland *et al.*, 1996) in the crack tip process zone and this phenomenon also help to extend the crack under tensile excursion of the cyclic load. As a consequence the crack growth resistance of the material decreases. This is substantiated through Fig. 4.23 which illustrates the crack tip profiles obtained after monotonic and cyclic J - R tests.

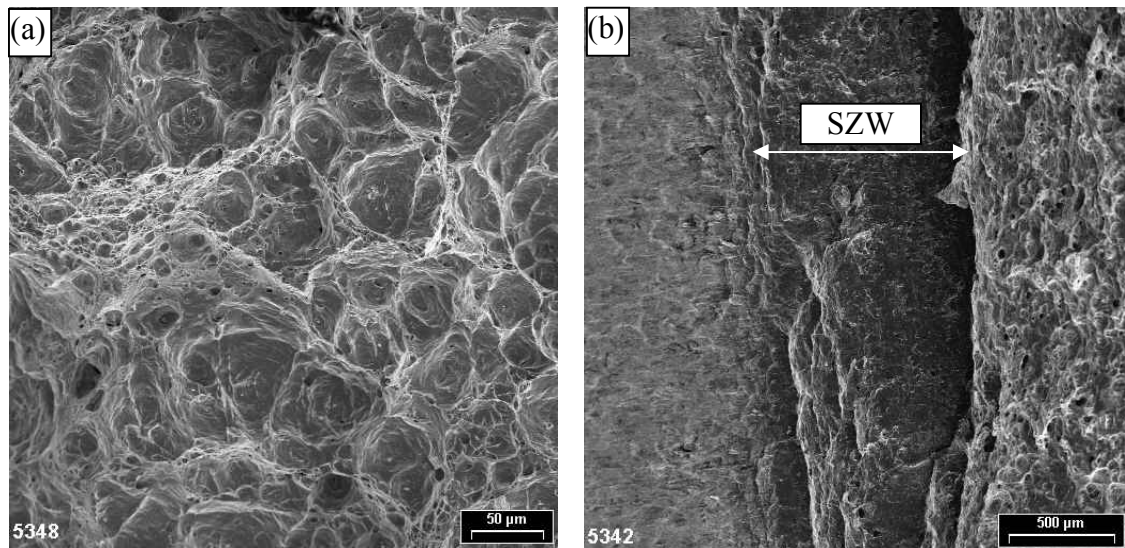


Fig. 4.20 Typical SEM fractographs recorded from broken fractured surfaces of AISI 304LN SS base metal after monotonic J - R tests: (a) crack growth region showing dimples, (b) stretch zone width (SZW) ahead of fatigue pre-crack and before actual crack growth marked by an arrow. Only parts of the fractured samples of interest are shown

It is evident from Fig. 4.24 that the voids formed ahead of crack tip under cyclic loading condition are mostly elongated and sharpened leading to crack tip re-sharpening phenomenon. In addition the crack profile of the cyclic J - R tested specimen, interrupted after compressive loading as shown in Fig. 4.24, shows irregular shape of the crack profile which exhibits propensity of the crack surface to branch out, leaving features of fissures on the fracture surface. The primary crack is found associated with several secondary cracks. A magnified view of the crack tip is also illustrated in Fig. 4.24(d).

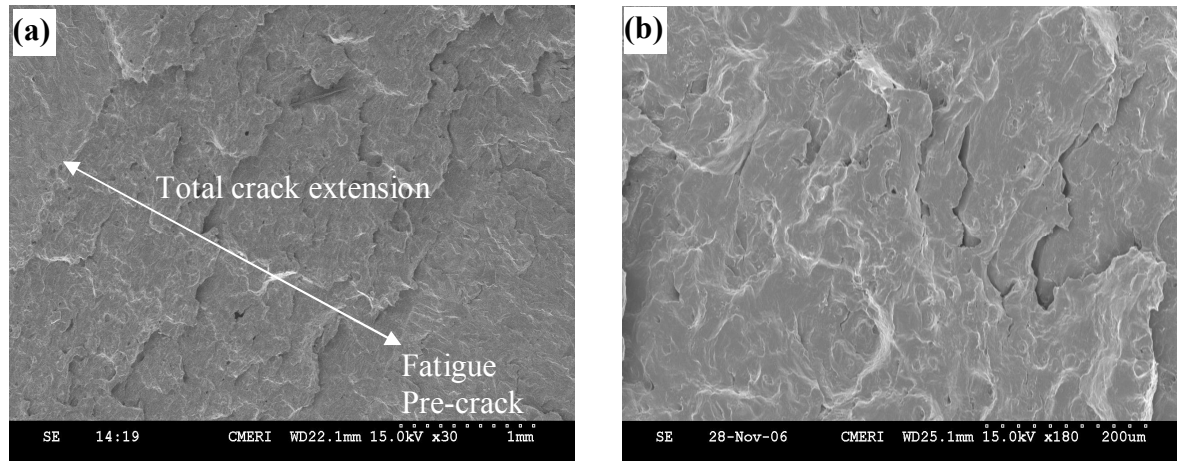


Fig. 4.21 (a) SEM photograph of the fracture surface of a AISI 304LN SS base metal specimen subjected to cyclic J - R test at $R=-1.2$ indicating fatigue pre-crack and the sub-critical crack extension regions (b) Magnified view of the crack extension region of the same specimen showing smeared voids and rubbed surfaces with secondary cracks

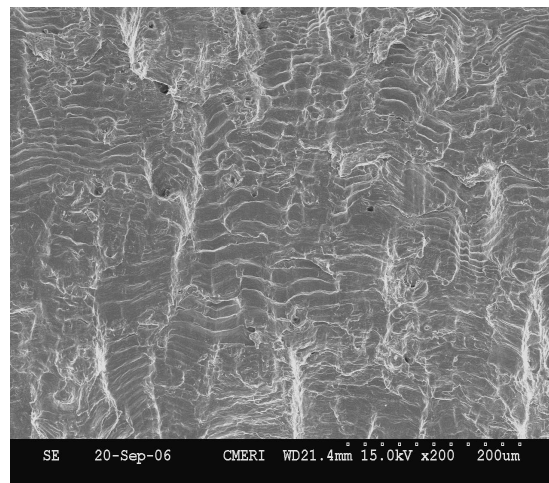


Fig. 4.22 Fracture surface under cyclic loading condition at $R= -0.5$ and $\Delta V=0.1$ mm showing striation marks

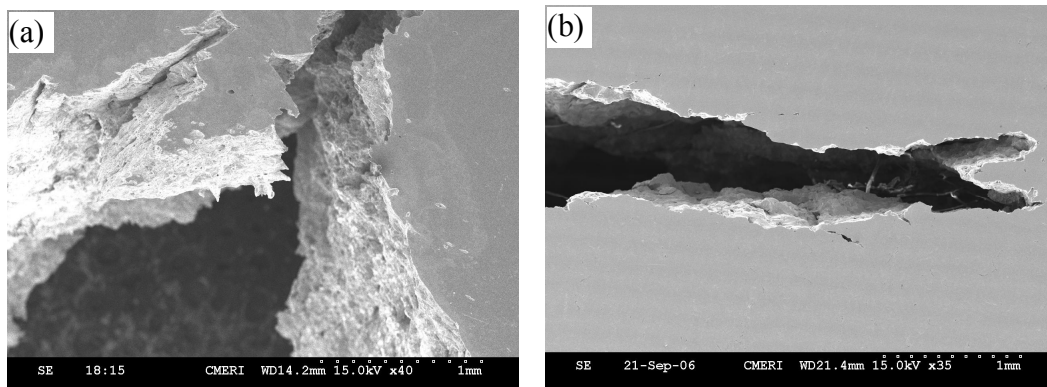


Fig. 4.23 Crack tip opening in (a) monotonic and (b) cyclic J -integral test

There is a large secondary crack originated from the primary crack in the case of cyclic J - R tests for negative R ratio. This grows parallel to the primary crack extension. Thus the total displacement observed during cyclic J - R tests comes from both primary and secondary crack extensions. The crack length calculations are usually done from CCL relation (as given by the eqn. (4.3) using total compliance) would thus result in higher magnitude of primary crack extension than what is actually happening to the primary crack tip in a specimen. This higher magnitude of primary crack extension would result in lowering of the magnitudes of energy absorbed because the expression (4.9) for J calculation incorporates crack length also. This is one of the contributing factors, in apparently lesser fracture resistance behaviour of the material during cyclic J - R tests (Roy *et al.*, 2010a).

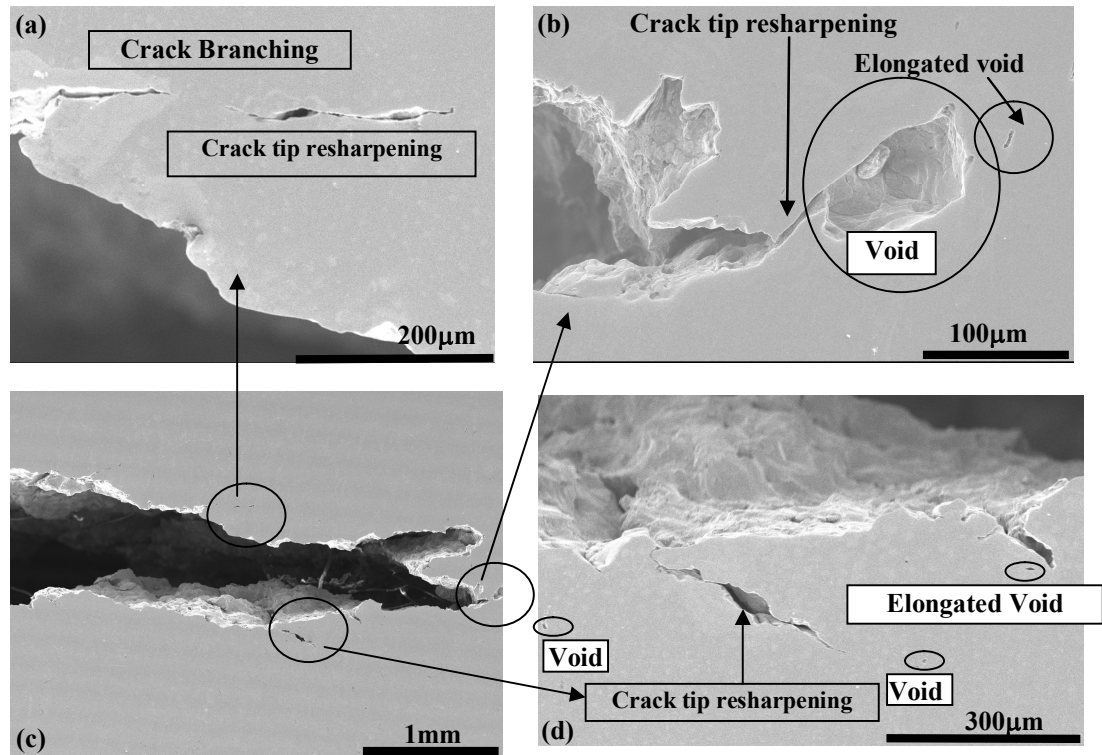


Fig. 4.24 Crack tip profile after cyclic fracture tests showing: (a) Crack branching (secondary cracks) and crack tip reshaping (b) Crack tip reshaping and void reshaping (c) crack tip profile of cyclic J - R test specimen (d) isolated voids, elongated voids and crack tip reshaping

Another major point to be noted here is that the crack branching in the case of cyclic loading makes the crack estimation in cyclic J - R conditions complex. Until now

there is no method by which both primary and secondary cracks can be estimated correctly during a test in order to construct hypothetically a perfect cyclic J - R curve. In absence of such developments, one is left with the conventional J - R curve approach, which only considers primary crack extension. Only merit of this approximate method is that it provides the lower bound value, hence it can be used in LBB analysis of the components reliably.

In generalization the above results and their analyses unambiguously indicate that the mechanisms of crack growth in monotonic and cyclic J - R tests are different for AISI 304LN SS base metal and its weldments.

4.4 Conclusions

The salient results obtained from this part of the investigation lead to the following major conclusions:

1. There is significant decrease in fracture resistance of AISI 304LN SS base metal and its weldment under cyclic loading compared to that under monotonic loading condition. The minimum J_Q value obtained by cyclic J -integral tests is almost one-fifth of that estimated under monotonic loading condition both for base metal and the weldments.
2. Fracture toughness decreases with decrease in load ratio, R . However, the lower bound J - R curves for AISI 304LN SS base metal and its weldment correspond to approximately $R = -1$. Thereafter, with further lowering of R -value fracture resistance of these steels increases marginal increasing trend.
3. Fractographic examinations of the broken samples of AISI 304LN SS base metal and its weldment, after monotonic and cyclic fracture tests, reveal that the ductile crack extension through micro void coalescence gets considerably influenced by smearing and fissure formation under cyclic loading condition.
4. The monotonic fracture resistance of weldments is approximately 50% lower than the base metal of AISI 304LN stainless steel.

Load controlled fracture behaviour of AISI 304LN stainless steel and its weldment

5.1 Introduction

Piping components of the primary heat transport system of nuclear power plants are expected to experience dynamic-cyclic loads with considerable plastic strains during seismic event. These components may experience 10-20 large amplitude load cycles during a typical earthquake event (Gupta *et al.*, 2007). Adequate protection of piping components from the consequences of earthquake thus demands detailed knowledge about deformation behaviour and characteristics of fracture resistance of the components of the piping system. It is discussed in Chapter 4, that reversible loading significantly affects fracture process in components due to cumulative damage by compressive plasticity originating from void flattening and crack tip re-sharpening. The above observations and the governing mechanism have support from other published literature (Marshall and Wilkowski, 1989; Kobayashi *et al.*, 1992; Tarafder *et al.*, 2003; Roy *et al.*, 2009) It is also known that for piping systems, under seismically induced loads, get subjected to neither fully stress controlled nor truly strain controlled state and their force response corresponds to combined load and displacement controlled condition.

The state of the art related to fracture behaviour of steels under superimposed cyclic loading indicates considerable deleterious effect due to imposition of compressive load cycles, the details of which have been discussed in Chapter 4. However, it has been observed that the extent of such deleterious effects depends up on the magnitude of the compressive load (via R ratio) and the frequency of load cycle (via plastic displacement, ΔV). There are limited investigations related to fracture behaviour of steels under superimposed cyclic loading in load control mode. Unlike displacement control tests where fracture resistance is assessed as function of R ratio and ΔV , one usually determines the number of cycles to failure in load-control tests to understand the fracture behaviour of structural materials. Miura *et al.* (1989) were pioneers to examine the effect of loading pattern on crack growth rate using circumferential through-wall cracked pipes.

Venukumar *et al.* (2004) and Gupta *et al.* (2007) have carried out displacement as well as load control cyclic tests on SA333 Grade 6 and AISI 304LN stainless steels during full scale pipe testing. These investigators have reported that number of cycles required to cause failure in load control tests depends on load amplitude, load ratio and initial crack length similar to that in tests related to fatigue crack growth rate (FCGR); but in displacement control mode number of cycles required to attain the peak load is dependent on the increment of plastic displacement in each cycle. Thus to understand the seismic effect on structural components, one must examine fracture behaviour of materials under both load and displacement controlled modes, a discipline of current interest with extremely limited information.

International Piping Integrity Research Group (IPIRG) (Scott *et al.*, 1993; Kramer *et al.*, 1997; Scott *et al.*, 1997) and Central Research Institute of Electric Power Industry (CRIEPI) (Miura *et al.*, 1997) have conducted fracture toughness tests on straight pipes and investigated the fracture behaviour of circumferentially cracked piping subjected to loading conditions that typically resemble seismic events. The IPIRG research was focused on A106 Grade B carbon steel and TP304 austenitic stainless steel materials. The IPIRG research has shown that inertial loading conditions (i.e., load controlled) are more prone to crack growth instability than displacement controlled loading. It has been suggested (Miura *et al.*, 1997) to consider load controlled data for the stability analysis of flawed pipe under pure inertial loading. These earlier investigations ascertained significant influence of cyclic nature of loads on fracture stability assessment. Most of the available data related to load controlled cyclic fracture tests (Venukumar *et al.*, 2004; Gupta *et al.*, 2007; Miura *et al.*, 1997) are, however, carried out on actual components. An attempt has been directed here to study the effect of the same using laboratory specimens (20 mm thick specimens fabricated from actual pipes) and to compare the results with available component data.

The objectives in this part of the investigation are: (i) to generate constant amplitude load controlled test data for base metal and weldment (ii) to compare the number of cycles to failure under load controlled and displacement controlled tests

(iii) to compare the obtained results with the available data for components and finally to make an attempt to generate a master curve for LBB analysis.

5.2 Experimental procedure

5.2.1 Specimen preparation and fatigue pre-cracking

The cyclic fracture tests under load control mode were planned on compact tension specimens on both weld and base metal of the investigated steels as in the case of monotonic and cyclic fracture tests under displacement controlled mode. The nominal specimen dimensions were as described in chapter 4. However, the actual dimensions of individual specimens employed for experiments are presented in Table 5.1. All specimens were fatigue pre-cracked prior to fracture tests, as described in section 4.2.1.

Table 5.1 Details of specimen dimension, estimated load (% P_{amp}) and no. of cycles to failure (N) under load-controlled cyclic fracture test of AISI 304LN SS and its weldment

W, mm	B, mm	a_{ini} , mm	ηbB	Test P_{amp} , kN	Mon. P_{max} , kN	% P_{amp}	N
Base Metal							
50.13	20.11	21.44	111.30	72.11	90.65	79.5	10
50.15	19.95	23.89	90.14	55.00	74.34	74.0	18
50.11	20.26	21.23	113.90	67.30	92.66	72.6	20
50.03	20.05	21.92	106.19	60.33	86.71	69.6	24
49.81	19.79	21.76	104.93	53.85	85.74	62.8	41
49.91	20.09	22.86	97.74	45.00	80.20	56.1	86
Weldment							
49.68	19.30	22.90	92.31	57.66	72.08	80.0	15
49.83	20.35	21.28	112.32	57.26	87.25	65.6	68
49.77	19.85	24.47	83.25	40.31	65.21	61.8	156
50.01	20.21	21.81	107.86	44.63	83.87	53.2	179
49.90	19.50	21.25	108.29	44.24	84.19	52.6	284
49.90	19.35	23.93	85.80	33.97	67.14	50.6	423

W= Width of specimen; B= Thickness of specimen; a_{ini} = Initial crack length; $\eta = 2 + 0.522 (b/W)$; b= unbroken ligament; P_{amp} = amplitude of cyclic loading; N= No. of cycles to failure

5.2.2 Load controlled cyclic fracture tests

After fatigue pre-cracking, the specimens were subjected to fracture under slow cyclic load at room temperature until failure. The failure was implied when the crack grew in an unstable manner rendering it incapable of taking any further load.

Fully reversed ($R=-1$) fatigue cycles with pre-determined load amplitudes was used during testing. The magnitudes of these load amplitudes correspond to 50% to 80% of the peak load (P_{max}) during monotonic J - R tests. As maximum load bearing capacity during monotonic J - R tests would vary with small deviation in specimen geometry, a number of monotonic J - R tests in addition to results reported in chapter 4 were carried out. The peak loads from these tests were used as a basis for developing a calibration curve to predict the required P_{max} value for load controlled test for a specimen with known remaining ligament. The specimen dimensions of these additional J tests and the corresponding P_{max} values are presented in Table 5.2. The method of estimation of P_{max} through calibration curve is discussed in the next section.

Table 5.2 Details of specimen dimensions and estimated monotonic load (% P_{amp}) under displacement-controlled J -integral test of AISI 304LN SS base metal and its weldment

Sl. No	Specimen Name	Width (W), mm	Thickness (B), mm	Crack length, a_i , mm	ηbB	Test P_{max} , kN
Base metal						
1	LNYBF2	49.98	19.85	25.97	73.54	49.20
2	LNYBF5	50.03	19.78	25.62	75.97	66.29
3	LNYB1R1	49.97	20.01	27.17	66.01	56.03
4	LNBLC4J	49.73	20.01	23.27	93.00	76.03
5	LNBLC3	49.80	20.10	24.64	83.15	67.63
6	LNBL1J	50.01	19.87	23.93	88.71	61.47
Weldment						
1	LYWC12J	49.75	20.03	25.03	79.72	62.53
2	LYWC13J	49.78	20.30	24.52	84.78	66.37
3	LYWC14J	49.75	19.68	23.90	86.69	64.86
4	LYWC23J	49.91	19.88	22.70	98.03	55.01

$\eta = 2 + 0.522 (b/W)$; b = unbroken ligament

5.3 Results and discussion

In this section the effect of cyclic loading with different load amplitudes on the load-LLD plots has been analyzed. The crack growth behaviour for these tests with superimposed cycling at different load amplitude has been studied for both base metal and weldments. The results of load controlled fracture tests were compared with that of displacement controlled fracture tests in order to bring forth the crack growth behaviour in the investigated steels under various types of superimposed cyclic loads/displacements. Finally a master curve has been constructed in order to illustrate load bearing capacity in

specimens under the condition of load excursions and its comparison has been made with similar data available on components.

5.3.1 Load controlled cyclic fracture behaviour of AISI 304LN SS and its weldments

The magnitude of maximum sustainable load (P_{\max}) is required for design of engineering components against cyclic load excursions in order to ensure that a component withstands specified number of load cycles. To determine this load under cyclic loading conditions, the maximum load during monotonic test is taken as reference. With this reference, a calibration curve has been constructed for various ligament sizes. A calibration curve is a plot between P_{\max} (during monotonic J test) and the remaining ligament, ηbB , where η is a constant, b and B are the unbroken ligament ($W-a$) and thickness, respectively, of the tested specimens; the magnitude of η is expressed as $2+0.522 (b/W)$. The calibration curves for the base metal and the weldment are shown in Fig. 5.1a and Fig 5.1b respectively. Once the calibration curve is constructed, P_{\max} values for cyclic fracture tests can be estimated for different values of remaining ligament of specimens employed during test.

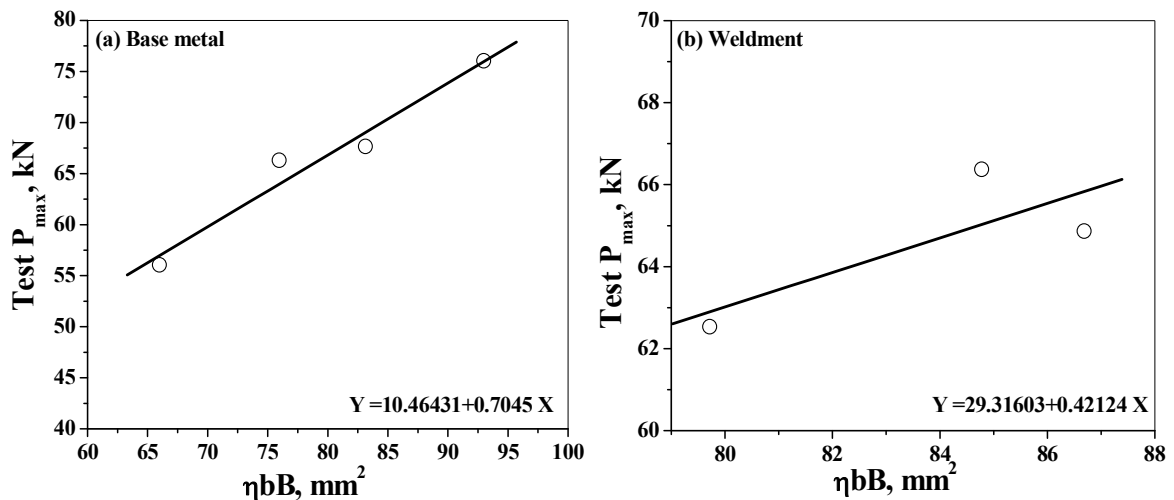


Fig. 5.1 Calibration curve for estimation of effective monotonic maximum load for cyclic tearing tests of AISI 304LN (a) base metal and (b) weldment

Typical load versus LLD plots obtained from load controlled cyclic tearing tests for base metal and weldments are shown in Fig. 5.2a and Fig. 5.2b respectively. The hysteresis records of load versus LLD of the tests show that the area of the hysteresis loop becomes larger as the number of load cycles increases. In all the tests it has been observed that initially there is stable crack growth up to certain critical size of crack; after

that all the specimens have rapid crack growth followed by the collapse of the remaining ligament. The results in Fig. 5.2a and Fig. 5.2b show that there is rapid increase in LLD around the peak load and towards the end of the test (instability). Crack growth in cyclic tearing consists of two parts: one is crack growth due to low cycle fatigue and the other is the accelerated crack growth due to monotonic tearing (Sherry *et al.*, 2005; Sherry and Wilkis, 2005). The rapid increase in LLD and crack growth rate towards the end of the test can be explained by the increased contribution of the static fracture (or tearing) mode. As the crack grows, the difference between the applied peak load and the instability load gets narrowed down and consequently the specimen fails by plastic collapse.

The results related to crack growth (Δa) versus number of cycles (N) for the base metal and weldment are shown in Fig. 5.3a and Fig. 5.3b respectively. The obtained results of Δa versus N typically depict the nature of crack growth, as is seen in conventional fatigue crack growth rate experiments, to be non-linear. The number of cycles to failure is dependent on the load amplitude, in agreement with conventional FCGR results. The number of cycles to failure of the specimens with crack located in weld metal is higher than for a crack located in the base metal for identical applied load range. The reason for sustaining higher number of cycles by the weldment compared to its base metal can be attributed to the fact that the weldment has higher crack growth resistance (as evident from Fig. 4.17 and Table 4.4) under cyclic loading condition.

5.3.2 Load controlled vis-à-vis displacement controlled cyclic fracture tests of AISI 304LN SS and its weldments

In this section, the displacement controlled tests have been examined with respect to load controlled cyclic fracture tests. Comparison between displacement controlled cyclic fracture tests and corresponding quasi static monotonic tests are discussed in the earlier chapter (Chapter 4). The results in Fig. 4.11 reveal that superimposed cyclic loading reduces both load carrying capacity and energy absorbing ability of AISI 304LN SS. These results also indicate that there is significant decrease in the crack initiation resistance of the material under cyclic loading. The extent of decrease in crack initiation resistance depends on the load ratio and the incremental plastic displacement as supported by evidences through results given in Fig. 4.12 and Fig. 4.13. Since the

resistance to crack initiation is governed by multiple independent variants, it is difficult to assess the applicability of the obtained results for achieving any criterion for fracture control.

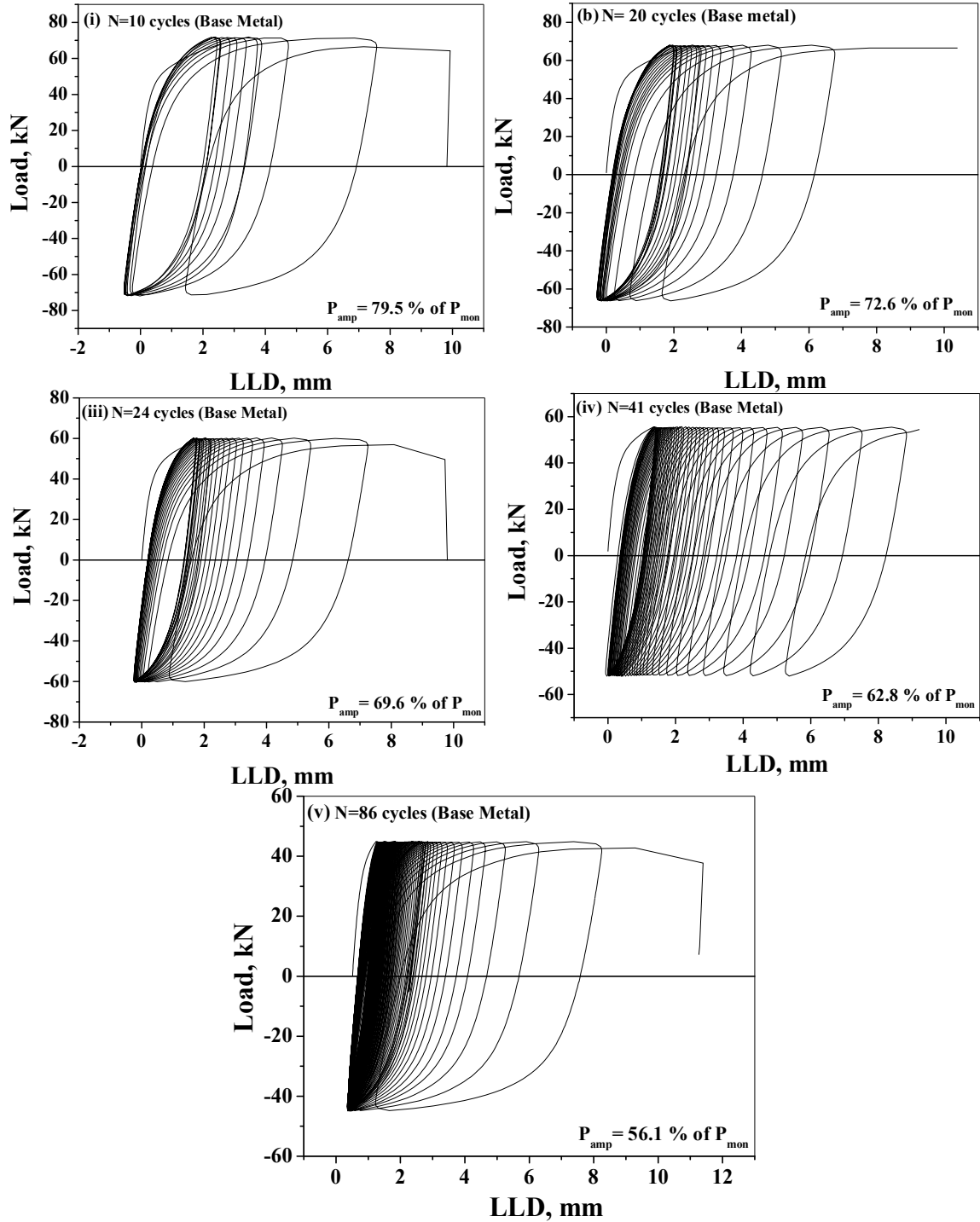


Fig. 5.2 (a) Typical load versus LLD obtained from load controlled cyclic tearing tests for base metal at various magnitude of P_{amp} exhibiting (i) N= 10 cycles, (ii) N= 20 cycles, (iii) N= 24 cycles, (iv) N= 41 cycles and (v) N= 86 cycles

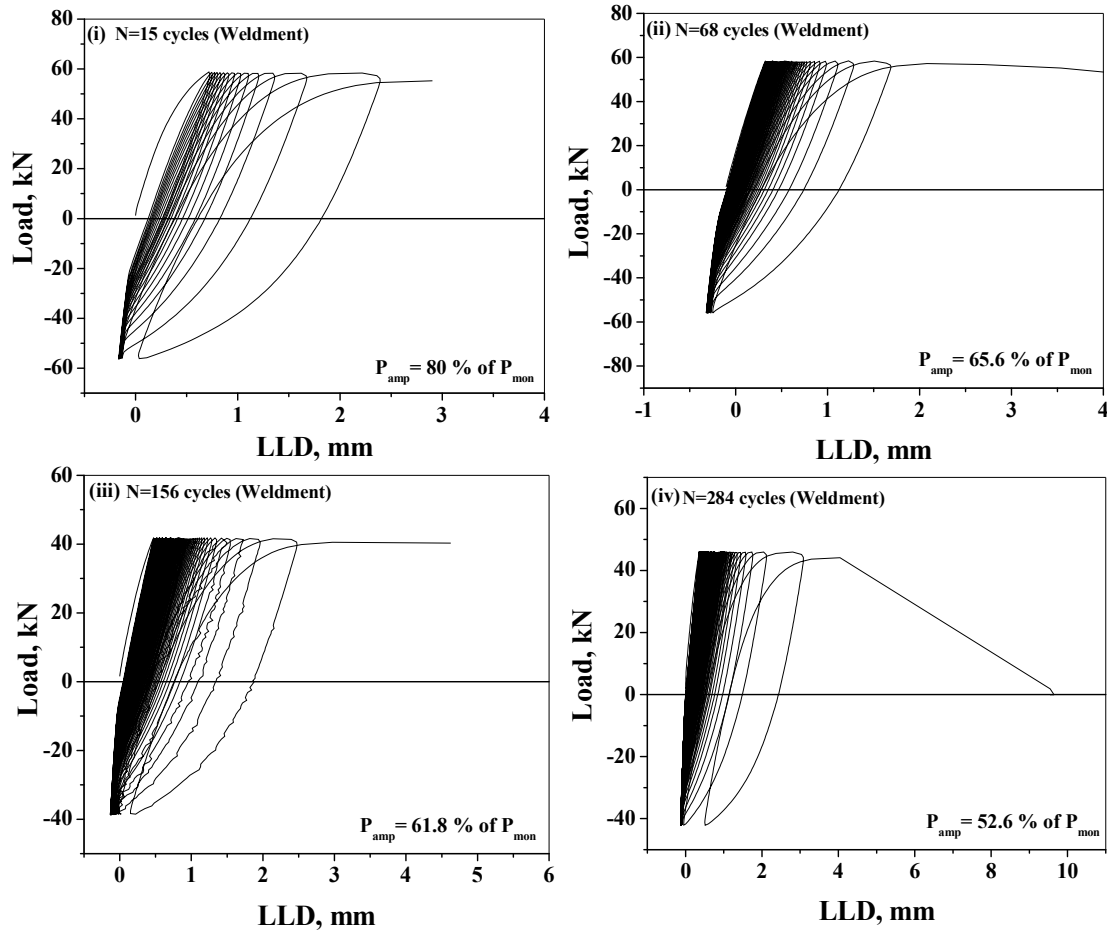


Fig. 5.2 (b) Typical load versus LLD obtained from load controlled cyclic tearing tests for weldments at various magnitude of P_{amp} exhibiting (i) $N= 15$ cycles, (ii) $N= 68$ cycles, (iii) $N= 156$ cycles and (iv) $N= 284$ cycles

The superimposition of cyclic loading for any type of J -integral analysis has to be dealt cautiously because significant amount of unloading during construction of J - R curves violates the basic principle of J -integral analysis. Hence all these analyses should be considered as relative rather than attempts to estimate accurate crack initiation resistance of the material under superimposed cyclic loading. A number of earlier investigators (Marshall and Wilkowski, 1989; Kobayashi *et al.*, 1992; Seok and Murty, 2000; Tarafder *et al.*, 2003; Roy *et al.*, 2009) have examined fracture resistance under displacement-controlled tests to simulate seismic loading condition, while a few (Miura *et al.*, 1994; Venukumar *et al.*, 2004; Gupta *et al.*, 2007) have highlighted the importance of load-controlled tests; but sufficient attention has not been paid to assess the applicability of the results obtained from load controlled tests.

The results of load-controlled tests as depicted in Fig. 5.3 indicate that the material fails in a limited number of load cycles even when the load amplitude (P_{amp}) is sufficiently below the maximum load bearing capacity of the material in conventional fracture tests.

Comparison of the variation of crack length (a) versus number of cycles (N) under both load and displacement controlled tests reveal the following:

(a) The plot of a vs. N under both load and displacement controlled tests exhibit apparently two linear regimes with a transition zone. The transition in case of load controlled tests (Fig. 5.3) seems to be smooth; whereas that in case of displacement controlled tests (Fig. 5.4) is found to be jerky.

(b) Under displacement-controlled tests crack extension continues till a specimen reaches its maximum load bearing capacity whereas under load-controlled tests, a specimen fails considerably below its maximum load bearing capacity. The obtained results are in good agreement with the report of Venukumar *et al.*(2004) related to full scale pipe testing of stainless steel under load and displacement control.

5.3.3 Master curve to account for cyclic tearing in components and in specimens

The leak before break (LBB) qualification requires rigorous assessment of fracture resistance of piping components with postulated flaws. Earlier research in this area have resulted in several reports such as NUREG-1061 (1984) and IAEA-TECDOC (1993), which describe the procedure for analyzing piping flaws for LBB qualification. The analysis of fracture characteristics of pipes considers the seismic loading as a one time applied load of magnitude equal to peak load at the postulated flaw location during the earthquake event. The assessment of pipe with flaw (or crack) is based on the monotonic tearing instability or net section collapse (NSC); there is no explicit consideration for the cyclic damage or the number of applied load cycles to failure. The existing reports related to fracture resistance under seismic loading condition (NUREG-1061, 1984; IAEATEC-DOC, 1993) describe the present LBB design procedures for pipes in detail. The required safety factors for LBB qualification are similar to those as described for flaw evaluation under level D loading in IWB-3600 of Sec. XI of the ASME Boiler and Pressure Vessel Code.

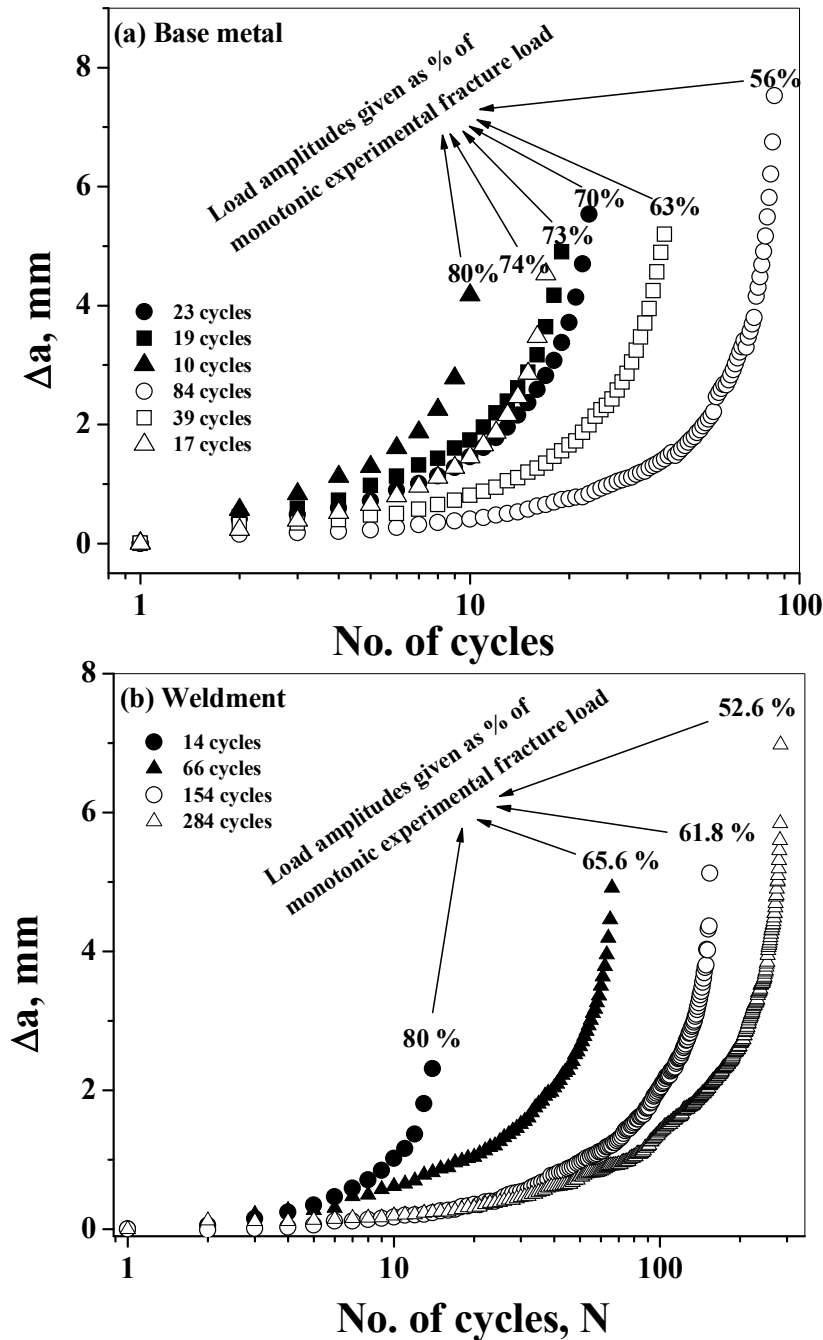


Fig. 5.3 Plots of variation of crack length with number of cycles obtained from load controlled tests of AISI 304LN stainless steel (a) base metal and (b) weldment

The report of nuclear regulatory board (NUREG-1061, 1994) recommends the following safety margins for the normal operating condition (NOC) plus safe-shutdown-earthquake (SSE) loads:

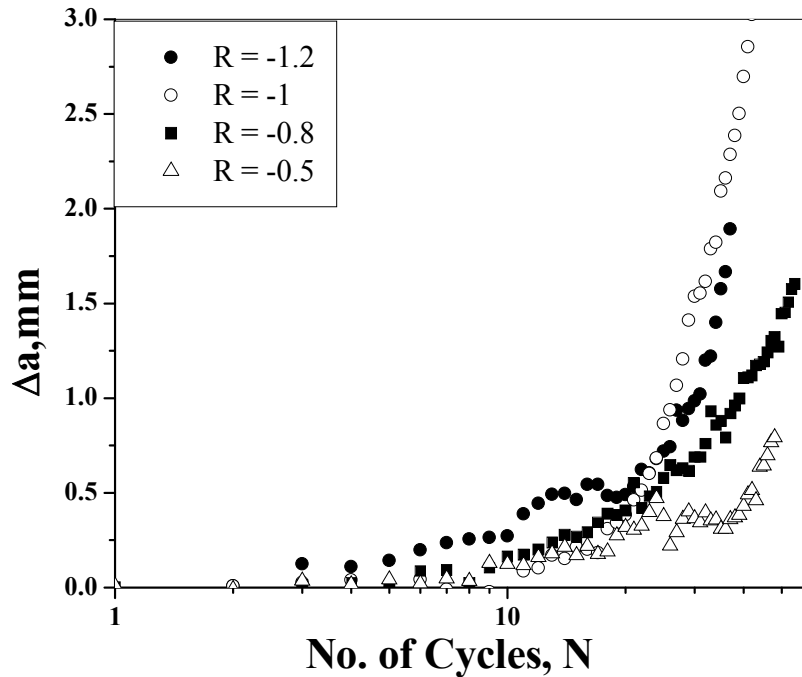


Fig. 5.4 Plots showing variation of crack length versus number of cycles under displacement controlled cyclic fracture tests of AISI 304LN stainless steel

(a) Margin to critical crack size: “The margin on the flaw size is determined by comparing the selected leakage size crack (LSC) to the critical size crack for normal operating plus SSE loading. There should be a margin of 2 to account for the uncertainties inherent in loads, material properties, etc. The limits are expressed below:

$$\text{LSC} < 0.5 \times \text{critical flaw size}$$

$$\text{or, } M_{\text{NOC}} + M_{\text{SSE}} < M_{\text{crit}} (\text{at } 2 \times \text{LSC}) \quad \dots (5.1)$$

(b) Margin on loads: “The margin on the load is determined by comparing the normal operating plus SSE loading to the critical load for the LSC. There should be a margin of $\sqrt{2}$.

$$(M_{\text{NOC}} + M_{\text{SSE}}) \times \sqrt{2} < M_{\text{crit}} (\text{at LSC}) \quad \dots (5.2)$$

Where M_{NOC} = margin on load under normal operating condition, M_{SSE} = margin on load during safe-shutdown-earthquake event and M_{crit} = Margin on load to account for critical size crack.

In the above equations, the evaluation of the critical load and the critical crack size are based on the monotonic collapse or monotonic fracture instability. Equations (5.1) and (5.2) do not account for the cyclic tearing as a failure mode nor do these ensure the safety

margins for the desired number of load cycles of the SSE load. The safety factors used in these equations are also not intended to cover the cyclic tearing damage and the number of load cycles to failure.

In view of the above discussions, a simplified material specific master curve was earlier constructed by Gupta *et al.* (2007) for pipe components of SA333 Grade 6 carbon steel and AISI 304LN SS derived from the results based on load controlled cyclic fracture tests; “a master curve is the plot of the cyclic load amplitude (given as % of maximum load recorded in corresponding monotonic fracture test) versus number of load cycles to failure (N_f)”. An attempt has been made here to generate similar master curve using results obtained from C(T) specimens of AISI 304LN base metal and its weldment. The master curves generated by earlier investigators (Gupta *et al.*, 2007) on full scale pipe components and on the laboratory specimens are shown in Fig. 5.5. This curve can readily be used in the current practice for LBB qualification for evaluating the critical load (which accounts for cyclic damage and number of load cycles) in terms of the percent of the monotonic critical load. The number of cycles to failure depends on the

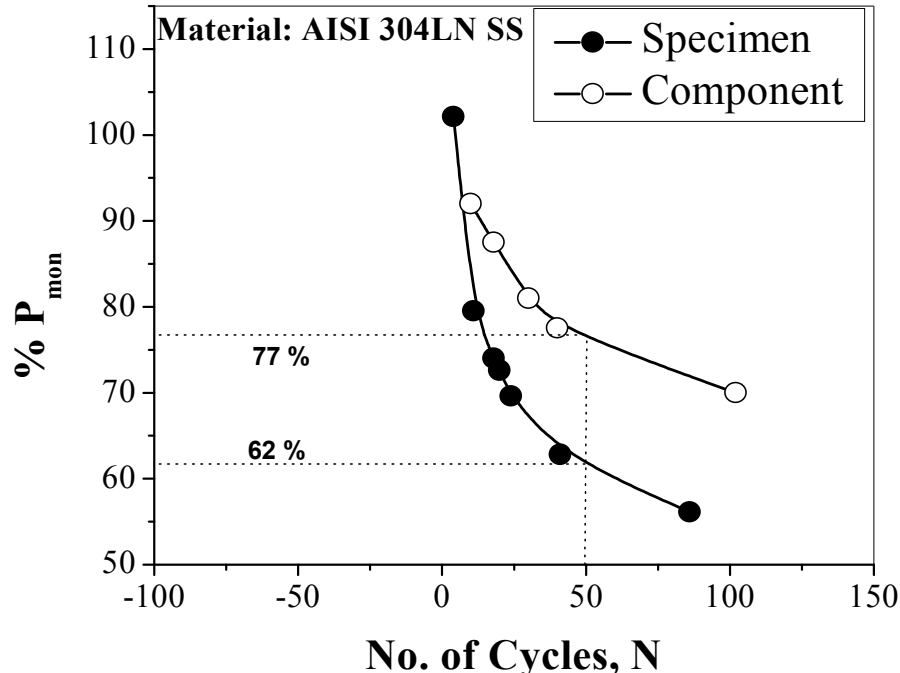


Fig. 5.5 Comparison of the variation of percentage maximum load under monotonic fracture test ($\%P_{\text{mon}}$) versus number of cycles (N) to failure for component and specimen

load amplitude and the initial crack length. The results in Fig. 5.5 shows that the cracked pipe can fail in a limited number of load cycles with load amplitude sufficiently below the monotonic fracture/collapse load.

Considering the uncertainty associated with intensity of earthquake, i.e., its magnitude, number of seismic load cycles, after shocks, etc. and uncertainties in the cyclic degradation of material, the factor of safety should be higher than that revealed by these material specific master curves. Alternately, one can fix margins considering higher number of seismic load cycles. Currently it has been decided to use a load reduction factor corresponding to 50 load cycles for SSE event, for the LBB qualification of the pipes (Gupta *et al.*, 2007). However, the number of cycles to which the piping components have to be LBB qualified is a matter of safety philosophy. It is seen from Fig. 5.5 that for pipe components made of AISI 304LN stainless steels, the failure load corresponding to 50 cycles is 77% of monotonic collapse load (P_{\max}). But it is obvious from the results generated from laboratory specimens, that the failure load corresponding to 50 cycles gets reduced to a more conservative value of only 62% of P_{\max} . This reduction in load for the same number of cycles for specimens vis-à-vis components could be attributed to two major factors (Roy *et al.*, 2011): (a) difference in the magnitudes in constraint factor in specimens and components, and (b) difference in crack geometry; in components there is embedded elliptical cracks whereas in specimens there is through thickness crack. Based on this observation the present results are indicative that the failure loads determined from laboratory specimens provide a conservative value for the load reduction factor compared to that of components in general.

5.4 Conclusions

The experimental investigations reported in this chapter illustrate the need to address the importance of load controlled cyclic tearing tests in understanding material response under seismic loading condition. The major conclusions are as follows:

1. The load controlled tests indicate that a material under investigation can fail in a limited number of load cycles with the load amplitude sufficiently below that monotonic collapse load.

2. The number of cycles that a material can withstand under load controlled tests depends on the load amplitude and the initial crack length. The number of cycles to failure is less for base metal compared to the weldment at constant applied load range.
3. Load controlled cyclic crack growth occurs by simultaneous interactive actions of mechanisms operative for low cycle fatigue and tearing. Crack growth occurs predominantly by (i) low cycle fatigue at the early stage and (ii) tearing at the later stage.
4. Comparison of the estimated results with that of reported ones related to load bearing capacity of specimens and components reveals that the former can withstand lower fraction of monotonic collapse load than that by the components.

A comparative assessment of acoustic emission and conventional load-displacement analysis for detection of crack initiation

6.1 Introduction

The principle of estimating fracture toughness by standard technique (ASTM E 1820-09, 2009) is based on indirect assessment of the point of crack initiation. But acoustic emission (AE) is capable of indicating the point of crack initiation directly during loading of a specimen; this technique is, therefore, often used for examining fracture process in metallic and non-metallic engineering structures. The AE technique is well matured as a system for continuously monitoring in-service structures as a NDE tool, but this method has limited applications in detecting crack initiation during fracture of ductile materials; the limitation is primarily due to the fact that initiation and growth of cracks in elastic plastic materials are found to be a relatively silent process (Blanchette *et al.*, 1983).

Several investigators (Palmer and Heald, 1973; Arii *et al.*, 1975; Masounave *et al.*, 1976; Clarke and Knott, 1977; Takahashi *et al.*, 1981; Khan *et al.*, 1982; Blanchette *et al.*, 1983; Dal Re, 1986; Camerini *et al.*, 1992; Ohira and Pao, 1986; Mashino *et al.*, 1996; Xin *et al.*, 1999; Sindi *et al.*, 2011) have carried out conventional fracture toughness tests in liaison with AE technique to justify the appropriateness of the standard methods for determining fracture resistance of materials; but so far no generalized guideline has emerged out from this type of ‘combined’ experiments. The major aim of this chapter is to examine results related to fracture toughness values of the selected steels estimated by these ‘combined type’ experiments in order to suggest a guideline.

Only a few reports (Palmer and Heald, 1973; Arii *et al.*, 1975; Masounave *et al.*, 1976; Clarke and Knott, 1977; Blanchette *et al.*, 1983; Camerini *et al.*, 1992; Ohira and Pao, 1986) are available that have attempted to estimate fracture toughness of ductile materials with the help of standard test practices in conjunction with AE technique. For example, Clark *et al.* (1977) have used acoustic emission to detect the initiation of cracks in pressure vessel steels like HY130 and A533B grades. These workers have concluded that the first appearance of high amplitude signals in AE could be attributed to the crack initiation processes. Camerini *et al.* (1992) have recorded the AE characteristics during

fracture toughness tests of pressure vessel steel, ASTM A 516 Grade 60, and have found that CTOD value corresponding to the first detectable acoustic emission signal from the crack tip of a loaded specimen is lower than the CTOD value estimated using standard methods (ASTM E 1820-09, 2009) for the initiation of stable crack growth. On the other hand, Blanchette *et al.* (1983) have observed that AE signal characteristics are unable to detect the onset of crack initiation in A516-70 steel. Thus, the earlier reports (Palmer and Heald, 1973; Arii *et al.*, 1975; Masounave *et al.*, 1976; Clarke and Knott, 1977; Khan *et al.*, 1982; Blanchette *et al.*, 1983; Camerini *et al.*, 1992; Ohira and Pao, 1986) do not provide any comprehensive guideline for detecting the point of crack initiation using AE signals generated during fracture toughness tests. Direct measurement of fracture resistance of nuclear piping material under superimposed cyclic loading condition has not been explored so far to the best knowledge of the author.

In this investigation time domain AE analyses have been carried out synergistically with monotonic and cyclic fracture toughness tests in order to examine the appropriateness of the detection of crack initiation by conventional fracture toughness test for AISI 304LN SS and its weldment.

6.2 Experimental procedure

The procedure for fracture toughness tests are already discussed in chapter 4 together with the details of specimen preparation and fatigue pre-cracking. The experimental procedure to record and examine AE response synergistically with load-CMOD data of fracture toughness tests are only elaborated in this section.

6.2.1 Acoustic emission during fracture toughness test

Acoustic Emission (AE) signals were recorded synergistically during the fracture toughness tests using a 32 channel Digital Image Signal Processing (DISP), acoustic emission system. A 150 kHz resonant (R15) transducer with 40 dB pre-amplification was used to monitor the AE signals. Petroleum jelly was used as acoustic couplant between transducer and specimen. The output from the transducer were amplified and transferred through a filter set at 0.2 volt to filter out the extraneous noises. Before starting the tests, the pinholes of all the CT specimens were preloaded to a level of approximately 1 kN.

This was carried out in order to eliminate spurious signals generated during cyclic J - R tests because of contact between the pins and pin holes. AE signals were monitored during such pre-loading and extraneous noises caused by the pin contact stresses were filtered. The testing machine and the pertinent loading fixtures were also preloaded using dummy (un-notched) test pieces in order to eliminate signals from the loading system. A schematic outline of the test set up to monitor AE from CT specimens is shown in Fig. 6.1. The AE system is interfaced to a computer for data acquisition and storage (Fig. 6.2).

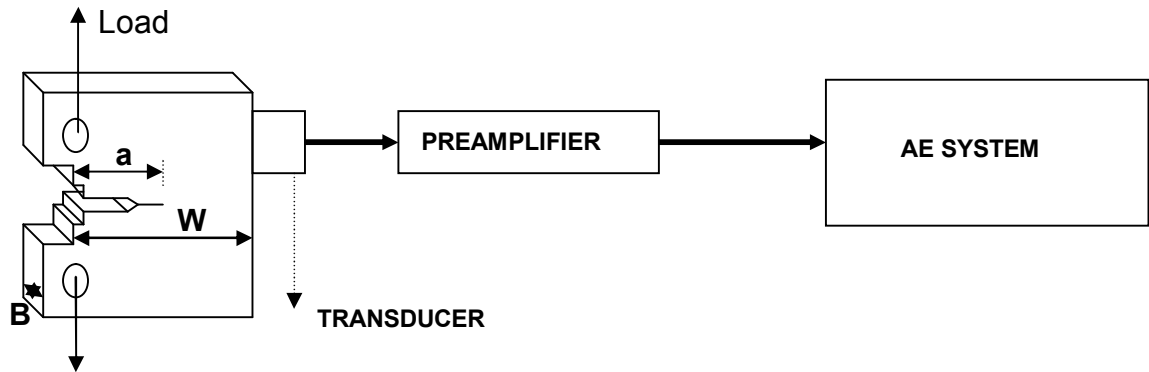


Fig.6.1 AE set up during fracture toughness test of CT specimen



Fig. 6.2 A 32 channel Digital Image Signal Processing (DISP), acoustic emission system interfaced with a computer

6.3 Results and discussion

The primary aim of this chapter is to elucidate the response of various AE signals acquired during monotonic and cyclic fracture toughness tests. The results related to monotonic and cyclic fracture toughness tests have been presented earlier in chapter 4. In this chapter, time domain analyses of AE signal characteristics has been carried out to directly identify the point of crack initiation in the selected steels.

6.3.1 Detection of the point of crack initiation by AE characteristics

An attempt has been made in this section to examine the nature of variation of energy and amplitude of AE recorded during the monotonic and cyclic fracture toughness tests of AISI 304LN SS base metal and its weldment. Similar attempts have been made earlier by several workers (Blanchette *et al.*, 1983; Clarke and Knott, 1977; Camerini *et al.*, 1992) on different grades of steels in order to characterize deformation and fracture behaviour of crack tip. It has been observed in AISI 304LN steels that the major acoustic emission activity occurs during the process of initial deformation prior to crack initiation. Blanchette *et al.* (1983) have obtained similar results while studying acoustic emission behaviour of A516-70 steel. Since the plastic zone to a large extent governs the fracture process that is operative, the AE energy versus time plots can be considered to distinguish the fracture processes.

The variation of energy and amplitude of AE for each sample was recorded simultaneously during the monotonic fracture toughness tests, and some typical results for some tested specimens of 304LN SS base metal and weldment are shown in Fig. 6.3 and Fig 6.4 respectively. The results in Fig. 6.3 and Fig 6.4 indicate that: (a) amplitude and energy of the AE events vary in an irregular manner with progressive loading, (b) the AE energy of the events increases at the onset of plastic deformation followed by a sudden jump at the point of crack initiation and thereafter exhibits fluctuations till the completion of the test and (c) the stable crack growth region is found to be associated with lesser number of signals, which corroborates with earlier findings like that of Blanchette *et al.* (1983) which indicate ductile crack growth is relatively a silent process.

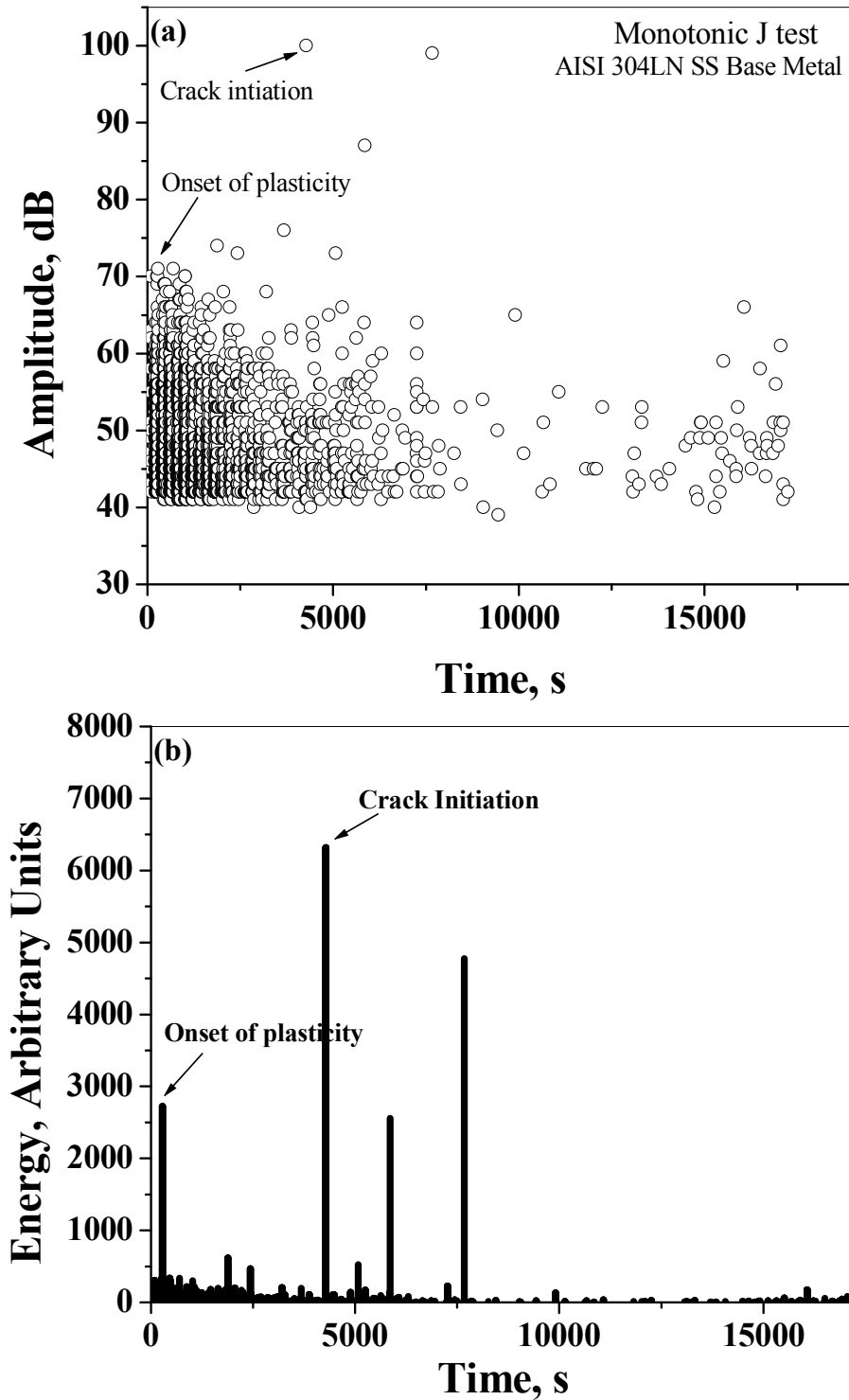


Fig. 6.3 Typical plot showing variation of AE (a) amplitude and (b) energy with time during a monotonic fracture toughness test of AISI 304LN SS base metal

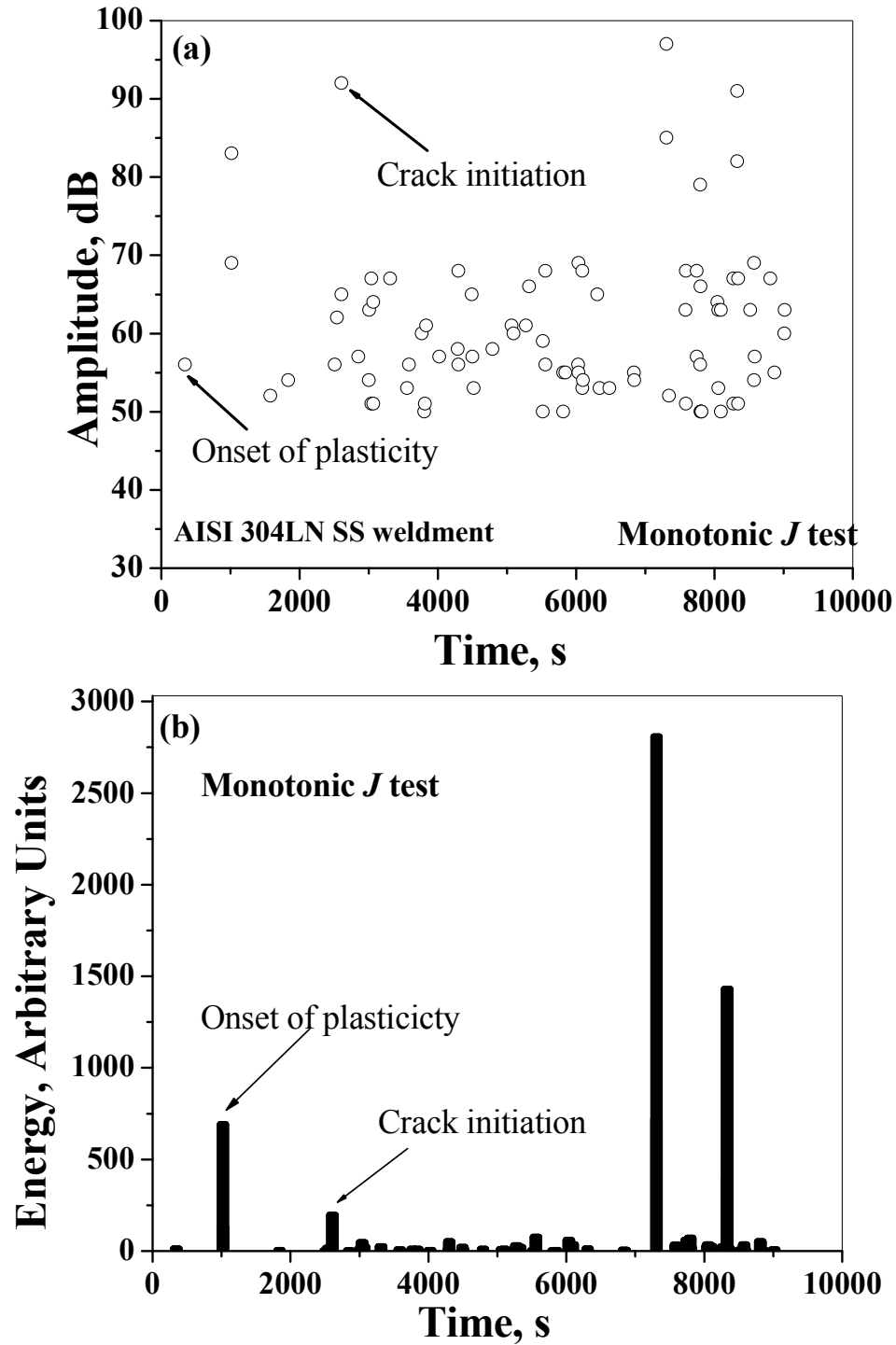


Fig. 6.4 Typical plot showing variation of AE (a) amplitude and (b) energy with time during a monotonic fracture toughness test of AISI 304LN SS weldment

The variations of AE energy and amplitude with time during cyclic fracture toughness tests for AISI 304LN SS base metal and weldment are shown in Fig. 6.5 and Fig. 6.6 respectively. These results as illustrated in Fig. 6.5 and Fig. 6.6 infer that: (a) the variation of AE energy and its amplitude with progressive loading depicts a continuous pattern i.e., absence of pronounced plastic zone formation and (b) the point of crack initiation is attributed to the sudden rise in AE energy associated with high amplitude signals, as marked by an arrow in Fig. 6.5 and Fig 6.6.

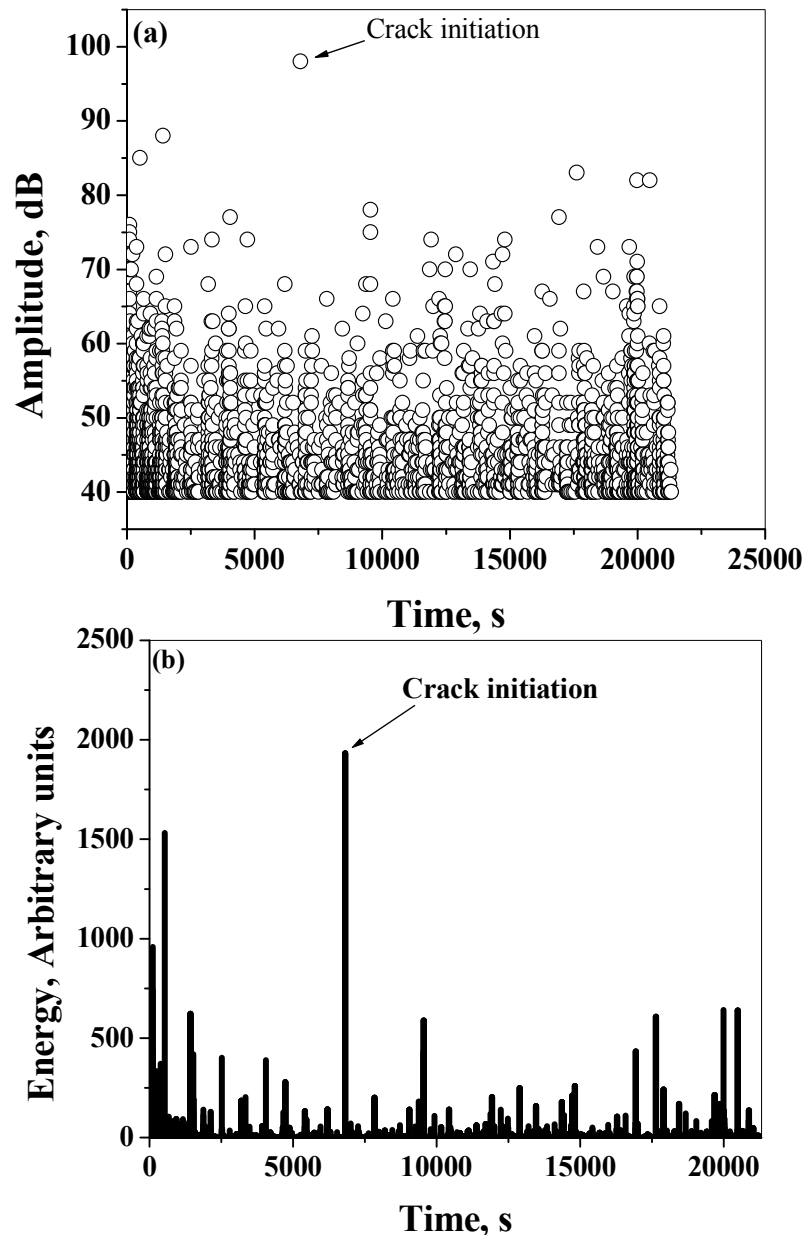


Fig. 6.5 Typical plots showing variation of AE (a) amplitude and (b) energy with time obtained during a cyclic fracture toughness test of AISI 304LN SS base metal

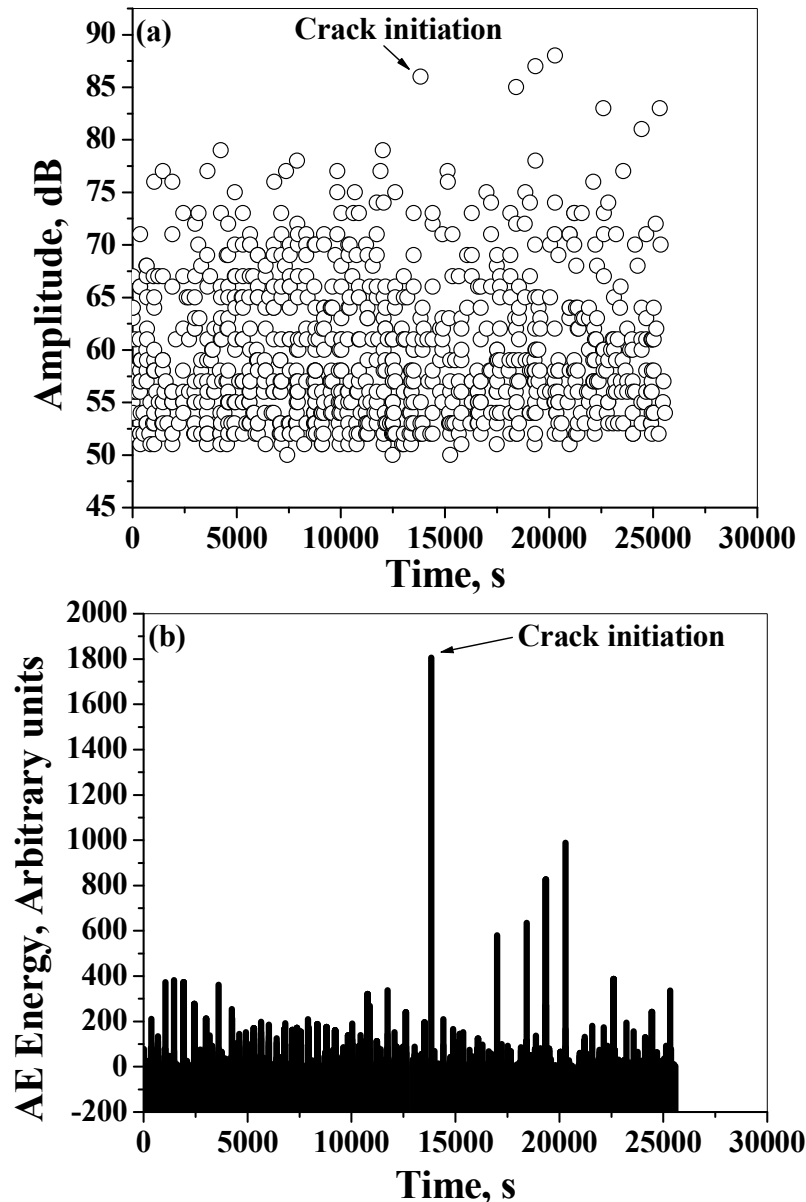


Fig. 6.6 Typical plots showing variation of AE (a) amplitude and (b) energy with time obtained during a cyclic fracture toughness test of AISI 304LN SS weldment

The characteristics of AE signals for monotonic and cyclic fracture toughness tests differ in two ways (Roy *et al.*, 2010b):(a) the number of AE events obtained in a cyclic fracture toughness test is larger than that encountered in monotonic fracture toughness tests. This can be attributed to the negative part of the stress cycle (for negative R ratio) during the cyclic fracture toughness tests and (b) the AE signals are continuous in case of cyclic J - R tests. It can be concluded from these observations that **synergistic analyses of**

peak amplitude and energy of AE signals assist in distinguishing the crack tip blunting from the point of crack initiation and subsequent stable crack growth.

6.3.2 Determination of fracture toughness by AE technique

Roy *et al.* (2008) have earlier observed that sudden rise in cumulative counts along with high decibel signal characterize the point of crack initiation in SA 333 Gr. 6 steel. The point of crack initiation in AISI 304LN SS is not associated with any sudden rise of AE cumulative counts (Fig. 6.7), but it is found to be associated with jumps in AE cumulative energy (Fig. 6.8) along with high decibel signals. Interestingly crack initiation in all the investigated steels under both, monotonic and cyclic fracture tests, can be detected using jumps in AE cumulative energy along with high decibel signals. Typical cumulative AE energy and amplitude versus time plots for AISI 304LN SS base metal and its weldment are shown in Fig. 6.9. The points of crack initiation in AISI 304LN SS base metal and its weldment, marked as ' a_i ' and ' b_i ' in Fig. 6.9 respectively, are characterized by the first sudden rise in cumulative AE energy along with high decibel signals. Further jumps in AE energy and amplitude versus time plot as seen in Fig. 6.9 could be either due to crack extension processes involving rapid shear linkage of growing voids, as documented by Clark and Knott (1977) or it could be due to formation of deformation induced martensite and subsequently breaking up of brittle martensite plates (Das *et al.*, 2008).

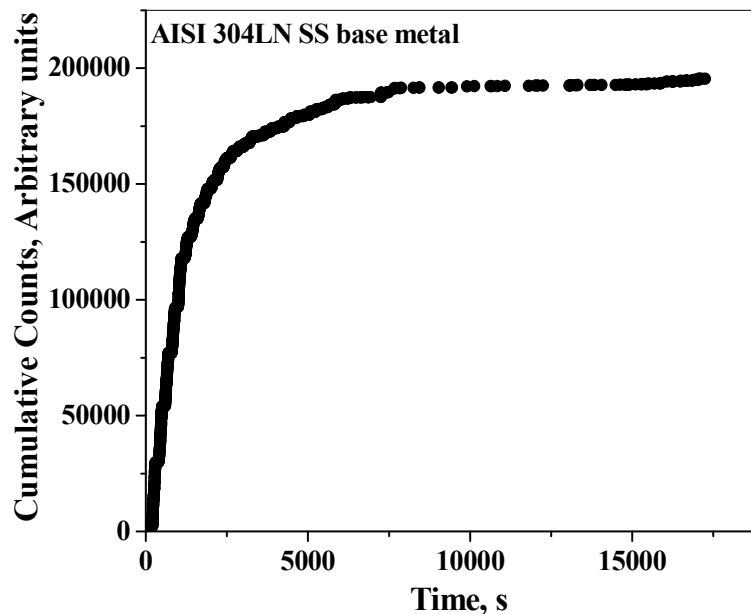


Fig. 6.7 Typical plot showing variation of AE cumulative counts with time obtained during monotonic fracture toughness test of AISI 304LN SS base metal

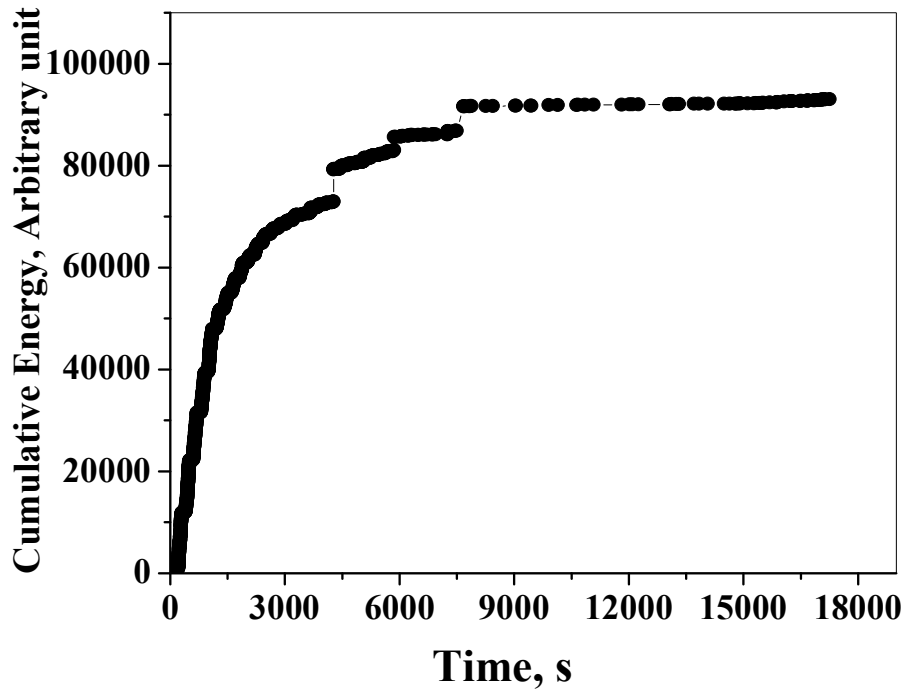


Fig. 6.8 Typical plot showing variation of AE cumulative energy with time obtained during monotonic fracture toughness test of AISI 304LN SS base metal

The loads corresponding to the point of crack initiation in AISI 304LN SS and its weldment during monotonic and cyclic fracture toughness tests are determined from the variation of load and AE energy with time, a typical plot is shown in Fig. 6.10. The obtained load is referred to as the critical load (P_{AE}) for fracture toughness calculation from acoustic emission activity. The fracture toughness value (J_{AE}) is then calculated using the following expression suggested by Dal Re (1986):

$$J_{QAE} = \eta A / bB \quad \dots (6.1)$$

where $\eta = 2 + 0.522 \frac{b}{W}$

A= Area under the load-CMOD plot

b= length of the un-cracked ligament

a, B and W are the dimensions of the specimen

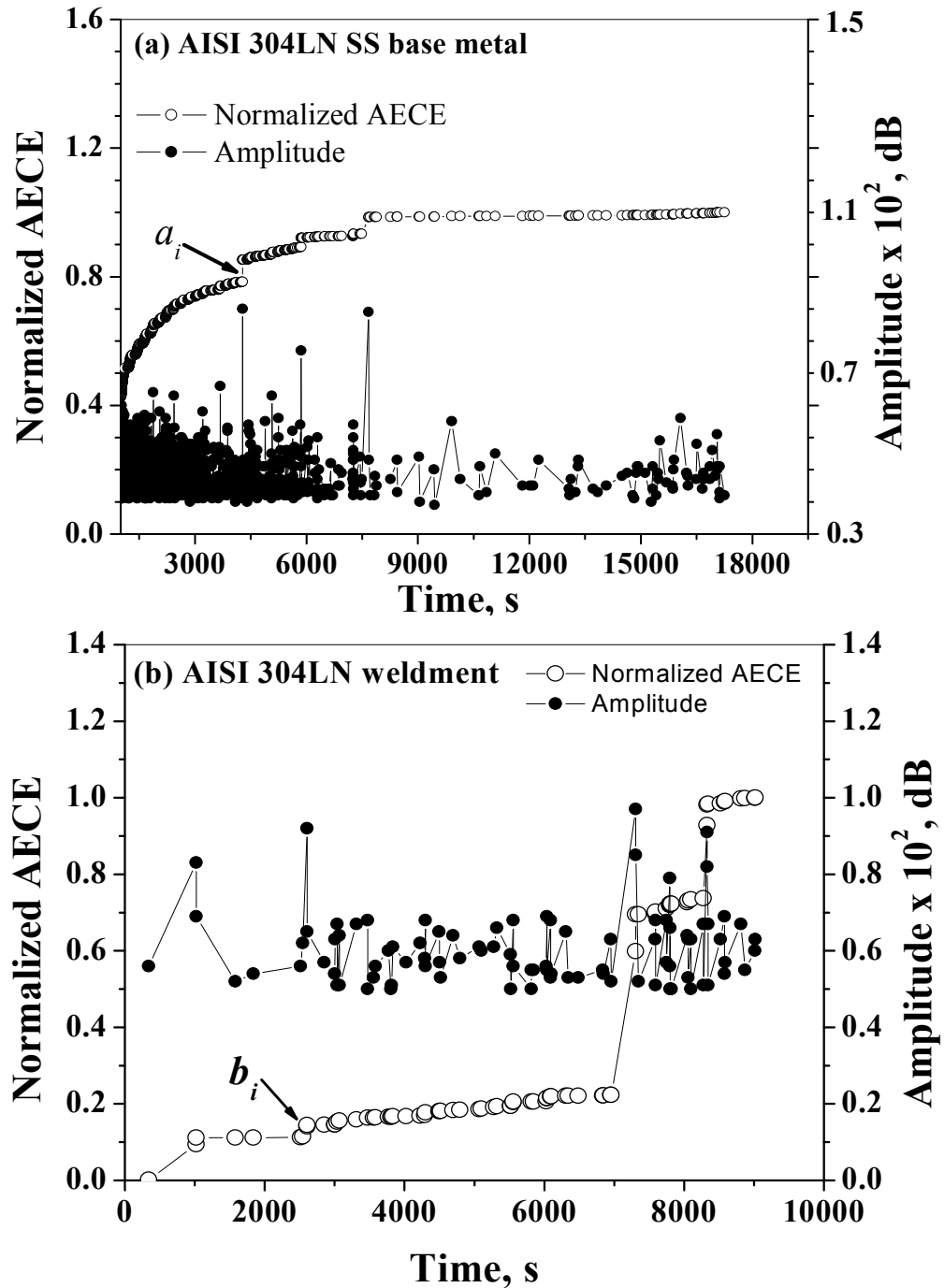


Fig. 6.9 Typical plots, obtained during fracture test of compact tension [C(T)] specimens of AISI 304LN SS (a) base metal and (b) weldment showing variations of acoustic emission cumulative energy (AECE) and acoustic emission (AE) amplitude with time. The AECE have been normalized with respect to the maximum value. The point at which crack initiates, has been indicated by arrows a_i and b_i .

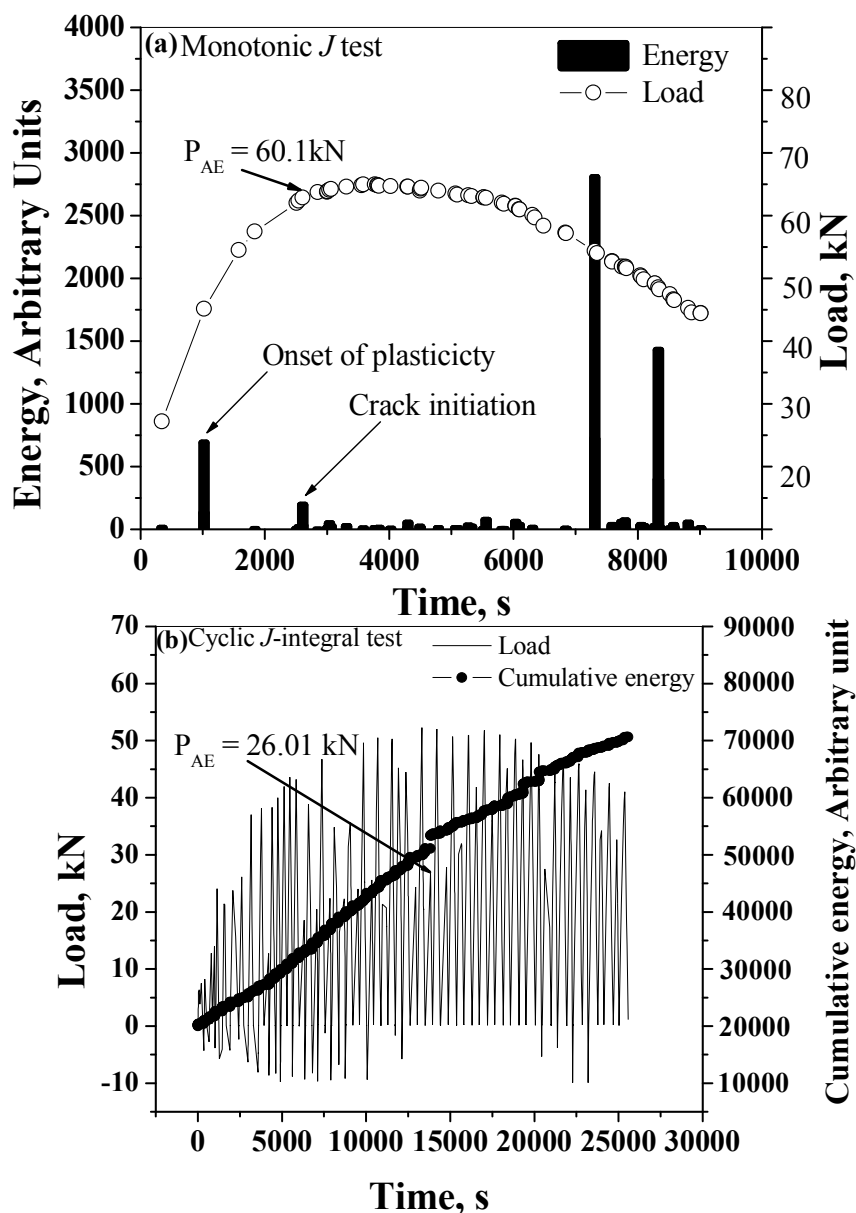


Fig. 6.10 Variation of AE energy and load obtained during (a) monotonic fracture toughness test and (b) cyclic fracture toughness test. P_{AE} indicates the critical load for fracture toughness calculation

The obtained fracture toughness values estimated from AE signal analyses are tabulated in Table 6.1 and Table 6.2 for monotonic and cyclic fracture toughness tests respectively. The average fracture toughness values estimated using AE characteristics (J_{QAE}) during monotonic fracture toughness tests of AISI 304LN SS base metal and weldment were found to be 761 kJ/m^2 and 273 kJ/m^2 respectively, whereas during a typical cyclic J - R test (J_{CAE}) at $R = -1$ and $\Delta V = 0.1 \text{ mm}$ these values were found to be 177 kJ/m^2 and 85 kJ/m^2

respectively. The difference in monotonic and cyclic J -integral tests could be attributed to the effect of crack tip re-sharpening that occurs in case of cyclic J -integral tests resulting in lower fracture toughness (Roy *et al.*, 2009). The estimated fracture toughness values for these materials by conventional procedure are also listed in Table 6.1 and 6.2. A comparison of J_{QAE} and J_Q for the two steels indicates that the former ones are almost 20–30% lower than J_Q for AISI 304 LN base metal whereas the difference is almost 50-60% for weldments. Similar comparison of J_{CAE} and J_Q under cyclic fracture toughness tests reveal that the former one is almost lower than the latter one by 35-45% for base metal and 12-22% for weldment, respectively. A comparative assessment of the estimated results is next carried out with the existing reports available. Ohira and Pao (1986) have reported that fracture toughness for A533B pressure vessel steel estimated using AE analysis is nearly 36% lower than that obtained by conventional J -integral test. In another instance Camerini *et al.* (1992) have obtained critical CTOD value corresponding to the first detectable AE to be three to nine times lower than the conventionally estimated CTOD value for crack initiation. The obtained results from this investigation are therefore found to be in good agreement with similar earlier reports (Blanchette *et al.*, 1983; Ohira and Pao, 1986; Camerini *et al.*, 1992).

Table 6.1 Comparison of monotonic fracture toughness values AISI 304LN base metal and its weldments estimated from conventional ASTM standard procedure (J_Q) and AE test (J_{QAE})

Type of steel	Specimen No.	J_Q (kJ/m ²)	J_{QAE} (kJ/m ²)
AISI 304LNSS base metal	LC1	1146	842
	LC2	1155	845
	LC3	1092	798
	CL1	915	635
	CL2	1024	718
	CL3	1076	733
AISI 304LNSS weldment	WC1	550	253
	WC2	587	272
	WC3	640	295

To rationalize the consistently lower value of J_{QAE} in comparison to J_Q , the following argument can be invoked. In ductile materials like AISI 304LN SS, the fracture toughness J_Q is ascribed at the intersection of an offset blunting line with the power law tearing curve.

Table 6.2 Comparison of cyclic fracture toughness values AISI 304LN base metal and its weldments estimated from conventional ASTM standard procedure (J_Q) and AE test (J_{QAE})

Type of Steel	Specimen code	ΔV (mm)	Stress Ratio (R)	J_{QC} (kJ/m ²)	J_{QAE} (kJ/m ²)
AISI 304LNSS base metal	LC4	0.1	-0.5	486	273
	LC5	0.1	-0.8	323	189
	LC6	0.1	-1.0	180	110
	LC7	0.1	-1.2	220	137
AISI 304LNSS weldment	WC5	0.1	-0.5	140	102
	WC6	0.1	-0.8	102	85
	WC7	0.1	-1.0	82	73
	WC8	0.1	-1.2	100	78

This procedure is followed in order to eliminate uncertainties associated with identification of the point of departure of the tearing curve from the blunting line. The offset of 0.2 mm essentially ensures that crack extension of 0.2 mm has already taken place. Acoustic emission, on the other hand, is an incipient process, and therefore indicates more precisely the point at which crack extension occurs in a massive manner along the crack front. It is thus naturally liable to be lower than the engineering definition of J_Q . In fact, identification of the J_{QAE} on the J - R curves in Fig. 4.10 brings out the fact that the J_{QAE} values represent points somewhere between the actual departure of the tearing curve from the experimental blunting line and the intersection of the offset blunting line with the tearing curve. It is logical therefore to assume that these represent significant extension of the crack after blunting. However, attempts were also made to compare the fracture toughness values obtained from AE signal characteristics with J_i (initiation toughness), which is defined as the point of deviation of linear and non-linear part of the J - R curve (Fig. 4.10 and Fig. 4.16). On comparison between J_i and J_{QAE} , J_{QCAE} values it is found that they are of the same order, the latter values being marginally lower.

Few critical examinations were carefully carried out to detect physically the crack initiation associated with variations in AE parameters, whereby tests have been interrupted on the basis of sudden jumps in acoustic emission cumulative energy (AECE).

The specimens were sectioned and the physical presence of crack initiation has been measured. Typical SEM fractograph during cyclic fracture toughness test of AISI 304LN SS weldment showing a crack of 120 μm length has been shown in Fig. 6.11 as a supportive evidence for actual crack initiation. Conventional analyses based on LEFM and EPFM principles suggest that crack length at fracture initiation could be of the order of 200 μm to 400 μm for the tested CT specimen. These values are estimated in the following manner: (a) LEFM principle accepts fracture initiation load corresponding to initiation of crack to a length (r) such that r/a is 0.02; considering specimen thickness to be 20 mm and that $a \approx B$, the initiation crack length would be $0.02 \times 20 \text{ mm} = 400 \mu\text{m}$, and (b) EPFM principle considers fracture initiation load corresponding to initiation and growth of crack to a length of 0.2 mm (i.e. 200 μm). However, length of the physical crack verified after interrupted tests suggest that the actual crack extension has occurred at considerably lower load and at a lower extent of crack extension. These estimations and the associated justifications provide support to the importance of AE in direct measurement of the point of crack initiation.

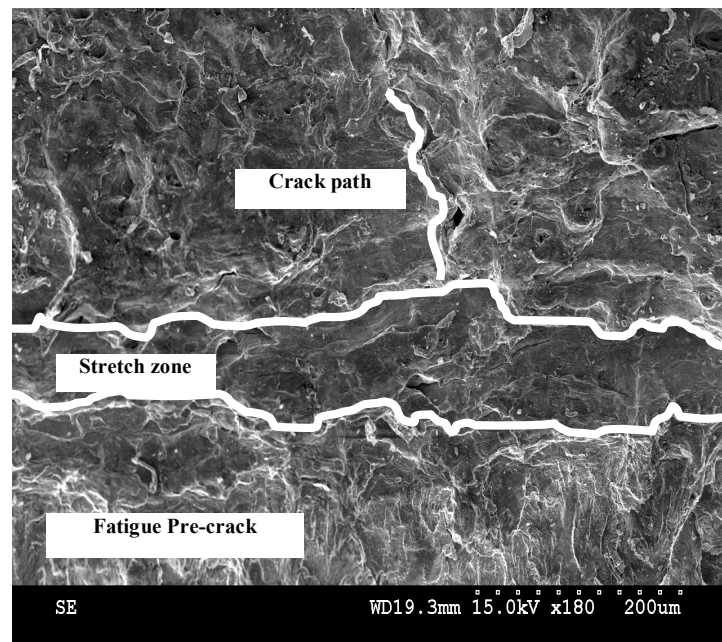


Fig. 6.11 Fracture surface observed after interrupted test of a typical cyclic fracture test specimen

6.4 Conclusions

The salient results and their analyses obtained from this part of the investigation lead to the following major conclusions:

1. Synergistic analyses of peak amplitude and energy of acoustic emission signals assist to reveal the onset of blunting and the point of crack initiation in steels possessing relatively higher fracture toughness.
2. Monotonic fracture toughness values for AISI 304LN SS base metal and weldments estimated using the characteristics of acoustic emission signal are found to be lower compared to their corresponding values estimated by standard J -integral technique by approximately 20-30% and 50-60% respectively. For cyclic fracture toughness tests, similar values are lower by 35-45% and 12-22% respectively for base metal and weldments.
3. Fractographic examinations of the broken samples from interrupted tests of AISI 304LN SS, after cyclic fracture toughness tests reveal the average size of physical cracks to be of the order of $120 \pm 5 \mu\text{m}$.

General conclusions and suggestions for future work

General conclusions

The major conclusions drawn at the end of the preceding chapters have been reviewed, outcome of the present experimental work and their analyses have been discussed and suggestions have been made for future scope of research in this chapter.

All critical engineering applications demand assessment of the structural integrity of components for their safe operation. The primary heat transport (PHT) pipings of advanced heavy water reactors (AHWRs) are such components in the nuclear power plants. These components are designed and operated on the basis of leak before break (LBB) concept. These PHT piping components made of AISI 304LN SS usually operate in the temperature range of 301-553 K and are used as circuit pipings of AHWR to carry the Heavy Water (D_2O) coming from the core channels. In order to ensure the structural integrity of piping components in service and to employ leak before break (LBB) concepts in their design, the materials of current interest, AISI 304LN SS and its weldment have to be rigorously characterized in terms of their mechanical properties with emphasis on its response to deformation and fracture behaviour. Understanding the deformation and fracture behaviour of 304LN SS and its weldment thus forms the major objective of this research.

The conventional studies on deformation behaviour show that the weldments possess comparable strength to that of base metal with substantial ductility. Deformation experiments at different strain rates suggest that flow behaviour of both AISI 304LN SS base and its weldments can get significantly altered. The microstructural investigations carried out in this work and similar reports in literature provide significant evidence for the formation of deformation induced martensite even at room temperature. Existing reports on deformation studies on AISI 304LN SS confirm that the volume fraction of deformation induced martensite varies with strain rate and provides considerable influence on mechanical behaviour. The variation of strength, ductility and strain rate sensitivity with deformation rate observed in this work therefore has to be examined in conjunction with the phase transformation.

Microstructural anisotropy can be one of the factors that can influence both deformation and fracture behaviour. Structural integrity approaches require information on changes in mechanical behaviour of materials due to orientation effects. The microstructural evaluations carried out in this study do not show any preferential orientation of grains. Even the ductile fracture resistance of the investigated material is not greatly influenced by the orientation of the crack plane, suggesting that the material would offer identical resistance to crack initiation/growth for various in-service stress conditions. However, the base metal has higher fracture toughness compared to its weldment as expected. The presence of δ -ferrite and microstructural inhomogeneity associated with the weldment can be thought to be responsible for its relatively low toughness values. The study also shows that the governing mechanism of crack initiation and growth in the selected materials is void nucleation, growth and coalescence as observed in highly ductile materials.

Conventional fracture resistance of structural materials is inadequate to safeguard structures against seismic loading conditions. Suitable experimental procedures have been designed and employed to study the influence of cyclic load excursions on the fracture resistance. The obtained results show that fracture resistance gets deleteriously affected due to cyclic loading. The influence of loading frequency and magnitude has been varied in these experiments through stress ratio and plastic displacements. A strong influence of both the parameters on the fracture resistance is observed. Moreover, the results also indicate that the adverse effect of both stress ratio and load amplitude gets saturated after a specified magnitude due to the contact of the fracture surfaces. Although, results of the cyclic fracture clearly show the influence of compressive load reversals as in seismic situation on the fracture resistance, these results bring forward another challenge of how to use the information directly for the purpose of design. Since both the stress ratio and plastic displacement influence fracture resistance curves to different extents, assigning a lower bound resistance curve through this method is considered difficult.

In the current design procedures, the allowable load on the component is generally compensated to account for the deleterious influence of seismic loading. This opens up a new avenue for investigating the number of load cycles that the component can withstand during seismic event prior to failure. Partially, this would eliminate the issues with

regards to the displacement controlled cyclic fracture evaluation. To address this issue, load control cyclic fracture experiments have been carried out, taking the collapse load during monotonic fracture as the reference. The load controlled fracture tests indicate that a material under investigation can fail in a limited number of load cycles with the load amplitude sufficiently below that monotonic collapse load. Under load controlled cyclic fracture tests crack growth occurs predominantly by (i) low cycle fatigue at the early stage and (ii) tearing at the later stage. Additionally, the obtained results on load-controlled cyclic fracture tests are compared with similar results on components. Comparison of the estimated results with that of reported ones related to load bearing capacity of specimens and components reveals that the former can withstand lower fraction of monotonic collapse load than that by the components.

An attempt in this investigation is also made to detect the onset of crack initiation in the selected materials during monotonic and cyclic fracture tests. The available standards on determining fracture resistance of materials suggest procedures using analysis of load–displacement plots. Acoustic emission (AE), on the other hand, is capable of indicating directly the crack initiation point during loading of a specimen. There are few available reports where various investigators have carried out conventional fracture toughness tests in liaison with AE technique; but so far no generalized guideline has emerged out from this type of ‘combined’ experiments. Results generated using such ‘combined’ experiment infer that monotonic fracture toughness values for AISI 304LN SS base metal and weldments estimated using acoustic emission signal characteristics are found to be lower compared to the values estimated by standard *J*-integral technique by approximately 20-30% and 50-60% respectively, whereas the same for cyclic fracture toughness tests are lower by 35-45% and 12-22% respectively for base metal and weldments. The AE technique thus proves to be a promising method for determining the ductile crack initiation.

In generalization, salient contributions of this investigation can be summarized as: (i) both load and displacement controlled fracture behaviour of AISI 304LN stainless steel have been revealed, (ii) the deleterious influence of plastic displacement (ΔV) and stress ratio (R) associated with superimposed cyclic loading condition on the fracture resistance of

stainless steel and its weldments has been illustrated, and (iii) it has been shown that the displacement controlled cyclic fracture experiments are inadequate to safe guard material during seismic loading. The proposed load controlled cyclic fracture experiments are demonstrated to be essential to know the maximum number of sustainable load cycles during seismic events.

Suggestions for future work

In the present investigation fracture behaviour under load and displacement controlled mode of the selected steel and its weldment has been carried out only at ambient temperature. Since the material is subjected to elevated temperatures (301-553 K) in its service life, future work should be directed to understand the monotonic and cyclic J - R behaviour of the material at elevated temperatures. Moreover, the material under investigation is found to undergo deformation induced phase transformation. Therefore, future studies can also be directed to investigate the effect of this transformed phase (martensite) on the fracture behaviour of the selected steels. In addition, PHT pipes carry Heavy Water (D_2O) with controlled chemistry under fixed partial pressure of oxygen and hydrogen. The effect of any variation in water chemistry and pressure is bound to affect the mechanical behaviour of the material. Hence, future work may be directed to study the fatigue and fracture behaviour under similar simulated environments.

References

Ayres, R. A. (1985), Thermal Gradients, Strain Rate and Ductility Sheet Steel Tensile Specimens, Metallurgical Transaction A, Vol. 16, pp. 37-43.

Anderson, T. L. (1995), Fracture Mechanics: Fundamentals and Applications, Third ed., CRC Press, Boca Raton, New York, pp. 265.

Arii, M., Kashiwaya, H. and Yanuki, T. (1975), Slow Crack Growth and Acoustic Emission Characteristics in COD Test, Engineering Fracture Mechanics, Vol. 7, pp. 551-556.

Bandstra, J. P., Koss D. A., Geltmacher, A., Matic, P. and Everett, R. K. (2004), Modeling Void Coalescence during Ductile Fracture of a Steel, Materials Science and Engineering A, Vol. 366, pp. 269–281.

Begley, J. A. and Landes, J. D. (1972), The J-Integral as a Fracture Criterion, ASTM STP 514, American Society for Testing and Materials, Philadelphia, pp. 24-39.

Benzerga, A. A., Besson, J. and Pineau, A. (2004), Anisotropic Ductile Fracture: Part I: Experiments, Acta Materialia, Vol. 52, pp. 4623–4638.

Blanchette, Y., Dickson, J. I. and Bassim, M. N. (1983), The Use of Acoustic Emission to Evaluate Critical Values of K and J in 7075-T651 Al Alloy, Engineering. Fracture Mechanics, Vol. 20, pp. 359-371.

Broek, D. (1982), Elementary Engineering Fracture Mechanics, Martinus Nijhoff Publishers, Third Edition, Netherlands.

Camerini, C. S., Rebello, J. M. A. and Soares, S. D. (1992), Relationship Between Acoustic Emission and CTOD Testing for a Structure Steel, NDT & E International, Vol. 25, pp. 127-133.

Christy, S., Pak, H. R. and Meyers, M. A. (1986) in: L.E. Murr, K.P. Staudhammer, M.A. Meyers (Eds.), Metallurgical Applications of Shock-Wave and High Strain-Rate Phenomena, Marcel Dekker, New York, NY, pp. 835–863.

Clarke, G. A., Andrews, W. R., Paris, P. C. and Schmidt, D. W. (1976), Mechanics of Crack Growth, ASTM STP 590, American Society for Testing of Materials, pp. 22-42.

Clark, G. and Knott, J. F. (1977), Acoustic Emission and Ductile Crack Growth in Pressure-Vessel Steels, Metal Science, pp. 531-536.

Dal, Re V. (1986), Fracture Toughness Measurement of a Ni-Cr-Mo-V Steel by Acoustic Emission, Journal of Acoustic Emission, Vol. 5-1, pp. 39-44.

Das, A., Sivaprasad, S., Chakraborti, P. C. and Tarafder, S. (2008), Correspondence of Fracture Surface Features with Mechanical Properties in 304LN Stainless Steel, *Materials Science and Engineering A*, Vol. 496, pp. 98-105.

Das, A. and Tarafder, S. (2008), Geometry of Dimples and Its Correlation with Mechanical Properties in Austenitic Stainless Steel, *Scripta Materialia*, Vol. 59, pp. 1014-17.

Dieter, G. E. (2001), *Mechanical Metallurgy*, Singapore, Mc Graw-Hill Book Company, SI Metric Edition, pp. 76-79.

Dowling, N. E. and Begley, J. A. (1976), Fatigue Crack Growth during Gross Plasticity and the J-Integral, *Mechanics of Crack Growth*, ASTM STP 590, American Society for Testing and Materials, pp. 82-103.

Dugdale, D. S. (1960), Yielding of Steel Sheets Containing Slits, *Journal of Mechanics and Physics of Solids*, Vol. 8, pp. 100-108.

Dunegan, H. L., Harris, D. C. and Tatro, C. A. (1968), Fracture Analysis by Use of Acoustic Emission, *Engineering. Fracture Mechanics*, Vol. 1, pp. 105-122.

Erdogan, M. and Tekeli, S. (2002), The Effect of Martensite Size on Tensile Fracture of Surface Carburized AISI8620 Steel with Dual-Phase Core Microstructure, *Materials and Design*, Vol. 23, pp. 597-604.

ESIS P2-92, ESIS Procedure for Determining the Fracture Behaviour of Materials, European Structural Integrity Society – ESIS, January 1992.

ASTM E 112-04 (2004), Standard Test Methods for Determining Average Grain Size, Philadelphia, PA, pp. 227-252.

ASTM E 62-08 (2008), Practice for Determining Volume Fraction by Systematic Manual Point Count, ASTM, Philadelphia, PA, pp. 1-34.

ASTM E 8M-08, (2008), Standard Test Methods for Tension Testing of Metallic Materials [Metric], ASTM, Philadelphia, PA, pp. 81-100.

ASTM E 1820-09, Standard Test Method for Measurement of Fracture Toughness, ASTM Philadelphia, PA, 2009.

ASTM E 647-03, Standard Test Method for Measurement of Fatigue Crack Growth Rates, ASTM Philadelphia, PA, 2003.

Garrison, W. M. (1984), A Microstructural Interpretation of the Fracture Strain and Characteristic Fracture Distance, *Scripta Materialia*, Vol. 18, pp. 583-586.

Gupta, S. K., Bhasin, V., Vaze, K. K., Ghosh, A. K., Kushwah, A. K. (2007), Effects of Simulated Seismic Loading on LBB Assessment of High Energy Piping, Transaction of ASME, Vol. 129, pp. 28-37.

Gurson, A. L. (1977), Continuum Theory of Ductile Rupture by Void Nucleation and Growth, Transaction ASME Journal of Engineering Materials and Technology, Vol. 99, pp. 2-15.

Hecker S. S., Stout, M. G., Staudhammer, K. P. and Smith, J. L. (1982), Effects of Strain State and Strain Rate on Deformation-Induced Transformation in 304 Stainless Steel: Part I. Magnetic Measurements and Mechanical Behavior, Metallurgical and Materials Transactions, Vol. 13A, pp. 619-626.

Heevens, J., Scwalbe, K-H. and Cornec, A. (1998), Fracture Mechanics: Eighteenth Symposium, ASTM STP 945, D.T.Reed and R.P.Reed eds, Philadelphia, pp. 374-389.

Heiple, C. R. and Carpenter, S. H. (1983), Acoustic Emission from Dislocation Motion, Acoustic Emission Non-Destructive Testing Monographs and Tracts, Vol. 2, pp. 15-103.

Heiple, C. R. and Carpenter, S. H. (1987), Acoustic Emission Produced by Deformation of Metals and Alloys-A review part-I, Journal of Acoustic Emission, Vol. 6, pp. 177-204.

Heiple, C. R., Carpenter, S. H. and Christiansen, S. S. (1990), Fracture of Boron Particles in 2219 Aluminium as a Known Acoustic Emission Source, Acta Metallurgica et Materialia, Vol. 38, pp. 611-618.

Hutchinson, J. W. and Paris, P. C. (1979), Stability Analysis of J-Controlled Crack Growth, ASTM STP 668, Philadelphia, pp. 37-64.

IAEA-TECDOC 710, International Atomic Energy Agency (1993), Applicability of the Leak Before Concept, Report of the IAEA Extra Budgetary Program on the Safety of WWER-440 Model-230 Nuclear Power Plants.

Irwin, G. R. (1957), Analysis of Stresses and Strains Near the End of a Crack Transversing a Plate, Trans ASME, Journal of Applied Mechanics, Vol. 24, pp. 361-371.

Joyce, J. A. (1988), Development of a Criterion for the Effect on the J-R Curve of Elastic Unloadings, Fracture Mechanics: Eighteenth Symposium ASTM STP 945, D.T.Reed and R.D.Reed, Eds, Philadelphia, pp. 647-662.

Joyce, J. A. (1990), Characterization of the Effects of Large Unloading Cycles on the Ductile Tearing Toughness of HSLA Steel. Journal of Testing and Evaluation, Vol. 18, No.6, pp. 373-384.

Joyce, J. A. and Culafic, V. (1988), Characterization of Interaction Effects Between Ductile Tearing and Intense Fatigue Cycling, International Journal of Fracture, Vol. 36, pp. 89-100.

Kaiser, S. (1983), On the Relation Between Stable Crack Growth and Fatigue, *Fatigue and Fracture of Engineering Materials and Structures*, Vol. 6, No1, pp. 33-49.

Khan, M. A., Shoji, T., Takahashi, H. (1982), Acoustic Emission from Cleavage Micro Cracking in Alloy Steels, *Metal Science*, Vol. 16, pp. 118-226.

Kobayashi, H., Kusumoto, T. and Nakazawa, H. (1992), The Cyclic J-R Curve and Upper Limit Characteristic of Fatigue-Crack Growth in 2.5Cr-1Mo Steel, *International Journal of Pressure Vessels and Piping*, Vol. 52, pp. 337-356.

Kramer, G., Vieth, P., Marschall, C., Francini, R. and Wilkowski, G. M. (1997), Stability of Cracked Pipe under Seismic/Dynamic Displacement-Controlled Stresses. NUREG/CR-6233-Vol-2 Report prepared for the U.S. Nuclear Regulatory Commission.

Landes, J. D. and Liaw, P. K. (1987), Conf: Effect of Load and Thermal Histories on Mechanical Behaviour of Materials, Denver Colorado P.K.Liaw and T.Nicholas Eds., pp. 241-246.

Landes, J. D. and McCabe, D. E. (1983), Elastic-Plastic Fracture, Second Symposium, vol II- Fracture Resistance Curves and Engineering Applications, ASTM STP 803, C.F.Shih and J.P.Gudas Eds, pII, Philadelphia, pp. 723-728.

Landes, J. D., Walker, H. and Clarke, A. G. (1979), Evaluation of Estimation Procedures Used in J-Integral Testing, *Elastic Plastic Fracture ASTM STP 668*, pp. 266-87.

Lee, W. S. and Chen, T. H. (2006), Rate-Dependent Deformation and Dislocation Substructure of Al-Sc Alloy, *Scripta Materialia*, Vol. 54, pp. 1463-1468.

Lee, W. S. and Lin, C. F. (2002), Comparative Study of the Impact Response and Microstructure of 304L Stainless Steel With and Without Pre-Strain, *Metallurgical and Materials Transactions*, Vol. 33A, pp. 2801-2810.

Marschall, C. W. and Wilkowski, G. M. (1989), Effect of Cyclic Loads on Ductile Fracture Resistance, *ASME Pressure Vessels and Piping*, Vol. 166, pp. 1-14.

Marschall, C. W. and Wilkowski, G. M. (1991), Effect of Cyclic Loading on Ductile Fracture Resistance, *Journal of Pressure Vessels Technology*, Vol. 113, pp. 358-367.

Mashino, S., Mashino, Y., Horiya, T., Shiwa, M. and Kishi, T. (1996), Analysis of Microfracture Mechanism of Titanium Alloy by Acoustic Emission Technique, *Materials Science and Engineering A*, Vol. 213, pp. 66-70.

Masounave, J., Lanteigne, J., Bassim, M. N., Hay, D. R. (1976), Acoustic Emission and Fracture of Ductile Materials, *Engineering Fracture Mechanics*, Vol. 8, pp. 701-709.

Mazille, H. (1995), An Acoustic Emission Technique for Monitoring Pitting Corrosion of Austenitic Stainless Steels, *Corrosion Science*, Vol. 37, pp. 1365-1375.

McClintock, F. A. and Irwin, G. R. (1965), Fracture Toughness Testing and Applications, ASTM STP 38, Philadelphia, pp. 84-113.

Meguid, S. A., (1989), Engineering Fracture Mechanics, Elsevier Applied Science.

Miura, N., Fujioka, T., Kashima, K., Kanno, S., Hayashi, M., Ishiwata, M. and Gotoh, N. (1994), Low Cycle Fatigue and Ductile Fracture for Japanese Carbon Steel Piping Under Dynamic Loadings, Nuclear Engineering Design, Vol. 153, No 1, pp. 57-69.

Miura, N., Kashima, K., Miyazaki, K. and Kanno, S. (1997), Effect of Negative Stress Ratio on Crack Growth for Cracked Pipe Subjected to Cyclic Loading with Large Scale Yielding, Fatigue and Fracture 1, edited by S. Rahman, K. K. Yoon, S. Bhandari, R. Warke, and J. M. Bloom, Book No. G01062. pp. 231-240.

Mogami, K., Hayashi, T., Ando, K. and Ogura, V. (1990), Elastic-Plastic Fatigue Crack Growth and Tearing Instability Behavior Under Cyclic Loads, International Journal of Pressure Vessels and Piping, Vol. 44, pp. 85-97.

Murr, L. E., Staudhammer, K. P. and Hecker, S. S. (1982), Effects of Strain State and Strain Rate on Deformation-Induced Transformation in 304 Stainless Steel - 2. Microstructural Study, Metallurgical and Materials Transactions A, Vol. 13, pp. 627-635.

Newman, Jr, J. C., Booth, B. C. and Shivakumar, K. N. (1988), Fracture Mechanics: Eighteenth Symposium, ASTM STP 945, D. T. Read and R. P. Reed, Eds, Philadelphia, pp. 665-685.

NUREG Report-1061, Report of the U.S. Nuclear Regulatory Commission Piping Review Committee (1984), Evaluation of Postulated Pipe Breaks, Vol. 3, Prepared by the Pipe Break Task Group.

O'Brien, D. M. and Ferguson, W. G. (1982), On the J-Integral Blunting Line for Soft Materials, International Journal of Fracture, Vol. 20, pp. R39-R43.

Ohira, T. and Pao, Y. H. (1986), Microcrack Initiation and Acoustic Emission During Fracture Toughness Tests of A533B Steel, Metallurgical and Materials Transactions A, Vol. 17, pp. 843-852.

Olson, R., Scott, P., Marschall, C. W. and Wilkowski, G. M. (1994), Comparison of Fracture Toughness Values from IPIRG-I Large Scale Pipe System Test and C(T) Specimens on Wrought TP 304 Stainless Steel, ASME Pressure Vessels and Piping, Vol. 280, pp. 241-254.

Palmer, I. G. and Heald, P. T. (1973), Application of Acoustic Emission Measurements to Fracture Mechanics, Materials Science and Engineering A, Vol. 11, pp. 181-185.

Parida, N., Sivaprasad, S., Tarafder, S., Ranganath, V. R. and Bhattacharya, D. K. (1999), Acoustic Emission: A Novel Technique for the Study of Fracture Micro-Mechanisms. Journal of Non-Destructive Evaluation, Vol. 19, pp. 51-55.

Paris, P. C. and Erdogan, F. (1963), A Critical Analysis of Crack Propagation Laws, *Journal of Basic Engineering*, Vol. 85, pp. 528-534.

Paris, P. C., Tada, H., Zahoor, A. and Ernst, H. (1970), The Theory of Instability of the Tearing Mode of Elastic Plastic Crack Growth, *ASTM STP 668*, Philadelphia, pp. 5.

Paul, S., (2003), Development of the Technical Basis for a New Regulatory Guide for Leak Before Break Applications, *Transactions of the 17th International Conference, SmiRT17*, Prague, Czech Republic, Aug. 17-22, Paper # G10-5.

Pickering, F. B. (1976), Physical Metallurgy of Stainless Steel Developments, *International Metals Review*, Vol. 21, pp. 227-268.

Prasad, P. (2004), Effect of Monotonic and Cyclic Loading on the Fracture Behaviour of SA333 steel, Ph.D Thesis, Indian Institute of Technology, Kharagpur.

Report No. MST/304IR-1, Evaluation of Fatigue and Fracture Behaviour of Narrow Gap Pipe Weldments of Similar and Dissimilar Metals, National Metallurgical Laboratory, Jamshedpur, India, March 2005.

Rice, J. R. (1968), A Path Independent Integral and the Approximate Analysis of Strain Concentration by Cracks and Notches, *Journal of Applied Mechanics*, *Transactions of ASME*, Vol. 35, pp. 379-386.

Roy, H., Parida, N., Sivaprasad, S., Tarafder, S. and Ray, K. K. (2008), Acoustic Emissions During Fracture Toughness Tests of Steels Exhibiting Varying Ductility, *Materials Science and Engineering. A*, Vol. 486, pp. 562-571.

Roy, H., Sivaprasad, S., Tarafder, S. and Ray, K. K. (2009), Monotonic vis-à-vis Cyclic Fracture Behaviour of AISI 304LN Stainless Steel, *Engineering Fracture Mechanics*, Vol. 76, pp. 1822-1832.

Roy, H., Sivaprasad, S., Tarafder, S. and Ray, K. K. (2010a), Crack Tip Damage Mechanism under Monotonic and Cyclic Loading Conditions, *Key Engineering Materials*, Vol. 417-418, pp. 105-108.

Roy, H., Bar, H. N., Sivaprasad, S., Tarafder, S. and Ray, K. K. (2010b), Acoustic Emission during Monotonic and Cyclic Fracture Toughness Tests of 304LN Weldments, *International Journal of Pressure Vessels and Piping*, Vol.87, pp. 543-549.

Roy, H., Sivaprasad, S., Tarafder, S. and Ray, K. K. (2011), Cyclic Fracture Behaviour of 304LN Stainless Steel under Load and Displacement Control Modes, *Fatigue and Fracture of Engineering Materials and Structures*, Accepted Paper DOI:10.1111/j.1460-2695.2011.01596.x.

Rudland, D. L., Brust, F. and Wilkowski, G. (1996), Fracture Toughness Evaluation of a 16-Inch Nominal Diameter TP304 Stainless Steel Pipe Used in Pipe Fracture Experiments, *NUREG/CR-6446*, BMI-2194.

Rudland, D. L., Brust, E. and Wilkowski, G. M. (1996), "The Effect of Cyclic and Dynamic Loading on the Fracture Resistance of Nuclear Piping Steels" Technical Report, Oct 1992-96. NUREG/CR-6440, BMI-2190, U.S. Nuclear Regulatory Commission, Dec.

Sandusky, D. W., Okada, T. and Saito, T. (1990), Advanced Boiling Water Reactor Materials Technology, Material Performance, Vol. 29, pp. 66-71.

Saxena, A. and Hudak Jr, S. J. (1978), Review and Extension of Compliance Information for Common Crack Growth Specimens, International Journal of Fracture, Vol. 14, pp. 453-468.

Scott, P., Olson, R., Wilkowski, G. M, Marschall, C. and Schmidt, R. (1997) Crack Stability in a Representative Piping System Under Combined Inertial and Seismic/Dynamic Displacement-Controlled Stresses. NUREG/CR-6233-Vol-3. Report prepared for the U.S. Nuclear Regulatory Commission.

Scott, P. (2003), Development of the Technical Basis for a New Regulatory Guide for Leak Before Break Applications, Transactions of the 17th International Conference, SmiRT17, Prague, Czech Republic, Aug. 17-22, pp. G10-5.

Seok, C. S., Kim, Y. J. and Weon, J. I. (1999), Effect of Reverse Cyclic Loading on the Fracture Resistance Curve in C(T) Specimen, Nuclear Engineering and Design, Vol. 191, pp. 217-224.

Seok, C. S. and Murthy, K. L. (2000), A Study on the Decrease of Fracture Resistance Curve Under Reversed Cyclic Loading, International Journal of Pressure Vessels and Piping, Vol. 77, pp. 303-311.

Sherry, A. H., Wardle, G., Jacques, S. and Hayes, J. P. (2005), Tearing-fatigue Interactions in 316L(N) Austenitic Stainless Steel, International Journal of Pressure Vessels and Piping, Vol. 82, pp. 840-859.

Sherry, A. H and Wilkes, M. A. (2005), Numerical Simulation of Tearing-fatigue Interactions in 316L(N) Austenitic Stainless Steel, International Journal of Pressure Vessels and Piping, Vol. 82, pp. 905-916.

Sindi, C. T, Najafabadi, M. H and Ebrahimian, S. A. (2011), Fracture Toughness Determination of Heat Treated AISI D2 Tool Steel using AE Technique, ISIJ International, Vol. 51, pp. 305-312.

Singh, P. K., Ranganath, V. R., Tarafder, S., Prasad, P., Bhasin, V., Vaze, K. K., Khuswaha, H. S. (2003), Effect of Cyclic Loading on Elastic-Plastic Fracture Resistance of PHT System Piping Material of PHWR, International Journal of Pressure Vessels and Piping, Vol. 80, pp. 745-752.

Speich, G. R. and Schwoeble, A. J. (1975), Acoustic Emission during Phase Transformation in Steel, ASTM STP 571, Philadelphia, pp. 40-58.

Srinivas, M., Kamat, S. V. and Rama Rao, P. (1994), A Fractographic Technique for Determining K_{max} and R, Journal of Testing and Evaluation, Vol. 22, No. 4, pp.302-308.

Takahashi, H., Khan, M. A., Kikuchi, M. and Suzuki, M. (1981), Acoustic Emission Crack Monitoring in Fracture Toughness Tests for AISI 4340 and SA533B Steels, Experimental Mechanics, Vol. 21, pp. 89-99.

Talonen, J., Nenonen, P., Pape, G. and Hanninen, H. (2005) Effect of Strain Rate on the Strain-Induced γ - α Martensite Transformation and Mechanical Properties of Austenitic Stainless Steels, Metallurgical and Materials Transactions A, Vol. 36A, pp. 421– 432.

Tarafder, S., Ranganath, V. R., Sivaprasad, S. and Johri, P. (2003), Ductile Fracture Behaviour of Primary Heat Transport Piping Material for Nuclear Reactors, Sādhana, Vol. 28, pp. 167-186.

Thomason, P. F. (1985), A Three-Dimensional Model for Ductile Fracture by the Growth and Coalescence of Micro-voids, Acta Metallurgica, Vol. 33 (6), pp.1087–1095.

Tvergaard, V. and Needleman, A. (1984), An Analysis of Ductile Rupture in Notched Bars, Journal of Mechanics and Physics of Solids, Vol. 32, pp. 461-490.

Venukumar, D., Murthy, D. S. R., Seetharaman, S., Gupta, S. K., Bhasin, V., Vaze, K. K., and Kushwaha, H. S. (2004) Cyclic Tearing and Crack Growth in Circumferentially Cracked Straight Pipes, Fatigue and Fracture of Engineering Materials Structures, Vol. 27, pp.1061-1072.

Wadley, H. N. G. and Mehrabian, R. (1984), Acoustic Emission for Materials Processing: an Overview, Materials Science and Engineering, Vol. 65, pp. 245-263.

Wells, A. A. (1961), Unstable Crack Propagation in Metals Cleavage and Fast Fracture, Proc. Crack Propagation Symposium Cranefield, pp. 210-230.

Wilkowski, G. M., Marschall, C. W. and Landow, M. (1990), Extrapolation of C(T) Specimen J-R Curves for Use in Pipe Flaw Evaluations, ASTM STP 1074, Philadelphia, pp. 56-84.

Xin, L., Cai, G. and Svensson, L. E. (1999), Investigation of Fracture and Determination of Fracture Toughness of Modified 9Cr–1Mo Steel Weld Metals using AE Technique, Materials Science and Engineering A, Vol. 270, pp. 260-266.

Zhang, J. and Jiang, Y. (2007), An Experimental Study of the Formation of Typical Dislocation Patterns in Polycrystalline Copper Under Cyclic Shear, Acta Materialia, Vol. 55, pp. 1831–1842.

CURRICULUM VITAE

Himadri Roy, born on July 29, 1979 in Jharkhand, received his Bachelor of Technology (Metallurgy) degree from Regional Engineering College, Durgapur, (presently known as National Institute of Technology, Durgapur), in 2002. He joined as a Junior Research Fellow (J.R.F) at the Material Science and Technology Division of National Metallurgical Laboratory, Jamshedpur, in 2003. He completed his Masters (M.Tech) degree from Indian Institute of Technology, Kharagpur in 2005. His keen interest in research has led him to join the Department of Metallurgical and Materials Engineering, Indian Institute of Technology, Kharagpur as a sponsored research scholar to pursue his doctoral work. He later on shifted to Central Mechanical Engineering Research Institute (CMERI) as Scientist in 2006, where he is presently employed.

His main area of specialization includes mechanical behaviour of materials, fracture mechanics, Non-Destructive Testing (NDT), Residual Life Assessment (RLA) and failure analysis of engineering materials. He has acquired Level-II certificate in ultrasonic testing from American Society for Non Destructive Testing (ASNT). He is an associate member of The Indian Institute of Metals (IIM). He is a keen researcher having approximately 30 publications in various journals and conferences. A part of the results contained in the present thesis has been published as shown below (only referred journals):

1. Roy, H., Sivaprasad, S., Tarafder, S. and Ray, K.K. (2009), Monotonic vis-à-vis cyclic fracture behaviour of AISI 304LN stainless steel, *Engineering Fracture Mechanics*, Vol. 76, Issue 12, pp. 1822-1832.
2. Roy, H., Sivaprasad, S., Tarafder, S. and Ray, K.K. (2010), Crack tip damage mechanism under monotonic and cyclic loading conditions, *Key Engineering Materials*, Vol. 417-418, pp. 105-108.
3. Roy, H., Parida, N., Sivaprasad, S., Tarafder, S. and Ray, K.K. (2008), Acoustic emission during fracture toughness tests of steels having varying ductility, *Materials Science & Engineering A*, Vol. 486, pp. 562-571.
4. Roy, H., Bar, H.N., Sivaprasad, S., Tarafder, S. and Ray, K.K. (2008), Acoustic emission during monotonic and cyclic fracture toughness tests of 304LN weldments, *International Journal of Pressure Vessels and Piping*, Vol. 87 (2010), pp. 543-549.
5. Roy, H., Sivaprasad S., Tarafder S. and K.K.Ray. Cyclic fracture behaviour of 304LN stainless steel under load and displacement control modes. Accepted in *Fatigue and Fracture of Engineering Materials and Structures*, DOI:10.1111/j.1460-2695.2011.01596.x.